Abstract

Biophysical Characterization of Somatosensory Responses in *Drosophila* Class IV Dendritic Arborization Neurons

Rajshekhar Basak

2021

Drosophila Class IV neurons are polymodal nociceptors that detect noxious mechanical, thermal, optical, and chemical stimuli. Escape behaviors in response to attacks by parasitoid wasps are dependent on Class IV cells, whose highly branched dendritic arbors form a fine meshwork that is thought to enable detection of the wasp's needle-like ovipositor barb. To study how mechanical stimuli trigger cellular responses, we developed a novel, tunable, focused 405-nm laser to create highly localized lesions to probe the conditions needed to evoke responses in Class IV neurons. Chapter 2 describes the development of the assay, physical properties of the stimulus, and its likeness to natural stimuli larvae encounter in nature.

Next, by imaging calcium signals in dendrites, axons, and soma in response to stimuli of varying positions, intensities and spatial profiles, we discovered that there are two distinct nociceptive pathways (Chapter 3). Direct stimulation to dendrites ("contact" pathway) produces calcium responses in axons, dendrites, and the cell body, whereas stimulation adjacent to the dendrite produces calcium responses in the axons only ("non-contact" pathway). The "non-contact" axonal pathway displays fast response times, high sensitivity, and is activated with or without direct stimulation of the dendritic arbor. In contrast, the slow, variable, and less sensitive "contact" dendritic

pathway is activated only by direct stimulation of dendritic processes. A mathematical model was developed to investigate the origin and magnitude of these cellular calcium responses. Because the axon signals to the central nervous system to trigger escape behaviors, we propose that the density of the dendritic meshwork in Class IV neurons is high not only to enable direct contact with the ovipositor, but also to enable neuronal activation by diffusing signals from damaged surrounding cells via the "non-contact" pathway. On the other hand, studies on dendritic morphology and dendrite tip dynamics suggest that evoked dendritic calcium signals via the "contact" response may facilitate morphological changes to the dendritic arbor following dendritic damage (Chapter 4).

Taken together, these *in vivo* studies provide detailed specifications of somatosensory properties in Class IV dendritic arbors and highlight the ability of compartments in individual Class IV neurons to respond to external stimuli via two distinct activation mechanisms. This ultimately contributes to the body of work on how individual nociceptive neurons integrate inputs and compute outputs.

***

Note: some sections of this document have been adapted from a manuscript currently under peer-review; a pre-print is available on bioRxiv (Basak et al., 2021).

Biophysical Characterization of Somatosensory Responses in *Drosophila* Class IV Dendritic Arborization Neurons

A Dissertation
Presented to the Faculty of the Graduate School
Of
Yale University
In Candidacy for the Degree of
Doctor of Philosophy

By
Rajshekhar Basak

Dissertation Director: Jonathon Howard

June 2021

GRADUATE SCHOOL OF ARTS & SCIENCES

YALE UNIVERSITY

Acknowledgements

Working in the Howard laboratory has been one of the most challenging and intellectually fulfilling experiences of my life. It is thus only appropriate that I begin this section with a heartfelt thank you to my advisor, Joe (Dr. Jonathon Howard), who kindly welcomed me into his laboratory in Spring 2016. Over the last half-decade, Joe has taught me how to question, analyze, and think. I am immensely grateful to him for his guidance and support for the last 6 years.

I have been fortunate to have overlapped in the Howard Lab with Sabo (Dr. Sabyasachi Sutradhar), who has been a mentor, collaborator, colleague, and dear friend – all at the same time. I have learned a tremendous amount about science, history, and Bengali culture through my daily interactions with him. It is not an exaggeration to say that Sabo has changed my perspective on the world for the better. I am sure that great things await him and all those who are lucky enough to associate with him.

Mohammed (Dr. Mohammed Mahamdeh), Ania (Dr. Anna Luchniak), Sonal (Dr. Sonal Shree), and Ashley (Dr. Ashley Arthur) have also been fantastic collaborators. I am grateful to Mohammed for teaching me the fundamentals of confocal microscopy, to Ania and Sonal for assisting with the countless experimental hurdles that accompanied our projects, and to Ashley for many helpful comments and suggestions with figures and manuscripts. To the many other members of the Howard laboratory: you have been great colleagues and I have benefitted greatly from your spirited discussions during lab meetings and sub-group meetings.

My gratitude also goes out to my thesis committee members, Damon (Dr. Damon Clark) and Yong (Dr. Yong Xiong), who kindly shepherded me through the many twists and turns in my thesis project. Each conversation with Damon and Yong, within and outside formal committee meetings, opened up new avenues that I had not previously considered. They have consistently provided kind and constructive feedback that has been critical for the completion of my project.

I was lucky to have not one, or two, but three amazing directors of graduate study during my time at Yale: Dr. Mark Solomon, Dr. Yong Xiong, and Dr. Karla Neugebauer. A big thank you to all three of them for their invaluable time and support.

Thanks to Doro (Dr. Dorothya Noble), Corey (Dr. Corey O' Hern) from the Physical & Engineering Biology program at Yale and the iPoLS community for giving me the opportunity to pursue a truly cross-disciplinary education. My sincere thanks to Dr. Pat Loria, Dr. Victor Batista, Dr. William Summers, and Dr. Andrew Miranker for their support and encouragement as well.

The Yale University Glee Club, The Yale Citations, Yale DISTILLED, and Yale-Canaan Venture Fellowship were instrumental in allowing me to pursue my passions external to scientific research during graduate school. I am thankful to all these wonderful organizations for the artistic and intellectual outlets they have provided me and others throughout my time at Yale.

A number of scientific mentors have played a very important role in my decision to pursue a Ph.D. in Biophysics. Dr. Maria Gulinello took a chance on me as a high school student and gave me my first exposure to scientific research. As an undergraduate research associate in Dr. David Fidock's lab, I saw the impact that basic

biological research can have on the lives of people around the globe. And Dr. V.P. Nair showed me the beauty and elegance with which physics can distill even the most complex problems. I am privileged to have been under their tutelage.

I would also not be here without the support of a great many high school teachers and college professors including, Steven Goldberg, Dan Browne, Scott Zimmerman, Alan Gardner, Tim Byrne, Andrew Adair, Eli Amzallag, Walter Muller, Dr. Timothy Boyer, Dr. Alexios Polychronakos, Dr. Brian Tiburzi, Dr. Darren Staloff, Dr. Mary Pearl, and Dr. Anne Kirschner. I was lucky to have you as teachers.

A warm thank you to my friends, including Max Farina, Dan Derosha, William Thompson, Christopher Wang, Mary Clare McMahon, Joshua Brooks, Slava Brodetskiy, Cheyn Shah, John Strub, Jessica Petrov, Jonathan Jove, Luke Espina, Chris Ushay, and Joseph Borrello. I am sure that many more adventures await.

To my partner Lauren, I cannot imagine these last few years without you. Cheers to many more sushi dinners, cilantro cocktails, jazz nights, and more.

Lastly, a big thank you to my brother, Ron, and my parents, Ratna & Prasanta, for their unwavering love and encouragement.

***

Table of Contents

Index of Figures

Index of Tables

The brain is the citadel of the senses;
this guides the principle of thought.

–Pliny the Elder (23 -79 A.D.)

Chapter 1:
Introduction

The big picture – interdependence of morphology and function in neurons

Our brains comprise billions of cells that interact with each other to build a nervous system of staggering complexity (Sjöstedt et al., 2020; Sherwood et al., 2012; Bassett and Gazzaniga, 2011; Hill and Walsh, 2005). At the most abstract level, this relies on the ability of neurons – cells of the nervous system – to receive, process, and relay information robustly. One of the fundamental goals of neurobiology is to uncover the macroscopic and molecular details unpinning this process.

The breathtaking diversity of neuronal structure and function makes this, both, an interesting and challenging pursuit (Kruger et al., 2003; Tas and Kapitein, 2018; Huang and Paul, 2019; Darmanis et al., 2015; Sjöstedt et al., 2020). As early as the 19th century, researchers identified the remarkable diversity of neuronal form and function across organisms and posited the Neuron Doctrine, which asserted that the nervous system is made up of distinct functional units – neurons – and supporting structures rather than a continuous matrix (Yuste, 2015; Shepherd, 1972; Guillery, 2005; Jones, 1999; López-Muñoz et al., 2006). While studying the heterogeneity of nerve cells,

Santiago Ramon y Cajal, one of the pioneers of modern neuroscience (Llin s, 2003; Sotelo, 2003; López-Muñoz et al., 2006), remarked in 1894:

> "the cerebral cortex is similar to a garden filled with innumerable trees, the pyramidal cells, which can multiply their branches thanks to intelligent cultivation, send their roots deeper, and produce more exquisite flowers and fruits every day."

Today, the human nervous system is known to comprise approximately 86 billion neurons, with hundreds, if not thousands, of distinct neuron types and classes (Bartheld et al., 2016; Lent et al., 2012; Herculano-Houzel, 2009). The often distinct morphological features seen in these neuron classes informs the number and types of cellular associations that individual cells can form, thus providing a structural basis for neuronal computation (Shepherd et al., 2005; Spruston, 2008; Vetter et al., 2001; London and Häusser, 2005). The resulting connections enables groups of cells to form and operate within cellular circuits that control a wide range of physiological processes (London and Häusser, 2005; Häusser et al., 2000; Branco and Häusser, 2010).

The high degree of branching seen in dendrites – spiny extensions in nerve cells – is particularly critical for establishing these neuronal connections (Häusser et al., 2000; Borst and Egelhaaf, 1994; Li et al., 2007). The storage and information processing capabilities of neuronal circuits is intricately related to the number of synaptic connections that a neuron can establish (London and Häusser, 2005; Vetter et al., 2001). Dendrites enable this process greatly by allowing neurons to form a large number of connections with a relatively small increase in the total cell volume (Chklovskii, 2004). For example, it is estimated that in cats, dendrites constitute 97%

of the surface area of spinal motor neurons (Ulfhake and Kellerth, 1981) and synaptic boutons occupy more than 80% of the surface area in proximal dendrites (Kellerth et al., 1979)

The morphometrics of dendritic arbors vary widely depending on the cell class being considered and are thought to be evolutionary adaptations designed for specific physiological functions. For example, olfactory sensory neurons in vertebrates are typically bipolar cells and possess arborized dendrites that locally innervate the surface of the epithelium in the nasal cavity (Morrison and Costanzo, 1990; Nagayama et al., 2014). This enables direct exposure of olfactory receptors on the ciliary surfaces to odorants. Purkinje cells in the human cerebellum, by contrast, are multidendritic neurons that have immensely intricate, space-filling dendritic arbors (upwards of 100,000 parallel fibers) than account for more than 90% of their total coverage (Hirano, 2018). This enables dendritic arbors of a single Purkinje cell to form synapses with hundreds of other cells. With the estimated number of Purkinje cells in humans estimated to be on the order of 10 million, this translates to approximately 1 billion cellular connections – the circuitry needed for complex cerebellar computations (Nairn et al., 1989) . Furthermore, aberrant dendritic architecture has been linked to a number of neurological pathologies, including Alzheimer's disease, Parkinson's disease schizophrenia, and autism spectrum disorders (ASD) (Martínez-Cerdeño, 2017; Moolman et al., 2004; Baloyannis, 2009; Solis et al., 2007; Anda et al., 2012; Dierssen and Ramakers, 2006; Newey et al., 2005; Kweon et al., 2017; Emoto, 2011; Šišková et al., 2014; Glausier and Lewis, 2013). Consequently, understanding the way in which these branched structures emerge, the principles that govern their growth and

maintenance, and their impact on cellular functions is a prerequisite for understating broader neural function.

The molecular determinants of dendritic morphology have been the subject of considerable study in the last two decades (Scott and Luo, 2001; Gao et al., 1999). Investigations, across a range of model organisms, have uncovered individual proteins, external cues, and entire signal transaction pathways that regulate dendritic growth, maintenance, and death (Jan and Jan, 2001). Efforts to map these findings to humans via identification of conserved elements or orthologues have and continue to inform many therapeutic and technological applications (Mirzoyan et al., 2019; Pandey and Nichols, 2011; Botas, 2007; Lai et al., 2000; Henricson et al., 2004; Hodge et al., 2019). Still, while these studies provide considerable *biochemical* insight into the dendritic morphogenesis and function, the *biophysical* properties of dendritic arbors remain less explored. How are dendrites activated? Do dendrites have a sensitivity threshold? How do signals propagate through dendrites? A desire for quantitative analyses of such questions motivated our work.

What is somatosensation?

The survival of organisms is heavily dependent of their ability to receive, process, and react to external cues. Somatosensation is the process by which organisms encode information such as pressure, heat, and pain (Lumpkin and Bautista, 2005). Somatosensory responses involve neurons that innervate the peripheral anatomy of organisms to form cell networks capable of integrating and reacting to external cues (Abraira and Ginty, 2013). The reception and eventual processing of

these stimuli is a highly complex process that has been the subject of vigorous study for many decades (Tominaga and Caterina, 2004; Zimmerman et al., 2014; Owens and Lumpkin, 2014; Lumpkin and Caterina, 2007). Somatosensory registration, the first step in the cascade that leads to behavioral responses, is necessarily dependent on the biological, physical and, mechanical features of the receptory cells. Somatosensory processing, on the other hand, refers to the interpretation of inputs and corresponding generation of outputs (Werner, 1977; Inui et al., 2004). Investigations of the multifaceted interplay between somatosensory registration and processing require insights from cell biology and biochemistry (i.e., what are the molecular players in this process?) just as it does physics (i.e., electrical and mechanical properties of sensory and motor neurons) and psychology (i.e., how does the organism "understand" and interpret these cues?).

In our studies, we were interested in the physical basis of somatosensory registration. What are the receptive properties of dendrites? How does the dendritic morphology of the receiving neurons enable or constrain function? While we were ultimately interested in uncovering features that are universal to all organisms, the sheer heterogeneity and complexity of somatosensory networks poses many challenges. Hypothesized to be independent processors of information (Gochin et al., 1994; Reich et al., 2001; Narayanan et al., 2005), a single neuron can be implicated in a staggering number of biological and behavioral circuits (Schüz and Palm, 1989; Beaulieu and Colonnier, 1989; Herculano-Houzel, 2009). A considerable body of work, nonetheless, has also established that many structural and functional features of individual neurons and entire nervous systems are conserved across higher- and lower-

order organisms (Reichert, 2009; Lichtneckert and Reichert, 2005; Hibi et al., 2017; Cuntz et al., 2010; Vormberg et al., 2017). This indicates that neuronal dendrites form and operate according to shared biological and physical principles. Model organisms with smaller and less complex nervous systems are thus desirable for investigating universal principles governing somatosensory reception and processing (Sattelle and Buckingham, 2006; Romanova and Sweedler, 2018).

Drosophila melanogaster as a model system

The *Drosophila melanogaster* nervous system is a fantastic vehicle for studies in neuroscience (Bellen et al., 2010; Bier, 2005). Since the pioneering work of Thomas Morgan in the 1910s (Morgan, 1910) and Seymour Benzer in the 1960s (Benzer, 1967), among many others, *Drosophila* has been adopted as a leading model organism for studies on neuronal structure, architecture, and behavior. Several reasons contribute to this. First, *Drosophila* display rapid fecundity, with the process of mating to eclosion occurring within a span of only 10-12 days at room temperature (20–22 °C) (Figure 1.1A). This, paired with the relative ease of fly husbandry, enables researchers to maintain and generate fly-lines of interest with quick turn-over (Hales et al., 2015).

Secondly, decades of work have established a validated and well-developed toolkit for visualization and genetic manipulation of individual neuron classes *in vivo* (Matthews et al., 2005; Hales et al., 2015). The ever-growing arsenal of experimental tools provides efficient and convenient ways to dissect cell-specific roles within their native context. For example, the UAS-GAL4 expression system, used extensively in our studies, can be leveraged to selectively visualize, or knock-down entire neuron

classes via cell-specific promoters with exquisite specificity (Duffy, 2002; Brand and Dormand, 1995). Likewise, the expression of transgenic proteins can be performed with relative ease (McGuire et al., 2004; Jenett et al., 2012a). The ability to combine the UAS-GAL4 system with repressors (for example, GAL80) or analogous binary tools like LexA/LexAop and Q-system offers additional "intersectional" strategies to simultaneously manipulate multiple genes or selectively express reporters in a subset of cells (Potter and Luo, 2011; Riabinina and Potter, 2016; Suster et al., 2004; Lai and Lee, 2006; Rodríguez et al., 2012). The widespread availability of fly lines (Jenett et al., 2012b; Cook et al., 2010; Perkins et al., 2015) and modular nature of these expression systems further allows researchers to conveniently generate new fly lines.

Third, the *Drosophila* nervous system, although capable of complex behavioral tasks – grooming, obstacle-avoidance, mating – is a relatively small system in comparison to that of vertebrates. With on the order of 100,000 neurons, the *Drosophila* nervous system provides a tractable model system in which researchers can identify and dissect the connectivity and roles of individual neuron classes (Halligan and Keightley, 2006; Scheffer et al., 2020). The aforementioned genetic tools, paired with electrophysiological and imaging techniques have already enabled connectomic studies of neuronal networks in the *Drosophila* brain at single-cell resolution (Chiang et al., 2011; Xu et al., 2020).

And finally, the *Drosophila* genome has many similarities with those of humans and other organisms. The *Drosophila* genome is estimated to have 60% homology to that of humans and 75% of all human disease genes have conserved or related *Drosophila* sequences (Bier, 2005; Pandey and Nichols, 2011; Fortini et al., 2000; Ugur

et al., 2016). Cumulatively, the combination of experimental ease, advanced scientific tools, and evolutionary conservation make *Drosophila* a remarkable model organism for questions in neuroscience, ranging from features of single cells to compound organismal behaviors. Our investigations centered around a sub-class of sensory neurons in *Drosophila* larvae, described below.

Classification of sensory neurons in *Drosophila* larvae

Drosophila larvae have 45 sensory neurons per abdominal hemi-segment. These neurons are broadly grouped into two classes: type I and type II. Type I neurons typically have few dendrites and are classified into two distinct types based on their localization in either (i) chordotonal (ch) organs or (ii) external sensory (es) organs (Orgogozo and Grueber, 2005). Type II neurons, on the other hand, are structurally complex cells that have highly arborized dendritic arbors and are thus categorized as multidendritic (md) neurons. Md neurons are further classified into three classes: the tracheal dendrite (td) neurons, bipolar dendrite (bd) neurons, and dendritic arborization (da) neurons based on finer structural and functional characteristics. In our studies, we chose da neurons as our model system (Grueber et al., 2002).

There are 16 da neurons in each hemi segment A2-A6 of *Drosophila* larvae. Owing to distinct morphological phenotypes, dendritic arborization neurons can be grouped into 4 sub-types: class I, class II, class III, and class IV. Class I neurons are the structurally least complex of all da neurons and form sparse, comb-like dendritic arbors that cover 14-17% of the larval hemi-segment. Class II neurons have bigger and more complex arbors that cover a larger surface area along the larval body wall (33-

39%). Class III and Class IV neurons, on the other hand, have extensively arborized structures, with the latter displaying the most complex morphologies of da neurons (>3000 branches per cell in third instar larvae). These two cell types provide 70-100% coverage of the body wall with minimal redundancy (Grueber et al., 2002, 2003). The spatial localization of these neurons is remarkably consistent between organisms with predictable organization along the dorsal, ventral and lateral regions of the larval body (Orgogozo and Grueber, 2005).

Da neurons collectively mediate larval behavioral responses to a range of sensory stimuli, ranging from innocuous to noxious. As a result, one of the great strengths of this model system is that it allows investigation of somatosensory properties across different regimes. It has been shown that class I-IV neurons are differentially responsive to varying types of stimuli. Class I neurons, for instance, have been implicated in proprioception resulting from body segment deformations during crawling (He et al., 2019; Vaadia et al., 2019). Class III cells are involved in low-force threshold mechanosensation (Tsubouchi et al., 2012), and Class IV cells are involved in polymodal nociception – encoding responses to high mechanical force, damaging thermal, optical, and chemical stimuli (Terada et al., 2016; Lopez-Bellido et al., 2019; Johnson and Carder, 2012; Robertson et al., 2013; Xiang et al., 2010; Hwang et al., 2007a) . In our studies, we have focused on studying how Class IV cells encode noxious mechanical stimuli in an ethological setting, described below.

The structure and function of Class IV dendritic arborization (da) neurons

Class IV da cells exhibit laminar radiation and localize in an 8-10 μm layer along the extracellular matrix between the larval cuticle and basement membrane/muscle in *Drosophila* larvae (Figure 1.1B). Via intricate, space-filling dendritic arborization networks (Figure 1.2) that interdigitate with neighboring cells, Class IV neurons, collectively, innervate close to 100% of the larval body wall (Grueber et al., 2002). How they achieve this coverage has been the subject of considerable investigation. From a physical perspective, the principles of (i) self-avoidance and (ii) tiling have emerged as key processes that help regulate the spatial distribution of dendritic arbors (Jan and Jan, 2010; Grueber et al., 2003; Soba et al., 2007; Xiang et al., 2010).

As the name suggests, self-avoidance refers to the ability of Class IV neurons to occupy space without overlap with its own sister dendrites. How do Class IV cells prevent overlap with its own or neighboring cells? Evidence shows that surface interactions between dendritic branches, mediated by Down syndrome cell adhesion molecule 1 (Dscam1) (Soba et al., 2007; Matthews et al., 2007), Turtle (Tutl) (Long et al., 2009)and Flamingo (Fmi) (Matsubara et al., 2011), play some role in regulating this process. For example, loss of Dscam1 leads not only to dendrite crossing but also irregular aggregation of branches; the introduction of one of the >38,000 Dscam isoforms to da neurons in Dscam mutants is sufficient to restore self-avoidance (Schmucker et al., 2000; Soba et al., 2007). Similar mutant and rescue experiments show that *fmi* regulates Class IV self-avoidance in a cell-autonomous fashion (Matsubara et al., 2011)

Tiling, on the other hand, refers to maximal coverage of the larval body wall (Figure 1.2C). This process ensures that that Class IV dendritic trees spread as widely as possible across a given region without redundancies, thereby facilitating efficient and unambiguous signal processing (Cameron and Rao, 2010; Jan and Jan, 2010; Grueber et al., 2002). Although the molecular basis for tiling is not known fully, it has been proposed that Down syndrome cell adhesion molecule 2 (Dscam2) (Cameron and Rao, 2010; Lah et al., 2014; Millard and Zipursky, 2008), tricornered (trc) and furry (fry) (Emoto et al., 2004) mediate this process via repulsive contacts between branches. Additionally, there is evidence suggesting that interactions with neighboring dendrites, the surrounding tissue, epidermis and cell substrate could provide growth or shrinkage cues. For example, it has been reported that ablation or removal of Class IV dendrites results in invagination of sister dendrites and neurites from neighboring cells into the empty territory (Sugimura et al., 2003; Grueber et al., 2003). Furthermore, interactions of Class IV cells with the surrounding cellular matrix and underlying epithelial cells is important for achieving appropriate dendrite morphology: for example, levels of the microRNA *bantam* (*ban*) in epithelial cells have been shown to affect dendrite scaling and growth (Parrish et al., 2009).

What is the evolutionary purpose of the aforementioned structural features? Just as C-fibers in mammals sense harsh touch, high temperature, and toxic chemicals (Abraira and Ginty, 2013; Delmas et al., 2011; Perl, 2007), Class IV da neurons serve as polymodal sensors that mediate nociceptive behavioral responses in *Drosophila* larvae. Uniform and non-redundant coverage of the body wall thus maximizes the ability of Class IV neurons to sense a variety of insults to the epidermal barrier, register, and

process noxious stimuli (Ganguly et al., 2016; Grueber et al., 2002). There is support for this idea from number of experiments: for example, larvae stimulated with a thermal probe (>38°C), exhibit characteristic rolling escape movements (Babcock et al., 2009; Tracey et al., 2003; Xu et al., 2006) that are mediated by Class IV neurons (Hwang et al., 2007a; Burgos et al., 2018; Ohyama et al., 2013) (Hwang et al., 2007; Ohyama et al., 2013); cell-specific silencing results in loss of this behavior. Similarly, Class IV neurons initiate rolling behaviors in response to mechanical stimuli; larvae exhibit distinct withdrawal responses Von Frey filament stimulation at forces greater than 50 mN (Hwang et al., 2007a; Zhong et al., 2010; Yamanaka et al., 2013). It has likewise been demonstrated that Class IV neurons are needed for withdrawal and escape responses in response to optical stimuli and chemical stimuli (Lopez-Bellido et al., 2019).

A number of studies have identified critical genes and proteins that confer Class IV neurons these sensory properties: for example, the gene *painless* and the transient receptor potential channel TrpA1, are needed for thermal nociception (Neely et al., 2011; Gu et al., 2019), gustatory receptor 28b is needed for optical nociception (Berni et al., 2012; Yamanaka et al., 2013) and a member of the DEG/ENaC family, *pickpocket1*, is required for mechanical nociception (Zhong et al., 2010; Ainsley et al., 2008). Although there is evidence that many of these genes and proteins mediate modality-specific responses, ongoing work is investigating the degree to which they initiate distinct or interdependent signaling pathways via coordination with other sensory structures like the chordotonal organs (Ohyama et al., 2013)

Although the aforementioned investigations are performed under highly idealized laboratory conditions, the polymodal sensory capabilities of Class IV cells are

indeed relevant in common ethological scenarios. Evidence from Daniel Tracy's laboratory showed how Class IV neuron-mediated nociceptive responses in *Drosophila* larvae enable them to escape stings from the parasitic wasps. For example, using its sharp tube-shaped ovipositor, the parasitic wasp *Leptopilina boulardi* injects its egg into the *Drosophila* larval body. The injected wasp larva then devours the larvae from the inside before hatching from the larval enclosure. As a defense mechanism during mechanical penetration of the cuticle, *Drosophila* larva initiate stereotypic turning responses (Hwang et al., 2007; Ohyama et al., 2013) as a means to escape the wasp attack. Class IV neurons not only perform somatosensory registration of the stimulus (i.e., the wasp puncture wound), but also encode directional cork-screw-like rolling preferences, distinct from the normal style of locomotion used during foraging, which likely offer larvae a higher chance at survival (Ohyama et al., 2013). It is posited that rolling is an effective escape strategy because rotation results in a body velocity twice that of forward crawling (Hwang et al., 2007b), thus increasing the possibility of evasion. While studies have identified a number of second-order motor neurons that are involved in mediating these behaviors (Yoshino et al., 2017; Chin and Tracey, 2017), Class IV neurons are thought to be the primary sensors without which necessary downstream neuronal circuits are not activated. Thus, given their critical ecological role in mediating larval behavior and survival, Class IV neurons are an ideal model for studies on somatosensory registration.

In our studies, we were particularly interested in wasp oviposition because it highlights a tangible ecological scenario where sensory registration of mechanosensory input to Class IV neurons is paramount. To study somatosensory properties of Class

IV neurons in this very context, we developed a method to emulate a wasp stinger with a high degree of spatiotemporal control. Chapter 2 details the development and characteristics of this assay. Using this method, we elucidated somatosensory properties of individual Class IV cells *in vivo*. Namely, (i) what is the sensitivity threshold of Class IV dendrites? How are Class IV cells activated? (ii) are dendritic responses compartmentalized or a global event across the arborized network? (iii) how fast do dendrites in Class IV neurons register stimuli? (iv) do class IV cells activate in an all-or-nothing fashion or are responses graded? (v) do different neuronal compartments have uniform or different sensitivities to mechanical stimuli? Insights into these questions will help clarify the physical basis underlying nociception via Class IV cells.

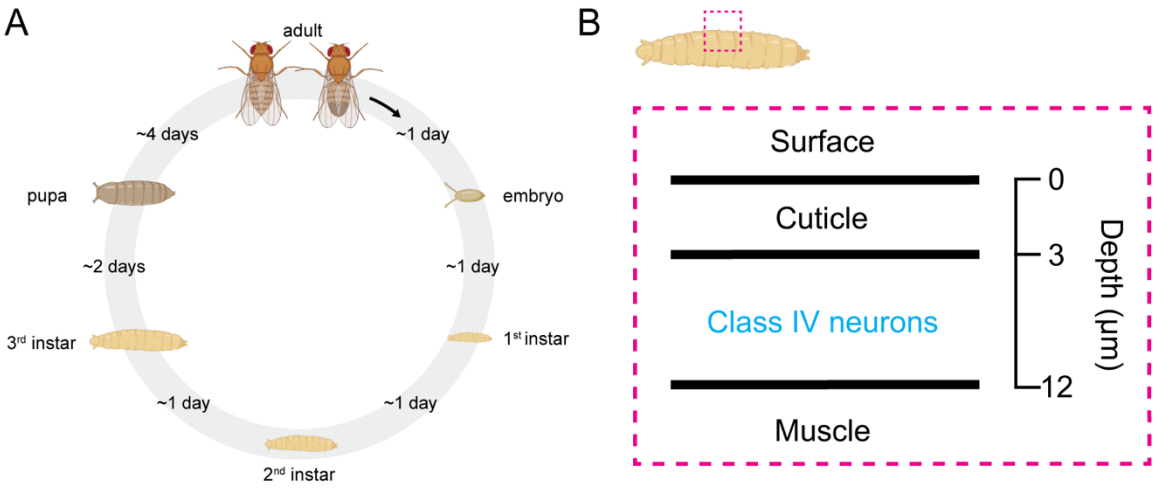

Figure 1.1: *Drosophila melanogaster* as a model system. (A) Life cycle of *Drosophila* from adult to eclosion occurs in ~10 days at room temperature (20–22 °C). Our studies focus primarily on 2nd and 3rd instar larvae. (B) Class IV neurons are sensory cells in *Drosophila* larvae that localize in a quasi-two-dimensional 8-10 µm layer beneath the cuticle and above the muscle/basement membrane layer.

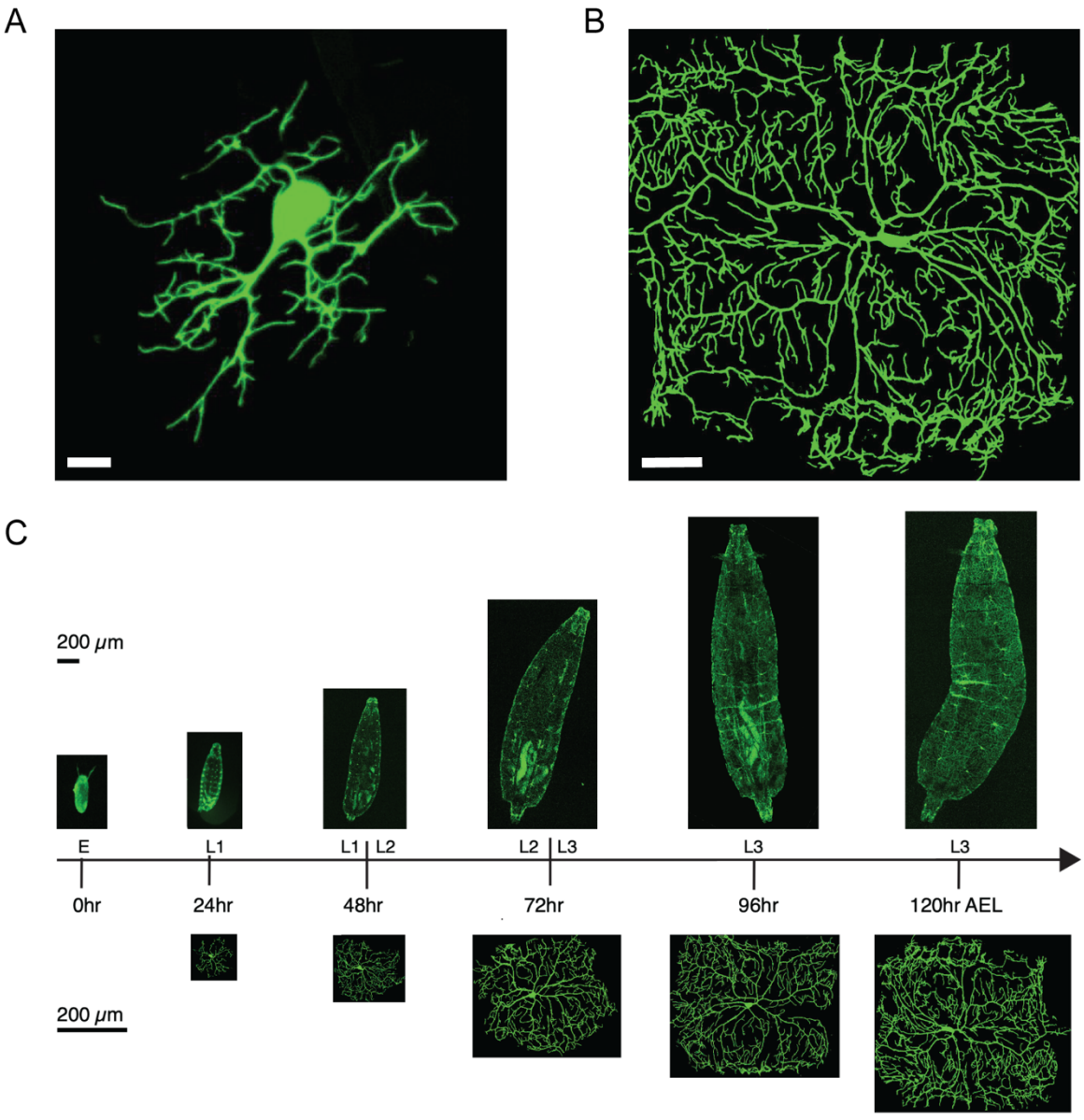

Figure 1.2: Class IV dendritic arborization neurons in *Drosophila* larvae display intricate branching morphology. (A) Image of a Class IV da neuron in a 1st instar larva (~18 hours AEL). Scale bar is 50 μm. (B) Image of a Class IV da neuron in a 3rd instar larva (~80 hours AEL). Scale bar is 50 μm. (C) Development of Class IV da neurons across the larval stage, from embryo to 3rd instar stage of development in whole larvae (top) and single neurons (bottom).

Dynamic remodeling of Class IV neurons

One of the most interesting studied features of the nervous systems in holometabolous insects like *Drosophila* is the perpetual remodeling of dendritic structure throughout the lifetime of the organism (Shimono et al., 2009; Consoulas et al., 2002; Veverytsa and Allan, 2013) (Figure 1.3). It has been shown that the nervous system in these organisms has the capacity to modify existing structures while also acquiring new features needed for a range of behavioral and cellular functions (Corty et al., 2009; Kuo et al., 2005). In *Drosophila*, for instance, entire classes of neurons are degraded during the pupal transition and replaced with new cells (Kuo et al., 2005; Williams and Truman, 2005; Shimono et al., 2009). Alternatively, the axons and dendrites of neurons can selectively undergo degradation and regeneration throughout the larval stages without loss of the cell body or nucleus (Consoulas et al., 2002; DeVault et al., 2018).

Class IV neurons demonstrate dendritic remodeling that persists from embryogenesis until they are degraded during pupal transition (Kuo et al., 2005) (Figure 1.3). Individual dendritic tips exhibit spontaneous growth and shrinkage on the second time-scale with each event lasting between 1-20 seconds (Howard Lab, *unpublished data*) (Figure 1.3). While the molecular underpinnings of this process are still under investigation, it has been proposed that microtubule dynamics and orientation (Herzmann et al., 2018, 2017; Williams and Truman, 2005), in conjunction with microtubule associated proteins like Katanin P-60 like 1 (Kat-60L1) (Stewart et al., 2012; Lee et al., 2009), may play an important role in mediating reorganization of dendritic tips.

Quantification of this dynamicity is a subject of ongoing study in our laboratory. Broadly, dendritic tips display three distinct behaviors: the trajectory of any dendritic tip can be segmented into periods of growth (G), shrinkage (S) and paused (P) states (Figure 1.4). Although contact-based transition to the shrinkage state is induced when a dendritic tip collides with another (Figure 1.4A), evidence shows that transitions between states in the absence of dendrite-dendrite contact-based repulsion can be explained by modeling tip dynamics as a spontaneous stochastic Markov process (Howard Lab, *unpublished data*) (Figure 1.4B). We use this quantitative framework to analyze morphological properties of Class IV arbors in Chapter 4.

Why do Class IV neurons consistently undergo this energetically expensive process? The ethological purpose of this dynamic remodeling is presently unclear. One theory is that dendrite tip dynamics may facilitate more robust coverage of the body wall that results in optimized ability to sense noxious cues that may otherwise go undetected. Another is that dendritic reorganization may be a reaction to external stimuli received; there is evidence in other systems that sensory-evoked neuronal activity contributes to remodeling of dendritic fields (Emoto, 2011; Vannini et al., 2016; Cline, 2001; Miller and Kaplan, 2003). Along this line of inquiry, in Chapter 4, we explore if direct stimulation results in changes to features of Class IV arbors via careful quantification of dendritic morphometrics.

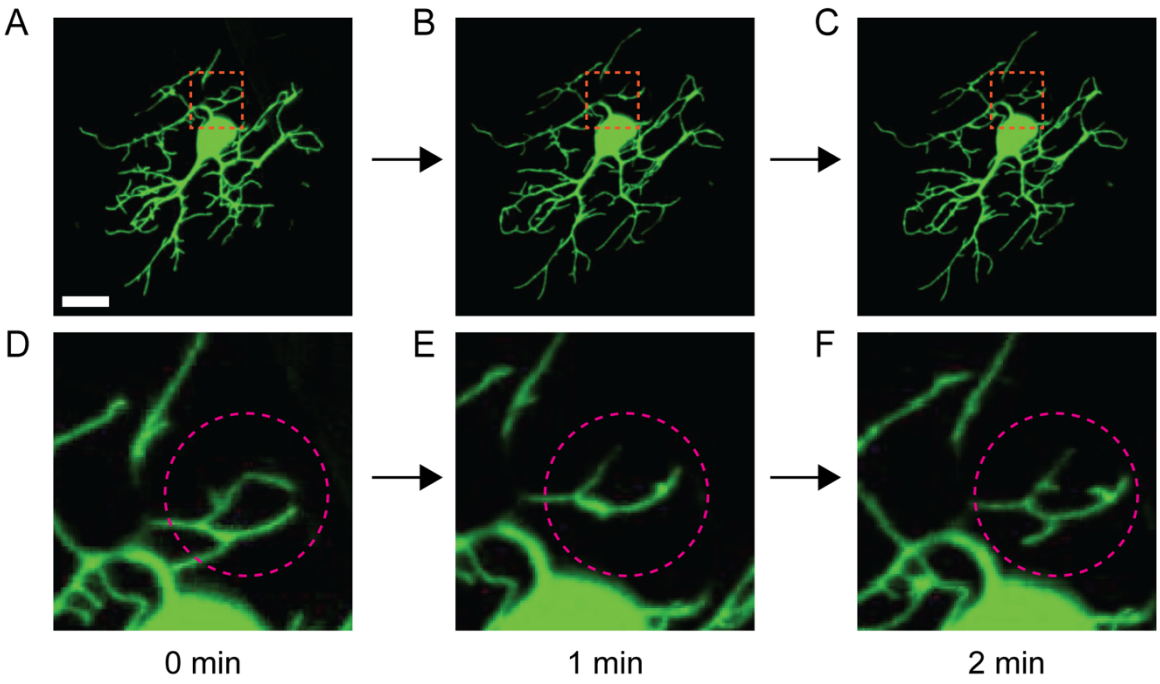

Figure 1.3: Class IV da neurons in *Drosophila* larvae display persistent remodeling of dendritic arbors via dynamics of dendritic tips. (A-C) Montage of a Class IV neuron (~18 hours AEL) undergoing dendritic remodeling over a 2-minute period. Scale bar is 50 µm. (D-F) Zoom in on region highlighted in panels A-C with dashed orange box. Magenta dashed circle highlights a region of interest where dendrite tip dynamics are clearly evident: (0 min), pruned (1 min) and regrowth (2 min).

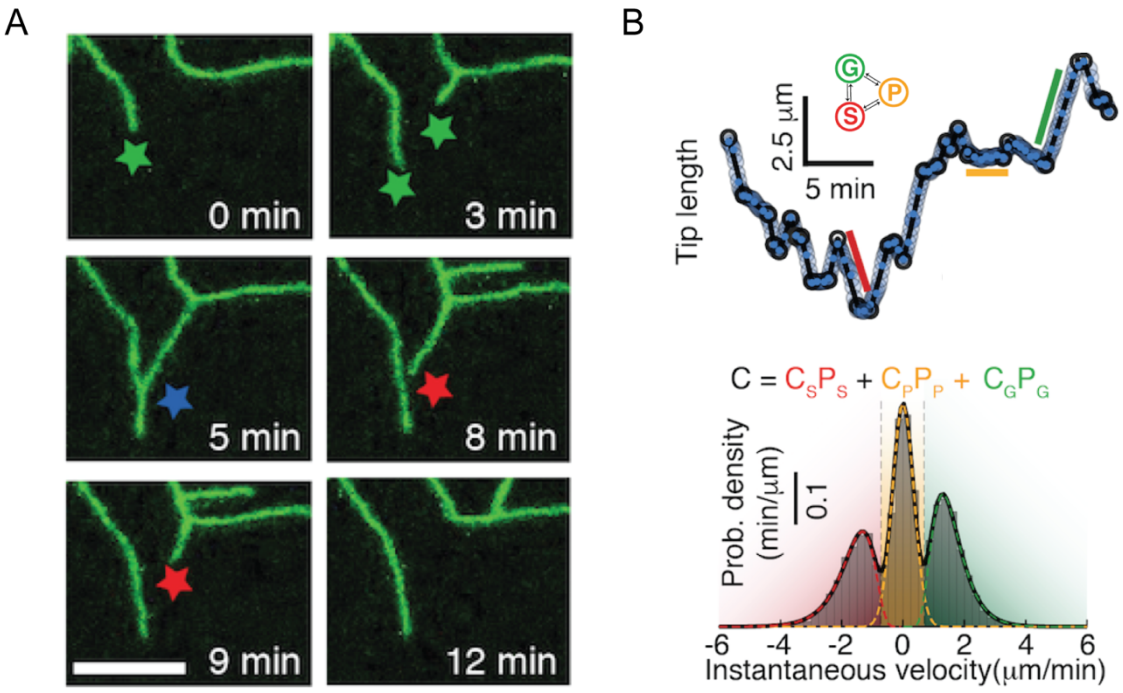

Figure 1.4: A three-state model encapsulates dendrite tip dynamics in Class IV da neurons. (A) Montage of a region of interest in a Class IV neuron demonstrating growth (green star), collision (blue star), and shrinkage (red star) events across a 12-minute period. Scale bar is 5 µm. (B) Dendrite tip trajectories can be quantified by segmenting processed tip traces into periods of growth, pause, and shrinkage. Example trace being segmented (top panel) The velocity distribution for all tips can be computed via quantification of the tip length trajectories into growing (green), shrinking (red) and paused (yellow) states. Example shown in bottom panel.

Calcium imaging as a technique to study neuronal function

The bioelectric nature of neurons is their most ubiquitous and perhaps, well-known, feature (Hodgkin and Huxley, 1952; Häusser, 2000). Accordingly, electrophysiological techniques have historically been the dominant tools using which neuronal properties are assessed. Patch clamping, for instance, allows direct measurement of action potentials in neurons with outstanding temporal resolution, signal-to-noise ratio, and sensitivity (Liem et al., 1995; Kornreich, 2007). However, this can be a technically challenging, laborious, and invasive process in living animals (Suk et al., 2019; DeWeese, 2007).

More recently, calcium imaging has emerged as an alternative powerful method for studying neuronal activity. Many studies have confirmed the relationship of neuronal excitability and intracellular calcium concentrations in a number of model systems (Ali and Kwan, 2019; Sabatini et al., 2001; Higley and Sabatini, 2008; Theis et al., 2016; Moreaux and Laurent, 2008; Stern et al., 2020; Deneux et al., 2016) Leveraging this association, calcium imaging uses sensors that modulate their fluorescence or shift their emission wavelength upon binding to calcium ions. This, effectively, results in a second-order measurement of neuronal depolarization (Tian et al., 2009; Wang et al., 2008; Akerboom et al., 2009).

This technique has numerous benefits. Foremost among them is that calcium imaging is an optical technique that enables direct visualization of neuronal activity *in vivo*. This allows for detailed analysis of Ca^{2+} signals within large cellular populations or compartments of single cells (for instance, individual dendrites) with a high degree of spatial and reasonable temporal resolution (1–100 Hz)(Russell, 2011). Furthermore,

ongoing developments in imaging and computational techniques are promising approaches that may help increase current resolution limitations via novel image processing and machine learning based approaches (Stringer and Pachitariu, 2019; Pnevmatikakis, 2019; Denis et al., 2020). Secondly, modern calcium indicators can be genetically encoded in specific cell populations without measurably altering native physiological conditions (Yang et al., 2018). This is a critical advantage as it bypasses the need for the insertion of chemical dyes (Deo and Lavis, 2018). Owing to rapid advances in fluorophore signal-to-noise ratios and binding kinetics (Sun et al., 2013; Ding et al., 2014), in some systems, genetically encoded calcium indicators even allow for imaging of neuronal dynamics down till the single synapse level (Reynolds et al., 2018).

In our studies, we relied extensively on the genetically encoded calcium indicator GCaMP6f, a 6th generation reporter in the GCaMP family (Chapter 3). Briefly, GCaMPs consists a Ca^{2+} binding domain, CaM, fused to a circularly permuted green fluorescent protein (GFP) (C-terminus) and a myosin light chain kinase domain (M13) (N-terminus). In its resting state, GCaMP6f exists in a low fluorescent state due to a water pathway that enables protonation of the GFP. When calcium is present, CaM undergoes a conformational change, and the hinge region is able to bind peptide chains on the M13. This interaction results in heightened emission via deprotonation of the GFP (Ding et al., 2014; Akerboom et al., 2009; Barnett et al., 2017). While the first GCaMPs suffered from low signal-to-noise ratios, slow binding kinetics and a shallow permissive temperature range, the newer iterations, like GCaMP6 and its successors,

have markedly improved features that make them excellent for monitoring intracellular calcium dynamics (Akerboom et al., 2012; Badura et al., 2014; Ye et al., 2017).

How does one interpret *in vivo* neuronal calcium signaling events? This is a challenging question because calcium dynamics observed via calcium indicators are the result of a lengthy cascade of events: registration of stimulus → depolarization of the membrane → opening of membrane ion channels (or release from internal cellular calcium stores) → influx of calcium → binding of calcium to the reporter → conformational changes to reporter structure → measurement via fluorescence → analysis of measurements. To complicate matters further, calcium is one of the most ubiquitous cellular messengers that is implicated in a wide range of cellular functions (Carafoli and Krebs, 2016; Cerella et al., 2010; Berridge, 2016) and the detailed impact of reporter kinetics on experimental observations is not fully understood (Sabatini, 2019; Higley and Sabatini, 2008). Still, while acknowledging these caveats, a large body of work studying the relationship between neuronal excitability and calcium signaling has made it possible to extract valuable information from intracellular calcium signals (Ali and Kwan, 2019). In our studies, although we did not infer individual rates of spiking from our calcium imaging data, signaling magnitudes offered insight into spiking trends (for example, all-or nothing vs graded responses), spatial information of cellular calcium transients (for example, signals in dendrites versus axons) and also served as a readout for synaptic input (for example, observing signal propagation between neighboring neurons). More detailed interpretations of each individual experiment is provided in the *Discussion* section of the corresponding chapter.

Our research questions

Our work focused on method development and investigating the physical basis for somatosensation in Class IV da neurons. To study this process in an ethological context, we first developed and optimized a assay that allowed us to emulate localized ovipositor-induced puncture wounds to the larval cuticle via controlled laser irradiation (Chapter 2). We then used this technique to perform a thorough biophysical characterization of cellular compartments by probing differential sensitivities across various parts of dendritic arbors in single cells using calcium imaging (Chapter 3). To our knowledge, this is the first reported investigation of somatosensory properties in individual dendritic arbors of *Drosophila* Class IV neurons. Finally, we attempted to situate our findings within the context of Class IV dendritic arbor morphology, development, and function (Chapter 4). Our *in vivo* data provide detailed specifications of somatosensory properties in Class IV dendritic arbors and proposes differing functional interpretations of dendritic and axonal calcium signals within the context of larval nociception. Taken together, this work contributes to our understanding of larval nociception, specifically, and how individual neurons integrate and process external input, more generally.

To measure is to know.

–Lord Kelvin (1824 - 1907)

Chapter 2:
Assay Development: Using Localized 405nm Laser Stimulation to Emulate a Wasp Ovipositor

2.1 Abstract

Drosophila class IV da neurons are nociceptive cells that mediate larval behavioral responses to noxious stimuli. A striking example of this ability can be seen in escape behaviors triggered in response to attacks from parasitoid wasps. As such, an understanding of the somatosensory properties in individual class IV neurons is of considerable interest. To study individual cellular responses within an ecological context, we developed a tunable optical assay using a 405 nm laser that delivers focal stimuli to the larval cuticle. In this chapter, we present the optical properties of the laser assay and characterization of the inflicted puncture wounds. Analysis of the geometric properties of the wounds demonstrate high resemblance to those inflicted by a wasp ovipositor. Stimulation of larvae is also accompanied by behavioral and single-cell nociceptive responses which we analyze in subsequent experiments. A discussion of the benefits and potential drawbacks of this approach is presented.

2.2 Introduction

What is nociception?

Nociception is the sensation of painful or injurious stimulation. The ability to detect noxious stimuli is important for organismal survival (Tracey, 2017). The peripheral nervous system senses noxious stimuli – mechanical, chemical, heat – through somatosensory cells called nociceptors, which signal to the central nervous systems to trigger appropriate behavioral responses (Nijs et al., 2012). Given their specialized role, it is of great biological and physical interest to study behavioral and cellular responses in nociceptive cells to these varying stimuli. A detailed understanding of the ways in organisms receive and process to external cues will provide considerable insight into the architecture and operational features of the peripheral nervous system.

Nociceptors possess highly specialized features that are optimized to specifically detect stimuli that could be injurious or harmful (Woolf and Ma, 2007; Tracey, 2017). This idea was first proposed by Sherrington over a century ago (Sherrington, 1903, 1907) . Imaging and electrophysiological studies have since confirmed the existence of specialized sensory neurons that are excited by differentially noxious levels of heat, cold, pressure, and chemicals – but not by innocuous stimuli such as gentle touch or low-intensity light (Dubin and Patapoutian, 2010). The evolutionary and biochemical complexity of nociceptors and their corresponding transduction machinery has been the subject of considerable study (McCleskey and Gold, 1999; Kavaliers, 1988; Chin and Tracey, 2017). In our

investigations, we were interested in studying the *biophysical* properties of nociceptors and their bearing on organismal survival. In particular, we focused on quantitation of somatosensory properties in individual nociceptive neurons. To do this, we had to select an assay that is compatible with confocal imaging experiments and allows precise delivery of stimuli to individual cells with high spatiotemporal resolution.

Commonly used nociception assays

Broadly, the most common noxious stimuli organisms encounter can be characterized into four different categories: mechanical, thermal, chemical, and optical. While there is some overlap between these classes, and there are other stimuli that do not fall neatly into this classification, these categories, together, encompass the vast majority of noxious ecological cues that organisms encounter in nature. Investigators have developed a number of assays to emulate these stimuli under controlled laboratory settings. Here, I provide a brief overview of commonly used nociceptive assays, along with their advantages and caveats.

The Von Frey esthesiometer is one of the first instruments that was widely used to perform controlled mechanical stimulation (Lambert et al., 2009; Deuis et al., 2017).The operating principle underlying Von Frey assays relies on the flexural rigidity of the attached filaments, also called Von Frey "hairs". A Von Frey filament of certain thickness, length, and material can exert an increasing amount of force up until the filament buckles (Fruhstorfer et al., 2001). This allows researchers to apply a reproducible force to a sample region. However, despite many developments in the filament materials and experimental protocols, Von Frey assays remain a crude, and

often hand-held, way of imparting forces to biological samples. Furthermore, while they are useful for mechanical stimulation in larger organisms (eg: mouse, rats, worms), the size and imprecision of Von Frey filaments make them ill-suited for studies on smaller organisms and single cells. Ongoing work is making great strides in developing automated Von Frey devices that render improved control and precision (Lambert et al., 2009; Campana and Rimondini, 2014).

More recent technology has made it possible to deliver very precise, automated, mechanical forces to biological samples with outstanding spatial precision – for example, even on targeted compartments within tissue or individual cells. Atomic Force Microscopy (AFM) (Gaub et al., 2019; Li et al., 2008; Spedden and Staii, 2013) and air-puff-based methods (Fleury et al., 2010; Kitamura and Häusser, 2011) are two such examples. Recently, an AFM-based approach was used to elucidate precise compartmental pressures required to generate sheer-stress induced opening of membrane channels in compartments of rat cortical neurons *in vitro* (Gaub et al., 2019). In the latter, carefully calibrated chambers deliver a gust of air to a sample. The velocity/pressure of the puff induces forces on the sample that result in analyzable deformations (Kling and Marcos, 2013; Kling et al., 2014; Kitamura and Häusser, 2011). Although less precise than AFM, air-puff based assays are commonly used to evaluate hyperalgesia in samples, both in research and clinical medicine (for example, diagnostic tonometry), primarily due to ease of use. Nonetheless, while these mechanical assays provide considerable physical insight into cellular structure and force regimes required to initiate cellular deformation, they are idealized experimental set-ups that do not

resemble natural conditions. If one is interested in studying behavioral/cellular responses under ecological conditions, different approaches need to be considered.

Assays imparting thermal stimuli have also been used extensively in the literature. Here, too, investigators have utilized, both, manual hand-held and more automated procedures to study organismal responses to thermal stimulation. In one commonly used example of the former, researchers deliver a thermal stimulus to samples using a modified metal thermal probe similar to a soldering iron (Deuis and Vetter, 2016; Chattopadhyay et al., 2012). Depending on the size of the probe, this type of assay can deliver focal stimuli within an approximately 500 µm X 500 µm localized region. Prior work has utilized this technique to study escape responses in *Drosophila* larva in response to thermal probes ranging from 23 °C to 65 °C directed at specific larval body segments (Oswald et al., 2011; Babcock et al., 2009; Tracey et al., 2003; Xu et al., 2006).

Infra-red-based laser assays are an alternative method that can be used to study thermal nociception (Ohyama et al., 2013; Terada et al., 2016). Due to the equipment and precision required, this type of assay has thus far been used for fillet preparations of *in vivo* samples or cultured *in vitro* cells. In these assays, samples are irradiated with long wavelength lasers (>800nm). Responses to this localized thermal stimulation can then be studied using patch-clamping or voltage/calcium imaging. For example, Terrada et al. used this technique to study differential responses in individual Class IV neurons by contrasting firing patters elicited in response to thermal versus other stimulus modalities (Onodera et al., 2017; Terada et al., 2016). Others have used similar set-ups to study behavioral responses to noxious thermal stimuli, and identified

characteristic escape sequences that comprised specific motions in *Drosophila* larvae – for example, bend-roll-escape crawl and bend-escape crawl (Ohyama et al., 2013). The use of thermal laser assays continues to be a very useful tool for studying somatosensation and nociception and has recently gained favor with investigators studying other model systems as well (Rodgers and Ryu, 2020; Ellström et al., 2019).

Chemically induced nociception has been studied in a range of organisms using exposure to varying concentrations of chemicals — for example, acids. Often, in these assays, researchers study behavioral responses following exposure to noxious chemicals, either in gaseous or liquid forms (HF et al., 2001; Lopez-Bellido et al., 2019; Im and Galko, 2012). Alternatively, samples can be exposed to the stimulus and then dissected for histological studies. A recent study proposed a new protocol for chemical nociception in *Drosophila* larvae using hydrochloric acid and analyzed behavioral and histopathological effects on the affected tissue (Lopez-Bellido et al., 2019). These studies offer the possibility for interesting comparisons between modality-specific behavioral and cellular responses in the future. However, it is worth noting that while such assays profess to emulate chemical stimuli organisms encounter in the wild, we derive greater value from such experiments as idealized set-ups through which we can probe cellular processes – not their ability to mimic ethologically realistic scenarios.

Finally, optical stimulation assays have become a mainstay in neuroscience due to the versatility of optogenetic actuators like channelrhodopsin and its counterparts (Fenno et al., 2011; Hegemann and Möglich, 2011). In these assays, organisms are genetically modified to express light-sensitive ion channels in neurons of interest. These neurons and their associated circuits can then be activated or inhibited via light

of specific wavelengths (Prigge et al., 2012; Honjo et al., 2012). Although the expression of these proteins is not in inherently noxious to organisms, this method has become relevant for studies on nociception because it can be used to study firing patterns and circuits underlying neurons that function in a nociceptive capacity. For example, optogenetic activation of Class IV neurons was used to identify neuronal pathways that mediate a number of escape behaviors in *Drosophila* larvae (Terada et al., 2016). The ever-improving millisecond-range temporal resolution and compatibility with modular expression systems (GAL4, LexA, etc) offered by such optogenetic techniques makes them well suited for a range of biological investigations, particularly in *Drosophila*.

Although these aforementioned assays provide a considerable number of options for studies on nociception, each of these techniques is accompanied with a number of drawbacks. These caveats manifest most often in trade-offs related to resolution, ease of experimental protocols, and similarity to natural conditions. For example, AFM- based assays offer high experimental precision and resolution, but are difficult to execute *in vivo* on live organisms. Similarly, optogenetic experiments of neurons, although procedurally straightforward, is a few degrees detached from natural stimuli that larvae encounter in the wild.

The best of all worlds – combining techniques to develop a new assay

For our study, we wanted to study nociception in individual Class IV neurons within the context of attacks from parasitic wasps. To do this, we sought to combine the best elements of the aforementioned techniques and develop a novel assay that is able to faithfully recreate puncture injuries. A number of considerations were

prioritized when we were conceptualizing this method: (i) we required control over the spatial/temporal properties of the stimulus. (ii) we required the ability to image individual Class IV neurons via confocal microscopy (iii) we required that the assay could be readily generalized to study other cell classes (iv) we required that experiments could be performed on whole-mount animals *in vivo* and (v) we required that the assay mimic ovipositor stings closely. Additionally, logistical considerations of compatibility with existing instrumentation in our laboratory were also important.

A laser-based technique offered the best combination of these desired features. We thus developed an assay that enabled tunable, highly localized stimulation of single neurons during calcium imaging on a confocal microscope set-up. Following, we present the properties of the assay, its ability to emulate ecological conditions, and important considerations for image processing during analysis. The development of this novel method laid the foundation for studies that we detail in subsequent chapters.

2.3 Results

Spatial and temporal features of our 405nm experimental set-up are tunable

To study nociceptive behavior in Class IV neurons during confocal imaging, we developed an assay using a 405nm laser to mimic focal stimuli to the larval cuticle similar to that of a wasp ovipositor (1- 15 μm diameter, tapering down to the tip) (Robertson et al., 2013; Hwang et al., 2007a) (Figure 2.1). Prior work has shown that short wavelength blue light is particularly noxious to *Drosophila*, thus making our choice of laser wavelength appropriate for studying larval nociception (Hori et al., 2014; Shibuya et al., 2018). The focus of the laser was calibrated, and the wattage and irradiance delivered to the sample was user-defined prior to each experiment. We use these tunable features of the stimulus in more detail later (Chapter 3).

Robust immobilization of larvae was required for imaging on our confocal microscope set-up (Figure 2.1A). This was accomplished by mechanically constraining the larva on a slide-bottom dish using a polydimethylsiloxane (PDMS) immobilization device (Mishra et al., 2014; Ghannad-Rezaie et al., 2012). The PDMS device was equipped with an internal cavity which was designed to accommodate larvae of a specific age/size. By applying suction using a syringe connected to the PDMS device through a hollow metal tube, we were able to physically constrain the larva (Figure 2.1B). Care was taken to ensure that larval samples were not over compressed or squashed during sample preparation. Once immobilized, larvae could be mounted on the imaging stage and imaged for ~30-45 mins without deleterious effects (12 out of 12, no fatalities). Experiments longer than 2 hours often resulted in a high larval fatality rate

(8 out of 12), likely due to suffocation or prolonged mechanical stress. For the bulk of our experiments, we illuminated larvae with 488nm to visualize GFP or GFP-tagged proteins (Figure 2.1C) for <45 mins. In addition, the 405 nm laser could be used to pulse individual Class IV cells at precise user-defined locations (Figure 2.1C, inset).

The wattage of our laser was tunable in our set-up. Using a manufacturer provided graphical user interface (Coherent, Palo Alto, CA), the wattage delivered to the sample could be defined in increments of 1% prior to each stimulation experiment. We measured the wattage output delivered through the microscope objectives at the sample plane using a watt-meter to ensure that increments in input %resulted in a corresponding linear increase in output wattage (also referred to as "Stimulus Intensity" or "Integrated Power") (Figure 2.2A). However, the total measured wattage values were lower than those listed on the company device specification sheet (for details of laser model, see *Materials and Methods*) due to loss of energy at mirror reflections required by our optical set up (Figure 2.1A). Nonetheless, this discrepancy was, minor and did not affect our intended purpose.

The spatial profile of our laser beam was also tunable. Using objective lenses of two different numerical apertures, we were able to create two different laser profiles: one with a tighter spatial profile (FWHM 0.5 µm) and another with a broad spatial profile (FWHM 1 µm) (Figure 2.2B) (See *Supplemental Calculations*). Importantly, the integrated power delivered in either case was the same. This effectively allowed us to modulate the irradiance of the stimulus (power per unit area) in our experiments by a factor of ~4X (Figure 2.2B, red vs blue), opening up an interesting avenue for investigations on somatosensory features in Class IV arbors.

To ensure acquired movies could be subsequently processed with ease, we synchronized the laser pulse with the camera image acquisition rate via a custom LabView macro. This effectively allowed us to limit exposure of the camera to the laser to only the precise number of frames that we intended. For example, in our typical experimental protocol, our camera exposure time was set to 100ms. Synchronization of the laser to the exposure time ensured that our 405 nm pulse could be delivered in multiples of 100ms. In most experiments, we opted for a 100ms pulse, which corresponded to only 1 frame (Figure 2.3A, B). Due to the ON-OFF dynamics of the system, activation of the laser shutter causes a transition lag-time that flanks the duration of the pulse (Figure 2.3C). This, however, did not affect our experiments as we were only interested in delivering a single, continuous pulse. These considerations are particularly important because, although the laser beam has a tightly focused profile, the gaussian tail of the beam results in saturation of the entire imaging field for the duration that the laser is on. Since our calcium indicator, GCaMP6f, is orders of magnitude less bright, this effectively results in loss of cellular signal for the frames that the laser is pulsed (see Figure 2.3A, f_s). In our protocol, we circumvent this caveat but utilizing pulses limited to 1-3 frames and dropping frames when the laser is active during image analysis. The resulting set of frames were then analyzed. In our system, we found that an exposure time of 100ms was sufficient to resolve initiation of calcium dynamics in Class IV neurons even after dropping the laser stimulus frame.

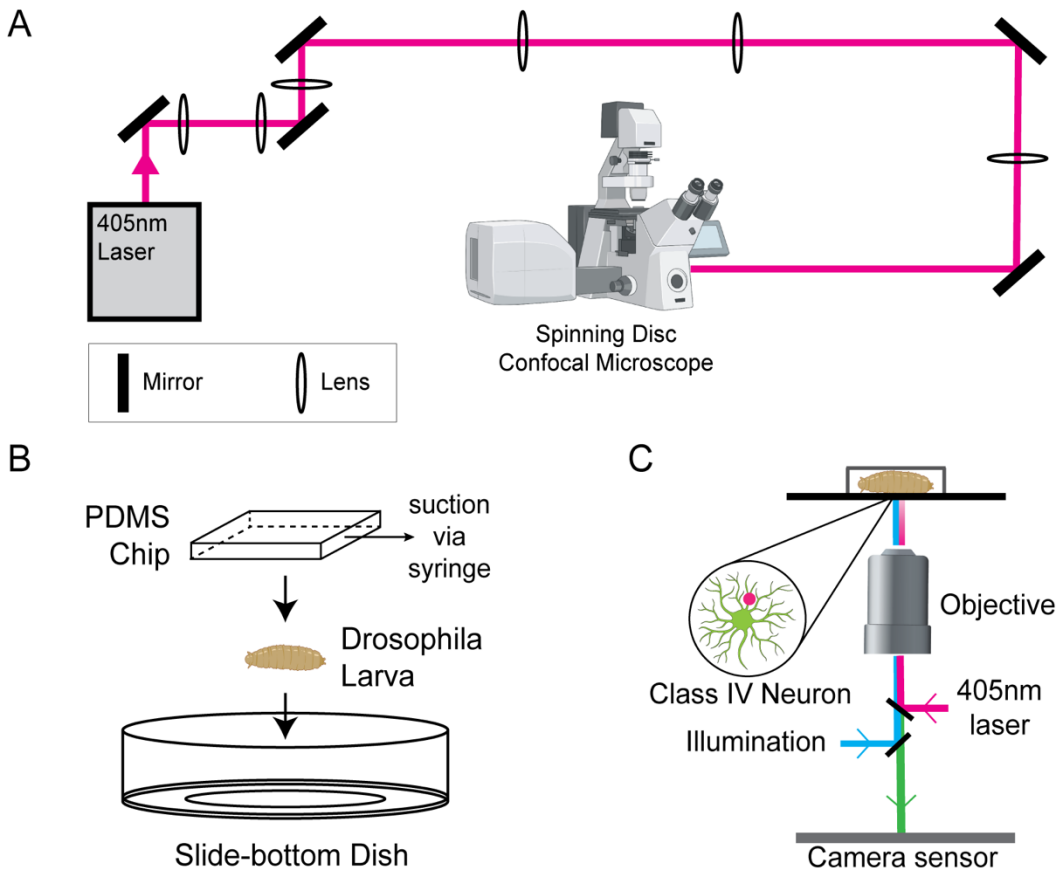

Figure 2.1: Imaging and sample-preparation set-up. (A) Schematic showing external laser and beamline on optical table to spinning disk confocal microscope. (B) Larval immobilization protocol. Immobilization device made out of Polydimethylsiloxane (PDMS) is used to constrain larval sample via mechanical pressure. PDMS device has a small internal cavity (not shown), which allows the larva to be immobilized without being excessively compressed. Suction is applied to the PDMS device via a syringe (not shown) to adhere the device to the slide bottom dish. (C) Schematic diagram depicting imaging set up and experimental protocol for imaging and stimulation. Inset shows cartoon of Class IV neuron being stimulated (magenta dot) on a proximal dendritic arbor. Location of laser stimulus is user-defined.

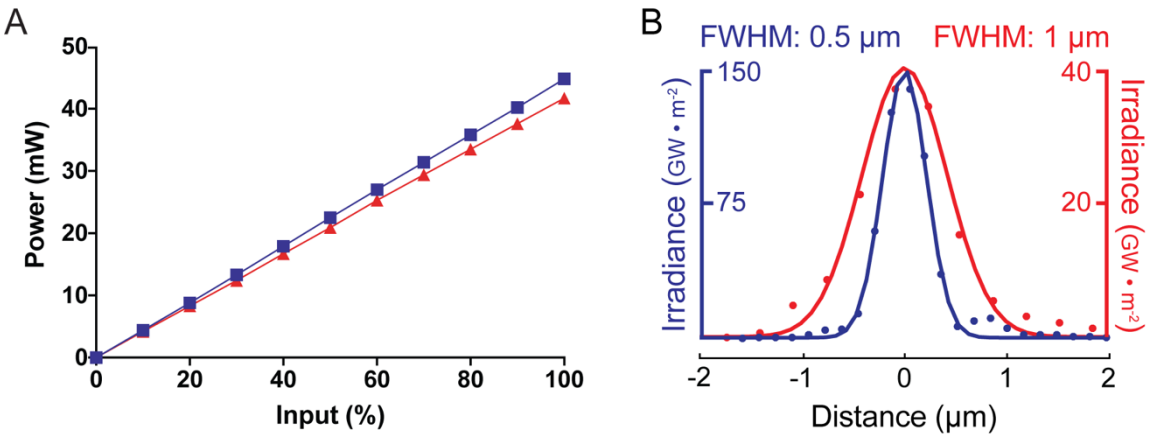

Figure 2.2: Physical parameters of 405nm laser stimulus. (A) Measured power output (mW) across various input values (%) from 405nm stimulus (through both 40X and 20X objective lenses) at the sample plane. Measurements were made using a microscope slide power sensor (S170C, Thor Labs) and a Touchscreen Optical Power and Energy Meter Console (PM400, Thor Labs) at the sample plane. Three different measurements were taken. (B) Line scans of spatial profiles of 405nm stimulus at two different irradiance settings – spatial profile of the laser at the sample plane through the 40X objective (FWHM: 0.5 µm, blue) and 20X objective (FWHM: 1 µm, red). Dots represent average values for n = 3 measurements, and lines represent a gaussian fit. Profile of the beam is radially symmetric (data not shown).

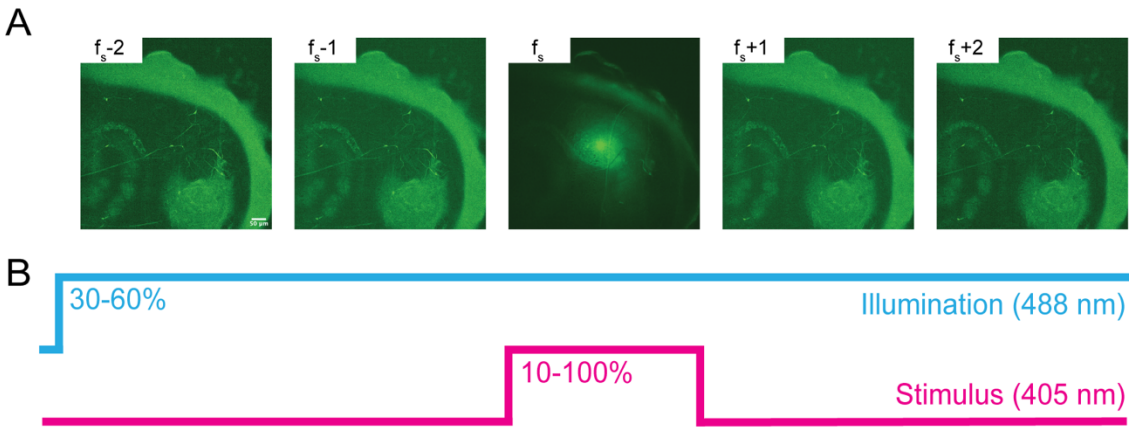

C

Camera	Transition	Exposure	Transition	Dead
	24.58 msec	75.43 msec	24.58 msec	-
TTL Signal	Low	High	Low	Low
Illumination				
Cycle Time	124.59 msec			

Figure 2.3: Temporal dynamics of laser stimulation. (A) Laser activation is synchronized with camera imaging rate. f_s denotes the frame when the laser was pulsed. Montage taken from stimulation experiment showing two frames prior to stimulation and two frames after stimulation. (B) Schematic diagram showing activation of illumination wavelength (488 nm, blue) and laser (405 nm, magenta) corresponding to montage frames in (A). (C) Laser ON- OFF dynamics. Opening/closing of the shutter causes a transition lag-time that flanks the duration of the pulse.

405nm stimulation emulates puncture wounds to the larval cuticle

After calibrating our set-up, we studied the effect of our 405nm on the larval body to ensure that our assay was simulating intended conditions – that is, highly localized stimulation akin to an insect stinger. Laser powers ≥ 80% (40mW, Figure 2.2A) induced visible puncture wounds, mimicking the insertion of an ovipositor clip into the larval cuticle (Figure 2.4A). The surrounding tissue also showed melanotic spots ~10 minutes after stimulation, which is an accompanying feature of mechanical penetration of larval tissue (200 ms exposure) (Figure 2.4B) (Galko and Krasnow, 2004).

We were also able to visualize the puncture wounds when Class IV cells expressing CD4-td-GFP were imaged via confocal microscopy (Figure 2.4C, D). Figure 2.4D shows a zoom-in of a Class IV neuron with the pulsed region highlighted by a magenta circle. Analysis of puncture injuries revealed that the diameters of the wounds were comparable to those caused by the insertion of the tip a wasp ovipositor (1-15 µm diameter), ranging between 2.8 – 3.5 µm. (Robertson et al., 2013) (Figure 2.4E, F). Varying the wattage allowed us to alter the puncture severity. Higher wattages resulted in deeper and wider wounds, whereas lower wattages emulated gentler stimulation. This allowed us to simulate conditions published in the literature where authors studied larval responses to penetration by an ovipositor to varying depths (Robertson et al., 2013). Analysis of the intensity profile at the puncture site showed that 405 nm stimulation resulted in complete loss of fluorescence – including the typical body autofluorescence – in the central region of the cut due to the absence of tissue (Fig 2.4 C-F).

There was a concern, however, that the observed lack of fluorescence was the result of highly localized photo-bleaching of the reporter tag, rather than an actual puncture wound. To test this, we performed a series of experiments where Class IV cells expressing a GFP construct (CD4-td-GFP) were stimulated, imaged and then re-imaged several minutes after stimulation. We hypothesized that if, in fact, the laser was causing only photobleaching, we would expect to see the bleached region recover within 10-20 minutes. However, if there was a puncture hole, the wound would be visible long after stimulation. To account for the possibility that both scenarios – photobleaching and puncture wounds – are possible depending on the integrated power of the light, we stimulated cells across a range of wattages and reimaged the same cells 20 minutes after stimulation.

Per our expectations, we found that low wattage stimulation (<50 %) caused localized photobleaching on the affected neuronal process. This was evident based on comparisons of the cellular region preceding and immediately following stimulation (Figure 2.5A, B). The inflicted site on the dendritic processes showed a highly localized dark spot as a result of photobleaching. However, the affected region showed full recovery when imaged 20 minutes after stimulation (Figure 2.5A, B). This suggested that low-wattage stimulation did not result breakage of the process or measurable punctures (Figure 2.5A, B). We found this to be the case across all cells stimulated at 10%, 20% and 40% input power.

However, when cells were stimulated with high wattage (>80%), we found that the 405 nm laser was able to definitively inflict puncture wounds a majority of the time. This was evidenced by the presence of a circular wound at the stimulation site that

persisted >20 minutes following stimulation (Figure 2.5C, D). Interestingly, the increased magnitude of the stimulus also caused observable cellular degradation of nearby processes which we did not see when cells were pulsed at lower wattages. We subsequently investigated the long-term impact of these injury wounds (Chapter 4).

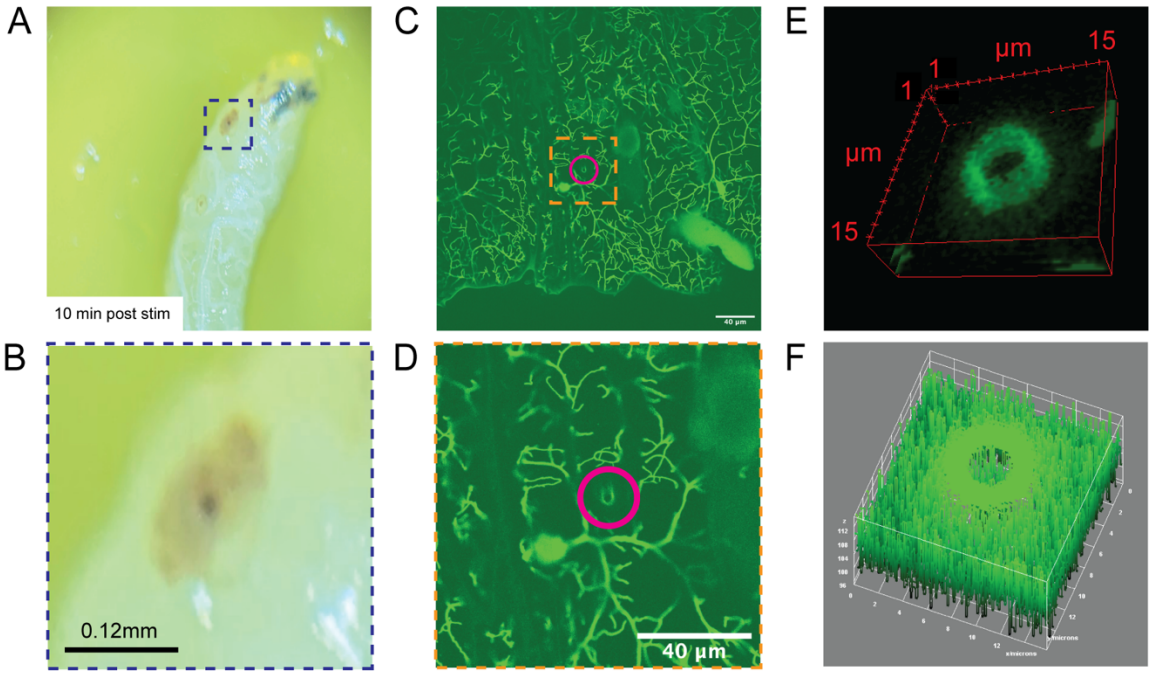

Figure 2.4: 405 nm pulse induces puncture wounds to larval cuticle. (A) Larval sample 10 minutes post-stimulation (200 msec | 405nm laser exposure) imaged through a dissection microscope. (B) Blow-up of region highlighted with dashed blue box in (A) showing the puncture wound (center), surrounded by a melanotic region. (C) Image of Class IV dendritic arbor expressing CD4-td-GFP in third instar larva (~70 hr AEL) pulsed with 405 nm laser (200 msec exposure). Magenta circle highlights region where 405nm laser was focused. (D) Zoom-in of dashed orange box shown in (C) showing puncture wound inflicted by 405nm laser. (E) 3-D collated confocal z-stack of sample in panel (C, D) showing depth of puncture wound (3-5 μm). (F) Intensity profile of central section (z-stack) shown in panel E highlighting no fluorescence in central region of puncture site.

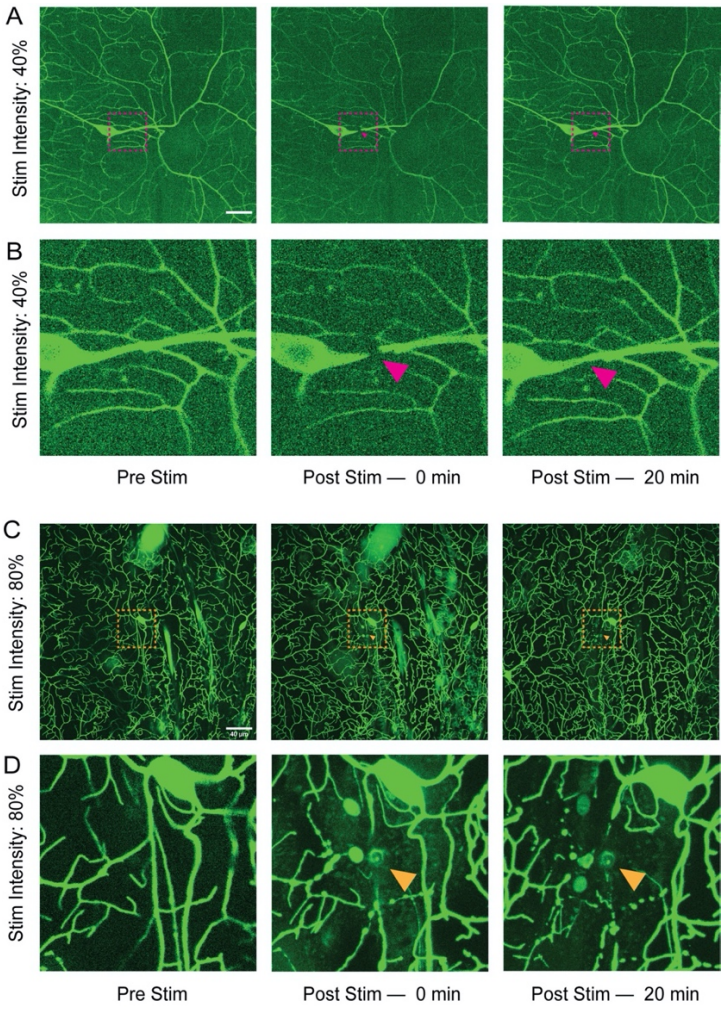

Figure 2.5: 405 nm stimulation causes bleaching versus cutting of dendritic processes depending on the wattage delivered. Panels shown are pre-stim (left), frame immediately following stimulation (center), and 20 minutes post -stimulation (right). (A) Montage of Class IV da neurons expressing CD4-td-GFP stimulated with 405 nm laser at 40% power. (B) Zoom-in of region indicated by the dashed magenta box shown in panel (A). Magenta arrow indicates region where laser was focused. Central panel shows localized bleaching of dendritic process; right panel shows same region after recovery (20 minutes post stimulation). (C) Montage of Class IV da neurons expressing CD4-td-GFP stimulated with 405 nm laser at 80% power. (D) Zoom-in of region indicated by the dashed magenta box shown in (C). Orange arrow highlights region where laser was focused. Central and right panels show puncture wound that does not recover (not photobleaching) 20 minutes post stimulation.

Observed puncture wounds are not the result of fluorophore-assisted cutting

To proceed with the intended purpose of our laser assay, we also had to ensure that expression of the reporter construct itself was not mediating cellular damage. That is, we had to confirm that our observed laser-induced puncture wounds were independent of the expression of GFP or the calcium indicator GCaMP. This is an important consideration because it has been suggested that expression of reporter constructs can aid in cellular damage via fluorophore-induced cutting.

To test this, we pulsed wild-type larvae at high intensities for a range of durations to see if we could impart focal puncture injuries even in the absence of reporter fluorophores. In the absence of reporter fluorescence, we relied on autofluorescence as a means to visualize the larval body. As cells show more robust autofluorescence at 405-408nm wavelengths, we utilized a widefield 405nm illumination – distinct from our focal 405 nm stimulation laser – to image the sample before and after a pulse. Using this method, we analyzed the puncture wounds 10 minutes after the pulse to understand the effect of our laser stimulus on the larval body.

Indeed, we confirmed that the injuries imparted by the 405nm stimulus were independent of any reporter constructs. Cuticles of wild-type larvae without reporters pulsed with our 405nm assay for 100 - 500 msec showed unmistakable puncture wounds 3-5μm (Figure 2.6A, B, D, E). To confirm this further, we plotted the fluorescence intensity at the puncture site 10 minutes after stimulation and confirmed the presence of a hole in the larval body via lack of fluorescence that persisted 20 minutes after stimulation (Figure 2.6C, F). Interestingly, we also observed that the region immediately surrounding the puncture site showed higher autofluorescence

after stimulation (Figure 2.6 B, E, insets). This was likely due to autofluorescence of aggregated tissue resulting from the localized puncture wound. Interestingly, imaging at widefield 405nm also demonstrated how regions radially surrounding the puncture site were bleached by the stimulus, demonstrating that small quantities of the 405nm laser are sufficient to cause photobleaching. Together, these experiments confirmed that our observed puncture wounds are not the result of fluorophore-assisted cutting.

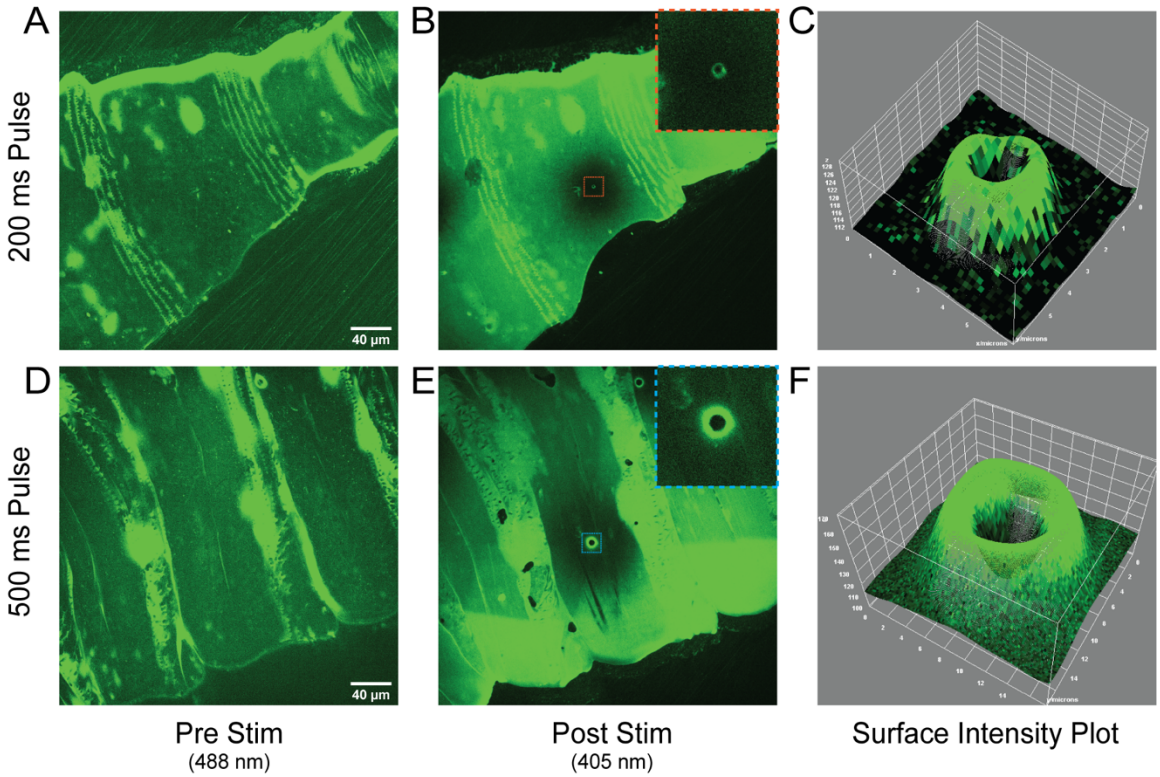

Figure 2.6: 405 nm stimulation-induced puncture wounds are not a result of fluorophore-assisted cutting. (A) Larva 70 hours AEL before stimulation imaged with 488 nm illumination. (B) Larva from panel (A) post stimulation with 405 nm laser (200 ms pulse), imaged with 405 nm widefield illumination 20 minutes post stimulation. Inset (top right) shown zoom-in of puncture wound region highlighted by orange dashed box. (C) Intensity profile of puncture region from inset in panel B 10 minutes after stimulation. (D) Larva 70 hours AEL before stimulation imaged with 488 nm illumination. (E) Larva from panel (D) post stimulation with 405 nm laser (500 ms pulse), imaged with 405 nm widefield illumination. Inset (top right) shown zoom-in of puncture wound region highlighted by blue dashed box. (F) Intensity profile of puncture region from inset in panel E 10 minutes after stimulation.

405nm stimulation triggers behavioral & cellular nociceptive responses *in vivo*

To test if our 405nm stimulus could initiate nociceptive responses in larvae, we probed individual Class IV neurons *in vivo* on whole mount immobilized larvae without the use of any anesthetics or sedatives. We then irradiated individual Class IV neurons and observed their overall behavioral responses while also studying responses at the single cell level using calcium imaging.

Constrained larvae pulsed with the 405-nm laser at ≥80% power for 0.1 s exhibited behavioral responses that manifest as tissue movements, including muscle twitching, writhing, crawling, and turning (Figure 2.7A). These behavioral responses were initiated immediately following stimulation and lasted between 1-30 seconds (Figure 2.7 A, B, D). We hypothesized that increased wattage would result in most robust responses. To test this, we stimulated larva with increasing wattage ranging from 20%to 80% in increments of 20%. Movement responses were indeed accentuated with increasing wattage, particularly at 80% and above (Figure 2.7B).

It was also important that our stimulation assay was not fatal to larvae upon delivery. To test if our stimulation assay was lethal, we quantified the survivability of samples 24 hours after stimulation: larvae were pulsed once under aforementioned imaged conditions and recovered. The same larvae were imaged 24 hours later. 100% of stimulated larvae (6 out of 6) were alive and crawling, confirming that our assay was non-lethal.

Direct stimulation of Class IV cells was also accompanied by large calcium transients in the dendritic arbors, which we observed through fluorescence changes in the genetically encoded calcium indicator GCaMP6f. These global calcium transients,

which have been shown to accompany activation/firing in neurons (Terada et al., 2016; Ali and Kwan, 2019; Higley and Sabatini, 2008; Sabatini et al., 2001), were further evidence of nociceptive responses triggered in response to stimulation. To study responses throughout individual Class IV neurons, we considered seven regions of interest (ROIs) sampling the entire dendritic tree: 4 ROIs on dendrites (magenta and blue), 2 ROIs on the axon (green) and 1 ROI on the soma (black) (Figure 2.7C). We then used the normalized fluorescence values (ΔF/F) in each ROI to quantify the magnitude and temporal dynamics of cellular responses (Figure 2.7D, *See Materials and Methods*). This subsequently allowed us to investigate differential responses in individual regions within the same dendritic arbor. We explore this more in Chapter 3.

Spontaneous calcium signaling events, however, have also been reported in Class IV neurons (Kanamori et al., 2013). Thus, we had to devise a protocol to distinguish these spontaneous calcium transients from those evoked by our stimulus. To do this, we developed a criterion during image processing wherein a cell was be deemed responsive only if the normalized fluorescence value of any cellular region of interest post stimulation exceeded five standard deviations above the baseline fluorescence level, $F_{o,}$, measured for at least 10 seconds prior to stimulation (*See Materials and Methods*). This stringent criterion ensured that we would not accidentally mistake a spontaneous calcium transient for an evoked calcium signal.

Thus, our focused 405-nm laser stimulus is a non-lethal nociceptive stimulus that mimics cuticle penetration by an ovipositor, producing both behavioral and cellular responses while offering high spatio-temporal control (intensity, geometry, duration).

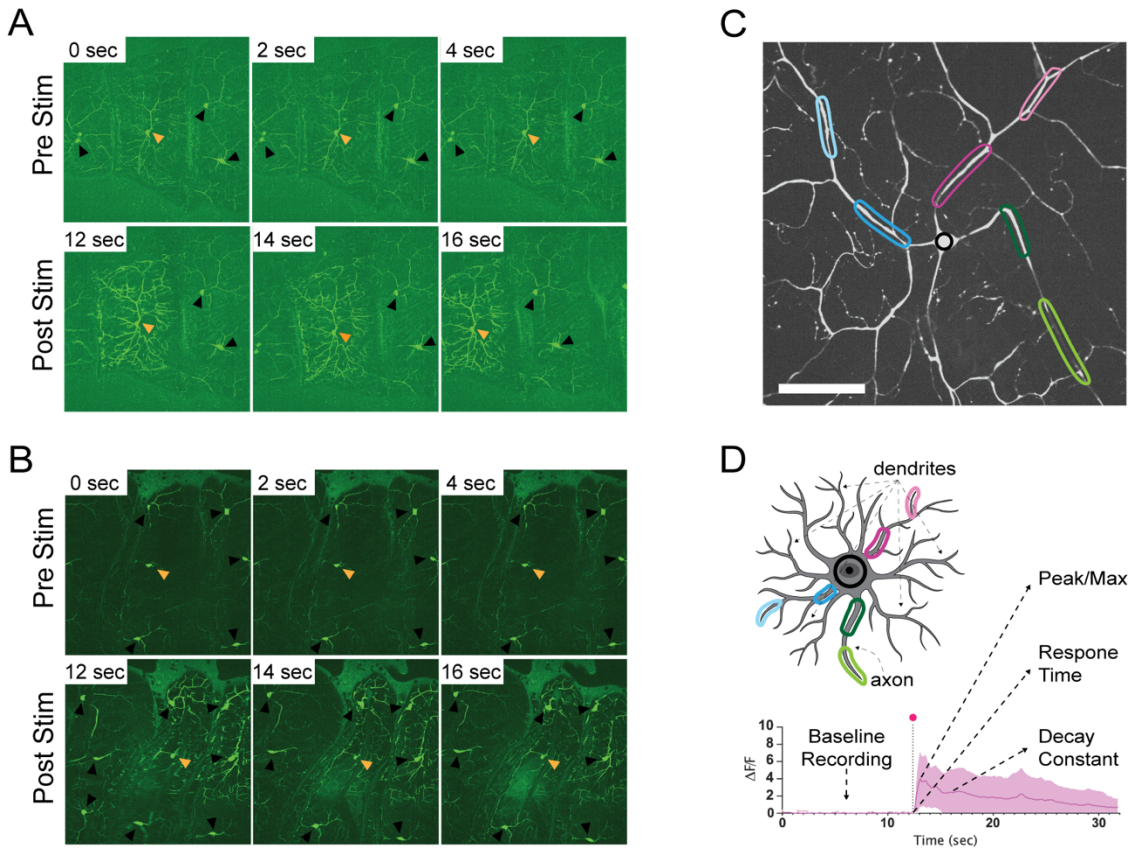

Figure 2.7: Focused 405 nm stimulation of *Drosophila* larvae triggers nociceptive behavioral responses and cellular calcium signaling events in Class IV neurons. Orange arrow head indicates stimulated cell. Black arrow heads indicate cell bodies of neighboring Class IV neurons to highlight movement of larvae post-stimulation. (A) Montage depicting behavioral and cellular response to 405 nm stimulation (40% power) in larvae expressing UAS-GCaMP6f. (B) Montage depicting behavioral and cellular response to 405 nm stimulation (80% power). (C) Image of Class IV neuron depicting seven regions of interest (ROI) sampled throughout the dendritic arbor for analysis. 4 on dendrites (magenta and blue), 2 on axon (green) and 1 on soma (black). ROIs are color coded to be darker for proximal ROIs and lighter for distal ROIs. Scale bar is 50 μm. (D) Schematic of Class IV neuron (top left) showing 7 ROIs and an example processed fluorescence trace (bottom).

Minimization of image background noise is necessary for accurate analysis of cellular calcium signaling events

During our tests, we observed that the magnitude of evoked calcium transients varied considerably from one experiment to another. While low-wattage irradiation caused small calcium transients, higher wattages resulted in large calcium transients (Figure 2.7). When analyzing these calcium transients using our protocol, we noticed that smaller calcium events were often being overlooked via our code. However, these same events were often visible to the naked eye. We thus hypothesized that our protocol for region of interest (ROI) selection was the cause of these discrepancies.

To test this, we studied a group of cells pulsed at low wattage (40% 405 nm) and plotted the ΔF/F traces of dendrites using two different ROI selection protocols. First, we drew a rectangular region around the process of interest while also including some neighboring regions of the cellular body. Then, we took the same process and drew an ROI that was carefully contoured to the shape of the process (Figure 2.8A).

As expected, the corresponding ΔF/F traces show that contouring of the dendritic process results in a larger signal magnitude (Figure 2.8B). This is because each ROI exports the mean fluorescence values in each frame for all pixels within its boundaries; increased background area encompassed within the larger ROI artificially depresses the average signal value. This effect becomes increasingly prominent when studying processes with calcium signaling events of smaller magnitude – our analysis script was missing these events since the Peak ΔF/F magnitude did not exceed our set threshold for a response (*See Materials and Methods*). Distal dendritic spines, which

are typically thinner, are also susceptible to the same problem. In light of this, we adopted the more tedious method of carefully contouring ROIs to the dendritic segment being studied as standard protocol for subsequent investigations of calcium signaling in Class IV neurons.

However, this, in turn, introduced new challenges during image analysis. Specifically, smaller traces from contoured ROIs were far more susceptible to movement artifacts since even minor muscle twitches could completely or partially remove the process being considered outside the ROI boundaries (as can be seen in Figure 2.8B; red and purple traces fluctuate more than the yellow and blue traces). Such scenarios are particularly problematic since accurate measurement of the baseline fluorescence, peak response magnitude, and response time require clean curves, and the abrupt removal/introduction of the cellular region of interest from the ROI boundaries results in jagged, artifact-filled traces.

To address this problem, we utilized Fiji stabilization plug-ins, Image Stabilizer and Template Matching, whenever we observed the presence of movement artifacts. Although these computationally expensive procedures necessarily increased the image processing and analysis time by over 5-10 X, the resulting traces allowed us to quantitively measure even calcium signaling events of small magnitude with a high degree of certainty.

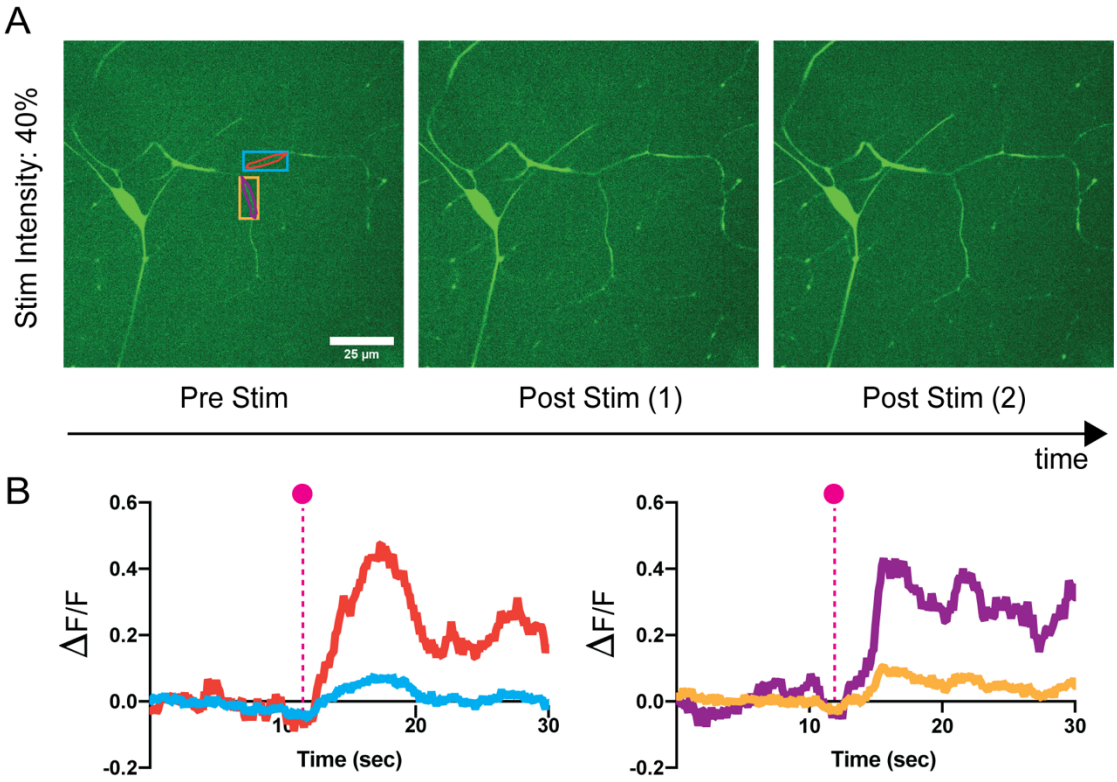

Figure 2.8: ROI dimensions are important for capturing smaller calcium signaling events. (A) Montage depicting Class IV neuron expressing UAS-GCaMP6f stimulated with 405 nm at 40% power. Colored shapes indicate user-defined ROIs along two dendritic arbors. Blue and yellow ROIs are larger; orange and purple ROIs have been carefully contoured to only encompass the dendritic process. (B) Micrographs showing ΔF/F magnitudes for each of the ROIs (color-coded as in panel A). Magenta dashed line/dot indicate timepoint when 405 nm stimulus was administered. Note that each set of ROIs (panel A) and their corresponding traces (panel B) are for the same region along the dendritic process.

2.4 Discussion

Prior work has utilized a range of stimuli to study nociceptive responses in Class IV neurons, including IR radiation, acids, and mechanical pressure. However, each of these techniques are accompanied with caveats on their experimental precision and ability to faithfully recapitulate ethological conditions. Here we have developed a non-lethal, tunable, *in vivo* assay for larval nociception using a 405 nm laser that causes puncture wounds to the larval cuticle similar to a wasp ovipositor. Calibration of the laser spot size allowed us to elicit wounds of similar shape and size to an ovipositor, and modulating the wattage and exposure time allowed us to emulate stings of varying depths and width. Using this system, we characterized sensory properties of Class IV neurons in whole-mount *Drosophila* larvae with a spatial resolution of 0.1615 μm (40X), 0.3225 μm (20X), and a 100 ms temporal resolution.

An important feature of our set-up is that our studies were performed on whole-mount larvae. This was accomplished by making minor modifications to a long-term imaging protocol published in the literature (Ghannad-Rezaie et al., 2012). Notably, this protocol enables sufficient immobilization of whole-mount larval samples without the use of any anesthetics or sedatives to allow for confocal imaging in a single z-plane for ~30-45 mins, if external factors (i.e., temperature at the microscope objective space, microscope z-drift) are controlled. Despite the many challenges that accompanied these *in vivo* experiments – for example, larval twitching during imaging – this set-up conferred us many scientific advantages. First, the use of anesthetics like di-ethyl ether or FlyNap (Carolina Biological Supply Company | 50% Triethylamine, 25% Fragrance

(Neutralizer), 22.63% Ethanol, 1.25% 2-Propanol, 1.13% Methanol) is often accompanied by aberrant cellular blebbing and/or degradation (data not shown). Controlling for this is paramount to our experiments as Class IV neurons localize close to the epidermis, and as such would be one of the first to be affected by any such changes. Secondly, the use of anesthetics and sedatives would have prevented us from visualizing behavioral responses that often accompany nociceptive stimulation. Furthermore, if nociceptive responses require fast coordination with other components of the central and/or peripheral nervous systems, the use of sedatives would have precluded us from capturing those details meaningfully.

The tunability of our assay is a critical strength that will enable diverse range of investigations in the future. The portability of the laser generation unit (Coherent, Palo Alto, CA) allows us to switch to utilize higher power units or alternative wavelengths via a simple plug and play mechanism. In addition, the ability to generate different spot-sizes via objective lenses of varying numerical aperture offers added versatility. It is also possible to modify the spot-size of the laser without the use of objectives via direct calibration of the laser beam-line mirrors, though this is more technically challenging.

Our approach, however, does have its own drawbacks. While a wasp ovipositor punctures via mechanical pressure, our laser is likely damaging the cuticle via highly localized heating of magnitude similar to an optical trap (Peterman et al., 2003), thus complicating comparisons. Additionally, scattered light from our optical stimulus on the surrounding tissue may also play a role in activating cellular photoreceptors via creation of reactive oxygen species (Lockwood et al., 2005). Still, in our investigations, we found that our stimulus generated behavioral responses and measurable lesions that

are similar to those caused by mechanical oviposition. Importantly, our stimulus caused highly localized physical breakage of cellular tissue and melanotic spots, which are hallmarks of mechanical penetration, and recognized differentiating factors when compared with other types of noxious stimuli (Tracey, 2017). Thus, despite the acknowledged drawbacks, our assay is a valuable addition to the arsenal of stimuli used in the literature and provides insight into cellular nociceptive responses.

Another downside of our experimental protocol was that our set-up is ill-suited for detailed analysis of whole-animal behavioral responses. Two main factors contribute to this. Firstly, the usage of 20 X and 40 X objective lenses on second instar larvae (~60-70 hours AEL) provide a view of only a fraction of the larval body. This prevents us from analyzing whole-body movements in larval samples. Secondly, since larvae are mechanically fastened during imaging, we are introducing constraints that directly affect the observation behavioral responses. Nonetheless, minor muscle twitching and contractions within the segments being imaged were often visible during imaging. Although we did not perform quantitation of these responses, modifications to the immobilization protocol may enable robust behavioral studies in the future.

Cumulatively, we developed a novel, tunable, focal optical assay that combines many of the most desirable features of existing nociception assays. We studied the effect of the local optical stimulation on larval samples and were able to reproducibly trigger behavioral and single cell responses *in vivo*. We also developed an image processing and image analysis protocol for quantitative characterization of calcium signaling events in individual neuronal compartments of Class IV neurons.

2.5 Materials and Methods

Live-cell Confocal Imaging. Larvae were timed and selected 68-72 hours AEL for imaging. Prior to imaging, larvae were washed in distilled water and gently rolled on a glass slide with a paintbrush to remove excess food and debris. Larvae were then placed on a Cellvis 35mm glass bottom dish (D35-20-1.5-N) and allowed to acclimatize for 60 seconds. Larvae were then immobilized using a single-layer PDMS device using a protocol as previously described (Mishra et al., 2014). Briefly, larvae were positioned on the center of the dish and gently constrained inside the PDMS cavity. The PDMS device was then adhered to the dish by applying slight suction using a 30ml syringe. No anesthetic was used. Samples were then mounted on the microscope stage, illuminated with Nikon lasers (488nm or 561nm at 30-50% laser power) and imaged at 8-10 Hz on a spinning disk microscope: Yokogawa CSU-W1 disk (pinhole size 50 µm) built on a fully automated Nikon TI inverted microscope with perfect focus system, an sCMOS camera (Zyla 4.2 plus sCMOS), and Nikon Elements software with either a 40X (1.25 NA, 0.1615 micron pixel size) or 20X (0.50 NA, 0.3225 micron pixel size). The temperature of the sample region was maintained using an objective space heater at 25°C. Samples were manually focused for each cell prior to image acquisition. No more than 3 cells were imaged from an individual larval sample. All data sets represent cells from at least four independent larval samples.

405nm Stimulation. Stimulation of Class IV da neurons was performed using a 405 nm laser (OBIS 405 nm LX 100 mW, Coherent, Santa Clara, CA) which was connected

to the microscope through an empty port. Wattage values of the laser were measured using a microscope slide power sensor (Thor Labs, Newton, NJ) at the sample plane. Activation of the laser was synchronized to the imaging rate using a custom LabView macro. The stimulus duration was then specified using the Triggered Illumination feature in NIS Elements (Nikon). Stimulus wattage was user-defined before each experiment (0-100%, 0-45 mW, Figure 2.2A) and administered for 100 – 500 ms. The precise location of the laser was calibrated using a custom graticule set in NIS Elements (Nikon) and tested prior to each experiment. For images targeting the soma, the laser was focused on the center of the cell body. Proximal dendrites were stimulated along a main branch 10-30 µm from the cell body. For distal branches, stimulus was administered to a branch 150-200 µm from the soma. Stimulation experiments were performed over 30-45 seconds wherein the stimulus was administered after 10-12 seconds of initial baseline recording for each cell.

Image Processing. Movies were analyzed using ImageJ (NIH). When necessary, movies were stabilized using the Template-Matching or Image Stabilizer plug-ins. For each cell, several regions of interest (ROI) were manually selected for each cell from 7 different locations along the entire dendritic tree to study any differential responses within the same cell: soma (1 ROI), axon (2 ROIs), dendritic arbors (4 ROIs). Care was taken minimize background by contouring the ROI region to encompass only the cellular region being considered. Corresponding fluorescence values for each ROI were extracted in Image J and imported into MATLAB (Mathworks). Baseline

fluorescence F_0 was calculated as the mean fluorescence for all frames before laser stimulation. The change in the fluorescence values from baseline was calculated as $\frac{F-F_0}{F_0-100}$ where 100 is the measured camera offset in our system. The time series data was then cleaned by applying a median filter (width 7) to remove outliers resulting from noise or movement. Data points were subsequently linearly interpolated between known values to generate a smooth curve before analysis (peak magnitude, response time, etc).

Calcium Imaging Response Criteria. The mean fluorescence value for all timepoints prior to the stimulus was designated as F_0. ROIs were scored as being responsive to the stimulus if the ΔF/F at any frame after stimulation was greater than 5 standard deviations above the baseline F_0. The largest ΔF/F value for all frames post stimulation was determined to be Peak ΔF/F. The first timepoint when ΔF/F was equal to or greater than 5 standard deviations above F_0 was scored as the Rise Rime (also referred to as Response Time or Latency).

2.6 Supplementary Materials

Theoretical calculation of laser spot-size through the objective lens

We recall that:

$$Magnification = \frac{Focal\ Length\ of\ Tube\ Lens}{Focal\ Length\ of\ Objective\ Lens}$$

$$Diameter\ of\ Back\ Focal\ Plane = 2 * Focal\ Length\ of\ Objective * Numerical\ Aperture$$

$$Spot\ Size\ of\ Laser\ = \frac{1.22 * Wavelength}{Numerical\ Aperture}$$

For our 40X water-immersion (WI) Objective (Numerical Aperture = 1.25), with 100% of back focal plane of the objective lens filled by the light:

$$Magnification = \frac{Focal\ Length\ of\ Tube\ Lens}{Focal\ Length\ of\ Objective\ Lens} = 40 = \frac{200mm}{f}$$

$$Focal\ Length\ of\ Objective\ Lens = \mathbf{5}\boldsymbol{mm}$$

The diameter of the back focal plane can be computed as:

$$d = 2 * Focal\ Length\ of\ Objective * Numerical\ Aperture$$

$$= 2 * 5 * 1.25 = \mathbf{12.5}\ \boldsymbol{mm}$$

$$Spot\ Size\ of\ Laser\ = \frac{1.22 * Wavelength}{Numerical\ Aperture} = \frac{1.22 * 405\ nm}{1.25} = \mathbf{395.28}\ \boldsymbol{nm}$$

For the 20X Air Objective (Numerical Aperture = 0.50), with 100% of back focal plane of the objective lens filled by the light:

$$Magnification = \frac{Focal\ Length\ of\ Tube\ Lens}{Focal\ Length\ of\ Objective\ Lens} = 20 = \frac{200mm}{f}$$

$$Focal\ Length\ of\ Objective\ Lens = \mathbf{10}\boldsymbol{mm}$$

The diameter of the back focal plane can be computed as:

$$d = 2 * Focal\ Length\ of\ Objective * Numerical\ Aperture$$

$$= 2 * 10 * 0.5 = \mathbf{10}\ \boldsymbol{mm}$$

$$Spot\ Size\ of\ Laser\ = \frac{1.22 * Wavelength}{Numerical\ Aperture} = \frac{1.22 * 405\ nm}{0.5}\ = \mathbf{988.2}\ \boldsymbol{nm}$$

2.7 Research Contributions

Dr. Mohammed Mahamdeh was instrumental in building the confocal microscope and optical set-up used for these experiments. Dr. Sean Christie (MVI) and Dr. Veikko Geyer were key players in helping transport the microscope set-up when our laboratory was relocating. Thank you to Dr. Maijia Liao for spearheading ongoing maintenance of the confocal microscope.

An experiment is a question which science poses to Nature
and a measurement is the recording of Nature's answer.

–Max Planck (1858 -1947)

Chapter 3:
Characterization of Somatosensory Properties in Dendritic Arbors of Class IV Neurons

3.1 Abstract

Using the laser assay described in Chapter 2, we studied somatosensory properties of individual Class IV neurons. We probed individual cells at varying magnitudes, irradiances, and characterized their responses using calcium imaging. We report the presence of two distinct signaling pathways: axonal and dendritic. The "non-contact" axonal pathway displays fast response times, high sensitivity, and is activated with or without direct stimulation of the dendritic arbor. In contrast, the slow and less sensitive "contact" dendritic pathway is activated only by direct contact with dendritic processes. Our mathematical model explains the observed dendritic calcium signaling magnitudes by considering physical and geometric properties of the stimulus and dendrites. Furthermore, analysis of cellular response magnitudes reveal that entire arbors of class IV neurons can differentiate stimuli of varying magnitudes and irradiance with uniform sensitivity. Taken together, our *in vivo* data provide novel insight into somatosensory properties of Class IV dendritic arbors.

3.2 Introduction

Class IV cells have elaborately branched dendritic arbors that tile the entire larval body wall in a dense meshwork (Ganguly et al., 2016). These neurons, which resemble mammalian purkinje cells, have been specifically implicated in noxious touch sensation (Tracey et al., 2003; Zhong et al., 2010). Silencing of Class IV neurons alone results in complete loss of larval ability to perform critical rolling defensive behaviors in response to noxious stimuli (Hwang et al., 2007a). A number of papers have also shown that Class IV neurons are polymodal cells capable of thermal nociception (Tracey et al., 2003; Babcock et al., 2009; Terada et al., 2016), chemical nociception (Lopez-Bellido et al., 2019) and optical nociception (Xiang et al., 2010; Yamanaka et al., 2013) by encoding distinct firing patterns in response to stimuli (Terada et al., 2016) . Identification of specific ion channels that mediate corresponding sensory transduction pathways has provided further color to the mechanistic details underpinning Class IV nociception (Babcock et al., 2011a; Tracey et al., 2003; Xu et al., 2006; Sokabe et al., 2008; Smith et al., 1996; Yan et al., 2012; Zhong et al., 2010; Kim et al., 2012; Hardie and Minke, 1992; Guo et al., 2014; Neely et al., 2011). However, while these studies provide considerable molecular insight, the macroscopic receptive properties of Class IV arbors as sensors remain an open question for investigation. Viewed from a physical perspective, nociceptors are effectively sensors that have been evolutionary optimized to detect specific inputs. Like sensors on a camera, the physical properties of these cells dictate the extent to which they can discern and react to stimuli. In this section, we investigate those features in detail.

It is accepted that different neuronal compartments play different roles within the context of cellular function (Jan and Jan, 2001). Dendrites are canonically accepted as cellular "antennae" that receive information via synapses; axons typically transmit information outward. However, in the context of nociception, it is unclear if the various cellular compartments share similar response properties to varying stimuli. A recent study demonstrated that compartments of rat cortical neurons have different capacities to discern stimuli of varying magnitudes *in vitro* (Gaub et al., 2019). It is not known if these findings generalize to other neuron classes *in vivo*; there is evidence suggesting properties of nociceptive systems are a result of evolutionary adaptions that are organism specific (Tracey, 2017). As such, similar comparative analyses of the various cellular compartments within individual Class IV neurons may provide improved insight into larval behavior and functional reasons underlying cell-specific dendrite morphogenesis. Technical challenges have thus far hindered such analyses in *Drosophila* Class IV neurons. However, developments in calcium indicators (Ye et al., 2017; Chen et al., 2013) and imaging protocols (Kakanj et al., 2020; Mishra et al., 2014; Ghannad-Rezaie et al., 2012) have now enabled detailed investigation of cellular compartments *in vivo* with improved spatial and temporal resolution. This opens the door for more granular examination of biophysical properties in Class IV neurons and their underlying circuitry.

In this work, we examined somatosensory properties of Class IV dendritic arbors *in vivo*. To do this, we used our tunable confocal microscopy-based laser assay that mimics wounds to the larval cuticle similar to an ovipositor jab (Chapter 2). We then used this technique to perform a thorough biophysical characterization of cellular

compartments by probing differential sensitivities across various parts of dendritic arbors in single cells using calcium imaging. Direct stimulation of larvae resulted in large calcium influxes into individual Class IV neurons. We studied these responses and found that stimuli trigger two distinct calcium signaling pathways based on the location of contact within the larval body: (i) the "non-contact" axonal pathway and (ii) "contact" dendritic pathway. We characterized both pathways. Analysis of the response magnitudes highlights different thresholds required to initiate axonal versus dendritic responses. We also investigated the temporal dynamics of calcium responses throughout the dendritic arbors of individual Class IV cells. To gain mechanistic insight in to the observed responses, we then developed a mathematical model using carefully measured physical parameters of dendritic arbors and our laser stimulus. Cumulatively, our *in vivo* data provide detailed specifications of somatosensory properties in Class IV dendritic arbors within a simulated natural scenario and proposes differing functional interpretations of dendritic and axonal spikes within the context of larval nociception. To our knowledge, this is the first systematic characterization of somatosensory sensitivities in Class IV da neurons.

3.3 Results

Different stimulation locations trigger two distinct calcium signaling responses

Prior work has indicated that the dense meshwork of Class IV neurons is designed to maximize their ability to sense and mediate escape behavior (Ganguly et al., 2016). If this is true, there should be no cellular responses if the stimulus does not directly make contact with the Class IV arbor. To test this, we harnessed the tight spatial profile of our laser to probe larvae in regions not tiled by Class IV arbors. We then took the same cell and stimulated Class IV arbors directly.

We found that larval behavioral responses (eg: muscle twitching) were triggered irrespective of the stimulus location (data not shown). However, we did observe differential calcium signaling responses in Class IV neurons depending on if the stimulus made direct contact with the dendritic arbor (Figure 3.1). We found that the "non-contact" condition consistently generated calcium transients in the axons of Class IV neurons, but not in the dendrites (Figure 3.1A, B). In contrast, direct stimulation of the arbor results in a calcium response throughout the entire cell (Figure 3.1A, B).

To control for any statistical anomaly and user-error in defining the stimulus location, we repeated the same experiment by stimulating larval samples three times: in the first two instances, we did not make contact with Class IV arbors in two different locations. In the third instance, we stimulated the dendritic arbor with direct contact of the laser. We found that, indeed, two different calcium signaling pathways can be triggered reproducibly based on the location of the stimulus. Only axons respond in the "non-contact" scenario (Figure 3.1A-B, E, color code of data points is adopted from

Figure 2.7C). When cells are directly stimulated, responses can be observed in the entire dendritic tree, including axons (Figure 3.1C-D, E, color code of data points is adopted from Figure 2.7C). These data confirm the presence of two distinct calcium signaling responses: (i) “non-contact” axonal response, and (ii) “contact” dendritic response.

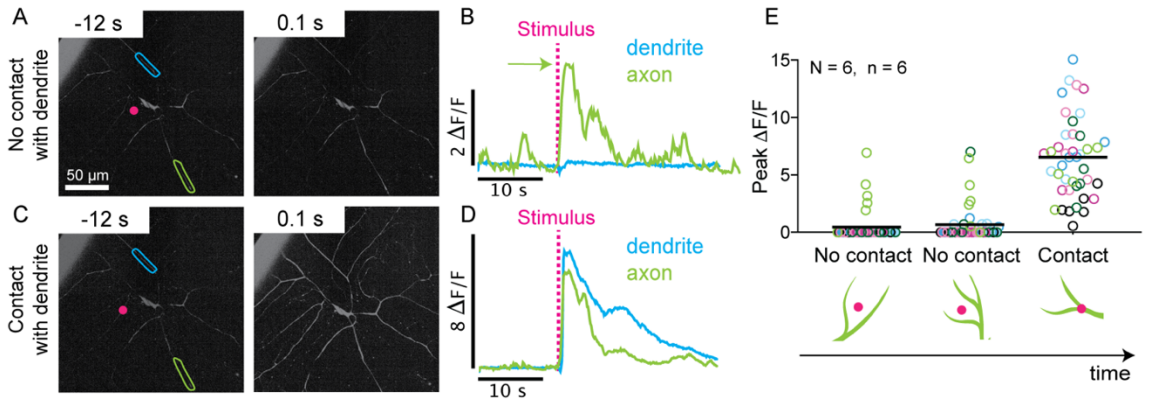

Figure 3.1: Axonal versus dendritic calcium signals in Class IV neurons are initiated based on the stimulus location. (A, C) Montage showing snapshots of same neuron expressing UAS-GCaMP6f stimulated without direct contact to the dendritic arbor (top row) and with direct contact with the dendritic arbor (bottom row). Scale bar is 50 µm. (B, D) Micrographs of normalized fluorescence responses from ROIs indicated in panel A, C (top corresponds to the "non-contact" scenario, bottom corresponds to direct contact scenario). Responses shown are for a dendrite (blue) and axon (green). (E) Magnitude of normalized fluorescence responses across all 7 ROIs (open circles, color coded as described previously in Figure 2.7C, see Materials and Methods) for cells stimulated 3 consecutive times. First two stimulations did not make contact with dendritic arbor. Third stimulation made contact with dendritic arbor. Black lines indicate means for all ROIs combined. N represents number of larvae; n represents number of cells.

"Non-contact" axonal responses are highly sensitive, graded, and initiated irrespective of stimulus location

To investigate the conditions under which the axonal "non-contact" pathway is triggered, we probed larval samples at various locations without making direct contact with the dendritic tree. Our stimulus intensity ranged from 10% to 100% laser power (~4mW-45mW). We also modulated the spatial profile of our 405nm laser (denoted by red and blue in figures), thus allowing us to deliver the same integrated power at two different irradiance settings (FWHM: 1 μm vs FWHM: 0.5 μm) (Figure 3.2A).

We first probed cells and scored the likelihood of responses by analyzing the percentage of axonal ROIs that respond under these varying conditions. An ROI was deemed responsive if the ΔF/F post stimulation was at least five standard deviations greater than F_0 (See *Materials and Methods*). We found that the axonal "non-contact" pathway displays graded behavior, with a larger percentage of ROIs responding with increasing stimulation power (Figure 3.2B). We found that the percentage of axonal ROIs that responded to "non-contact" stimuli increased from 10% (FWHM 1 μm) and 30% (FWHM 0.5 μm) at 10% laser power to 70-80% at 100% laser power (Figure 3.2B). Thus, the "non-contact" stimulus reproducibly evokes responses from Class IV axons, with narrower profiles giving larger responses at lower total intensities.

We then characterized the magnitude of calcium responses in each ROI across the varying wattage and irradiance settings. The magnitudes of calcium responses were also graded, with increased wattage resulting in larger ΔF/F values. Both irradiances showed similar calcium signaling magnitudes for axonal ROIs across all power settings

(Figure 3.2C, D) (Table 3.1). Although we previously observed some dendrite ROI responses (Figure 3.1B), the actual magnitude of their responses were ~0 ΔF/F (black line), reconfirming that axons are primarily activated in the "non-contact" pathway (Figure 3.2C, D). Interestingly, distal regions on the axon demonstrated higher magnitudes across all stimulation intensities (Figure 3.2C, D, light green versus dark green, color code from Figure 2.7C). This could be due to a higher density of calcium channels in distal regions where functional synapses are known to localize. Our data thus demonstrate that axonal calcium transients are not elicited on an all-or-nothing basis but are proportional to the intensity of our laser. Previous work has reported relationship between calcium signaling magnitudes and neuronal spiking rates (Ali and Kwan, 2019)). Thus, our observed differential calcium signaling magnitudes likely underscore cellular initiation of behavioral responses proportional with the severity of the stimulus. It has been suggested that nociceptors are activated only when sensory input exceed thresholds beneath which stimuli are determined to be innocuous (Perl, 2007). In fact, localized thermal infrared stimulation of Class IV neurons results in an abrupt increase in cellular activity beyond certain temperatures (Terada et al., 2016). Contrastingly, in our experiments, we see that our stimuli consistently elicited axonal responses even at low stimulation intensity settings with a graded increase towards higher stimulation intensity settings. This could be because our stimuli exceeded any existing cellular activation threshold even at the lowest wattages studied. Alternatively, it is possible that Class IV neurons encode different classes of stimuli (thermal vs optical vs mechanical) with differing thresholds.

We then studied the response times for axonal ROIs by computing the first time point where $\Delta F/F$ after stimulation exceeded five standard deviations above the baseline fluorescence F (Figure 3.2E, inset). The latencies of the "non-contact" axonal responses, decreased with increasing intensity (Figure 3.2E). The narrower stimulus (0.5 µm FWHM) gave shorter latencies than the wider stimulus. For example, the latencies at 100% power were 0.39 ± 0.17 s (mean ± SD, n=12) for 0.5 µm FWHM and 0.52 ± 0.38 s (mean ± SD, n=18) for 1 µm FWHM.

We next inquired if the "non-contact" axonal pathway is dependent on proximity of the stimulus to the cell body or axon. To test this, we stimulated the same group of cells seven times at 80% intensity, with each stimulus progressively further away from the soma. We then analyzed the magnitude of cellular ROIs. Our assay revealed that axonal ROIs are capable of responding irrespective of the stimulus distance from the soma. Furthermore, there is no statistical difference between the calcium signaling magnitudes as a result of changing location (Figure 3.2F) (Ordinary One-way ANOVA, $p = 0.8501$, *not significant*). These findings indicate that stimulation of untiled regions surrounding those heavily innervated by Class IV neurons is sufficient to initiate Class IV neuron activation, regardless of location (*See Discussion*).

In summary, these experiments show that the high responsiveness and graded profile of the "non-contact" axon pathway, and the ability of Class IV neurons to fire without direct stimulation, regardless of location. This spotlights the robust integration of Class IV neurons with the overall larval body.

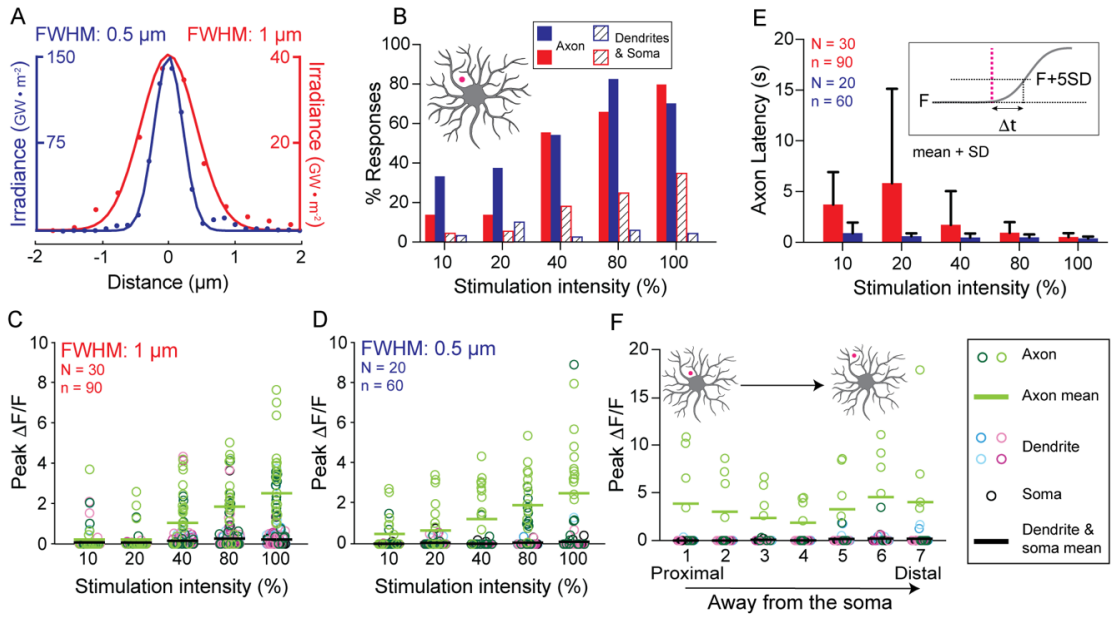

Figure 3.2: Characterization of "non-contact" axonal calcium signaling responses in Class IV neurons. N represents number of larvae; n represents number of cells. (A) Line scans of the spatial profiles of the narrower 405-nm laser profile (0.5 µm FWHM, blue) and the wider 405-nm laser profile (1 µm FWHM, red). While they have the same total power (intensity), the irradiance (on the y-axes) of the narrower profile is four times larger. (B) Frequency of calcium transients in the two axonal ROIs (solid bars) and the five dendritic and somal ROIs (striped bars) in response to "non-contact" stimulation across a range of intensities (10 -100%). Red and blue correspond to wider (red) and narrower (blue) profiles. (C-D) Peak $\Delta F/F$ values for cells stimulated with no contact. Open circles indicate ROIs color-coded as in Figure 2.7C. Lines denote means of axon ROIs (green) and dendrite/soma ROIs (black). Statistical comparisons for these data are in Table 3.1. (E) Axonal response latencies. Red and blue histograms correspond to wider and narrower stimuli. Inset: the latency is defined as the time when $\Delta F/F = F + 5SD$. Statistical comparisons for data are shown in Table 3.2. (F) Peak values of $\Delta F/F$ for seven consecutive "non-contact" stimuli (0.5 µm FWHM, 80% Stimulation intensity) at increasing distances from the cell body. Ordinary One-way ANOVA test shows no difference between axon means ($p = 0.8501$).

	Figure 3.2C	Figure 3.2C	Figure 3.2C, D	Figure 3.2C, D
	Axon (green line) (FWHM: 1 µm) vs. **Dendrite & Soma** (black line) (FWHM: 1 µm)	**Axon** (green line) (FWHM: 0.5 µm) vs. **Dendrite & Soma** (black line) (FWHM: 0.5 µm)	**Axon** (green line) (FWHM: 1 µm) vs. **Axon** (green line) (FWHM: 0.5µm)	**Dendrite & Soma** (black line) (FWHM: 1 µm) vs. **Dendrite & Soma** (black line) (FWHM: 0.5 µm)
10%	p = 0.9317 (ns)	p = 0.1117 (ns)	p = 0.9751 (ns)	p = 0.8456 (ns)
20%	P = 0.7630 (ns)	p = 0.0175 (*)	p = 0.7790 (ns)	p = 0.9719 (ns)
40%	p < 0.0001 (****)	p < 0.0001 (****)	p = 0.9896 (ns)	p = 0.1417 (ns)
80%	p < 0.0001 (****)	p < 0.0001 (****)	p >0.9999 (ns)	p = 0.0032 (**)
100%	p < 0.0001 (****)	p < 0.0001 (****)	p >0.9999 (ns)	p = 0.0193 (**)

Table 3.1: Comparison of Magnitude of Responses shown in Figure 3.2. Sidak's multiple comparisons test results shown for comparisons.

	Figure 3.2E
	Axon Response Time (FWHM: 1 µm) vs. **Axon Response Time (FWHM: 1 µm)**
10%	p = 0.2011 (ns)
20%	P = 0.0004 (***)
40%	p = 0.4851 (ns)
80%	p = 9710 (ns)
100%	p > 0.9999 (ns)

Table 3.2: Comparison of Response Times for axon ROIs stimulated under the "non-contact" condition as shown in Figure 3.2E. Sidak's multiple comparisons test results shown.

Sensory properties of entire dendritic field are homogenous, and magnitude of "contact" dendritic responses are nonlinearly dependent on stimulus intensity

Having observed features of the "non-contact" axonal response, we next investigated how various parts of the dendritic arbor respond under the contact dendritic pathway. Prior work has reported that evoked dendritic calcium transients occur in an all-or-nothing fashion beyond a cellular threshold (Terada et al., 2016). To test this, we stimulated dendritic arbors of Class IV neurons in three different locations: (i) soma, (ii) proximal dendrites, and (iii) distal dendrites (Figure 3.3A, B, C, insets) at varying wattages and studied their calcium signaling responses. Varying the stimulation location also allowed us to investigate if different parts of Class IV arbors have comparable sensory properties, or if certain regions were more sensitive to stimuli, as has been demonstrated in rodent *in vivo* models (Gaub et al., 2019).

To quantify the likelihood of responses for each stimulation condition, we computed the percentage of all seven ROIs in each cell that displayed calcium transients in response to stimulation ("% Responding"). We found that stimulation in the soma, proximal dendrites, and distal dendrites all evoked global calcium transients in a graded, dose dependent manner (Figure 3.3A, B, C). Lower wattages resulted in fewer ROI responses overall, whereas higher wattages resulted in majority of ROIs responding. While the percentage of ROI responses were very similar between soma and proximal dendrite stimulated cells, interestingly, cells stimulated on a distal dendrite showed fewer ROI responses across all stimuli wattage (Figure 3.3C).

We next analyzed the magnitudes of calcium transients. Increasing wattage at all locations – soma, proximal, and distal – resulted in a graded, non-linear increase in

Peak ΔF/F (Figure 3.4A, B, C). In addition, the average magnitudes of responses were very similar between soma and proximally stimulated cells (Figure 3.4A, B). However, similar to the response frequency, cells stimulated distally displayed average magnitudes that were lower (Figure 3.4C). We investigate the cause of this observation in a following section (Figure 3.6). To discern any differences in the response magnitudes between axon and dendrite ROIs, we computed their means separately (black and green lines). In contrast to the "non-contact" axonal pathway, both, axonal and dendritic ROIs respond with similar magnitudes when Class IV cells are directly irradiated by the stimulus (Figure 3.4D, E, F) (Table 3).

We were also curious if different dendritic sections along the arbor respond differentially. We hypothesized that regions proximal to the stimulus location may display different response magnitudes as compared with distal regions due to any localized damage caused by the stimulus. Intriguingly, analysis of individual dendritic ROIs reveal that the dendritic contact pathway elicits a global cellular response with consistent magnitude throughout all cellular regions. Axonal, proximal and distal ROIs respond similarly, on average, within each combination of experimental conditions (wattage, stimulation location) (Figure 3.4A-C). Furthermore, responses in all dendritic compartments were coincident after stimulation; the observed cellular response was a global cellular event.

Cumulatively, these experiments highlight the properties of the contact dendritic pathway. They show that the dendritic field of Class IV neurons are equipped to discern stimuli of differing magnitudes. Although it does require direct contact with

neuronal processes, the dendritic pathway is initiated regardless of which part of the arbor is stimulated. Furthermore, in all cases, the cellular response is a global response that causes all parts of the cell to respond with similar magnitude.

Magnitude of "contact" dendritic responses are dependent on irradiance of stimulus

To test the impact of changing stimulus geometry on the contact dendritic pathway, we performed the same set of aforementioned experiments under both irradiance settings, one with a broader profile (FWHM: 1 µm) and one with a tighter profile (FWHM: 0.5 µm) (Figure 3.2A). These two settings correspond to higher and irradiance (Figure 3.2A) but the same integrated power (Chapter 2). We found that both irradiance settings were able to trigger cellular calcium signals with similar frequency (Figure 3.3A, B, C). However, the higher irradiance setting resulted in larger calcium signaling magnitudes as compared with the lower irradiance setting (Figure 3.4 A & D, B & E, C & F). While the general features of the dose response curve were similar for both irradiance settings – graded, non-linear – the high irradiance setting caused steeper increases in Peak $\Delta F/F$ magnitudes with each unit increase in stimulation wattage (Figure 3.4A-F). Differences between dendritic responses across the two irradiance settings were statistically significant at higher stimulation wattage >40% (Table 3.4). However, the magnitudes of axon responses were consistent between both irradiance settings for all stimulus locations, reinforcing again that axonal calcium transients are distinct from dendritic calcium transients (Table 3.4).

Interestingly, doubling the wattage or halving the FWHM of the stimulus evoked Peak $\Delta F/F$ values of similar magnitude (Figure 3.4 A-F). For example, cells stimulated on the soma with the tight spatial profile (FWHM: 0.5 µm) at 80% stimulation intensity results in a Peak $\Delta F/F$ value of ~5 (Figure 3.4A). Reducing the stimulation intensity by half to 40% or doubling the FWHM of the laser to the broader profile (FWHM: 1 µm), both, result in Peak $\Delta F/F$ of ~2 (Figure 3.4A, D). This hinted to us that the stimulation intensity or peak irradiance alone cannot explain the observed calcium signaling magnitudes. Instead, the stimulus geometry, dendrite geometry, and integrated power must be considered together. We explore this feature of the data further in the model section (Figure 3.6).

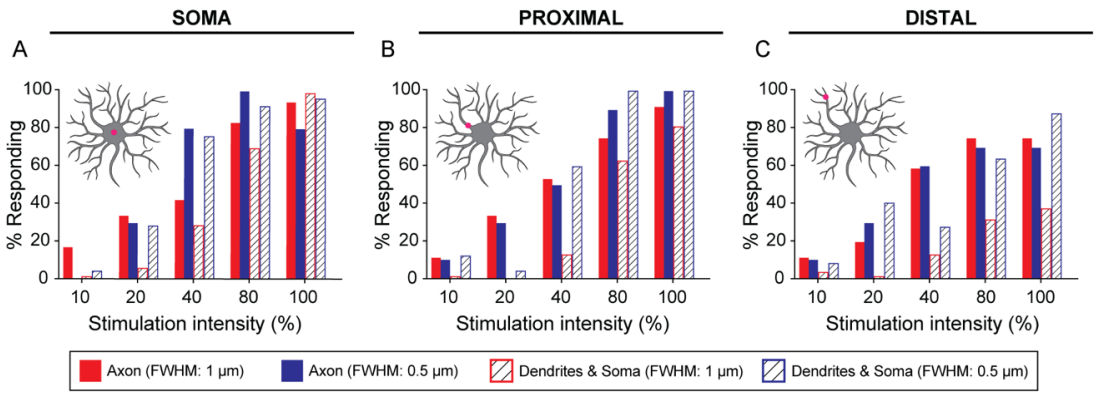

Figure 3.3: Frequency of dendritic calcium transients from direct stimulation of Class IV dendritic arbors – "contact pathway". N represents number of larvae; n represents number of cells. Red histograms indicate data from cells stimulated with broader spatial profile (FWHM: 1 µm). Blue histograms indicate data from cells stimulated with tighter spatial profile (FWHM: 0.5 µm). Open circles indicate ROIs, color coded by cellular location as described in *Materials and Methods*. Lines denote means of axon ROIs (green) and dendrite/soma ROIs (black). (A-C) Frequency of calcium transients from cells stimulated on the (A) cell body, (B) proximal dendrite, and (C) distal dendrite.

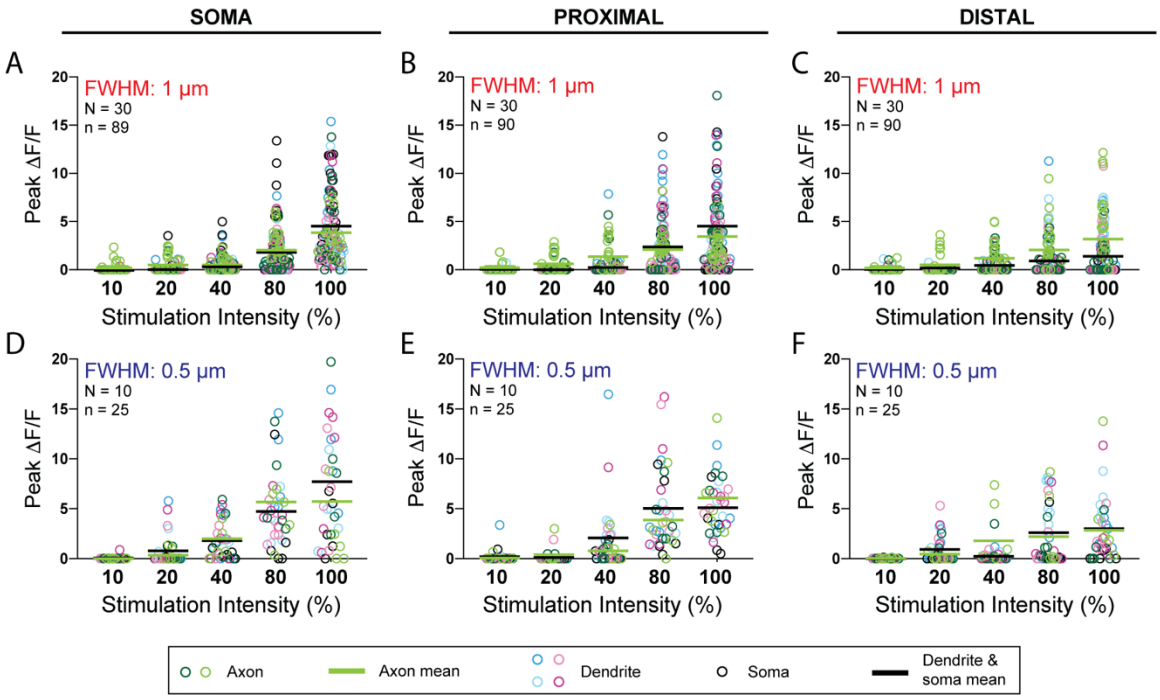

Figure 3.4: Magnitudes of "contact" dendritic calcium signaling responses in Class IV neurons are nonlinearly correlated with stimulus wattage. N represents number of larvae; n represents number of cells. Green lines denote mean of axon ROIs. Black lines denote mean of dendrite and soma ROIs. (A-C) Magnitudes of calcium transients from cells stimulation on (A) cell body (B) proximal dendrite and (C) distal dendrite using a broader stimulus profile (FWHM: 1 µm). (D-F) Magnitudes of calcium transients from cells stimulation on (D) cell body (E) proximal dendrite and (F) distal dendrite using a tighter stimulus profile (FWHM: 0.5 µm).

	Soma Stim	Prox Stim	Distal Stim	Soma Stim	Prox Stim	Distal Stim
	Axon (green line) (FWHM: 1 µm) vs. Dendrite & Soma (black line) (FWHM: 1 µm)	Axon (green line) (FWHM: 1 µm) vs. Dendrite & Soma (black line) (FWHM: 1 µm)	Axon (green line) (FWHM: 1 µm) vs. Dendrite & Soma (black line) (FWHM: 1 µm)	Axon (green line) (FWHM: 0.5 µm) vs. Dendrite & Soma (black line) (FWHM: 0.5 µm)	Axon (green line) (FWHM: 0.5 µm) vs. Dendrite & Soma (black line) (FWHM: 0.5 µm)	Axon (green line) (FWHM: 0.5 µm) vs. Dendrite & Soma (black line) (FWHM: 0.5 µm)
10%	p = 0.9975 (ns)	p = 0.9998 (ns)	p = 0.9998 (ns)	p > 0.9999 (ns)	p > 0.9999 (ns)	p > 0.9999 (ns)
20%	p = 0.8916 (ns)	p = 0.9006 (ns)	p = 0.6027 (ns)	p = 0.9993 (ns)	p = 0.9991 (ns)	p = 0.9904 (ns)
40%	p = 0.9993 (ns)	p = 0.2950 (ns)	p = 0.0041 (**)	p > 0.9999 (ns)	p = 0.6824 (ns)	p = 0.2377 (ns)
80%	p = 0.9981 (ns)	p = 0.9921 (ns)	p = 0.0010 (***)	p = 0.9593 (ns)	p = 0.7610 (ns)	p = 0.9954 (ns)
100%	p = 0.4851 (ns)	p = 0.3031 (ns)	p = <0.0001 (****)	p = 0.5376 (ns)	p = 0.8493 (ns)	p > 0.9999 (ns)

Table 3.3: Comparison of magnitude of Ca^{2+} responses between axons and dendrite/soma ROIs for the "contact" dendritic pathway as shown in Figures 3.4 A-F. Sidak's multiple comparisons test results shown for comparisons.

	Soma Stim	Prox Stim	Distal Stim	Soma Stim	Prox Stim	Distal Stim
	Axon (green line) (FWHM: 1 µm) vs. Axon (green line) (FWHM: 0.5 µm)	Axon (green line) (FWHM: 1 µm) vs. Axon (green line) (FWHM: 0.5 µm)	Axon (green line) (FWHM: 1 µm) vs. Axon (green line) (FWHM: 0.5 µm)	Dendrite & Soma (black line) (FWHM: 1 µm) vs. Dendrite & Soma (black line) (FWHM: 0.5 µm	Dendrite & Soma (black line) (FWHM: 1 µm) vs. Dendrite & Soma (black line) (FWHM: 0.5 µm)	Dendrite & Soma (black line) (FWHM: 1 µm) vs. Dendrite & Soma (black line) (FWHM: 0.5 µm)
10%	p = 0.9998 (ns)	p > 0.9999 (ns)	p > 0.9999 (ns)	p > 0.9999 (ns)	p = 0.9998 (ns)	p > 0.9999 (ns)
20%	p > 0.9999 (ns)	p = 0.9999 (ns)	p > 0.9999 (ns)	p = 0.8078 (ns)	p > 0.9999 (ns)	p = 0.0675 (ns)
40%	p = 0.2251 (ns)	p = 0.9626 (ns)	p = 0.9434 (ns)	p = 0.1265 (ns)	p = 0.0605 (ns)	p > 0.9999 (ns)
80%	p < 0.0001 (****)	p < 0.0563 (ns)	p > 0.9999 (ns)	p < 0.0001 (****)	p = 0.0016 (**)	p < 0.0001 (****)
100%	p = 0.0746 (ns)	p = 0.0012 (**)	p = 0.9940 (ns)	p < 0.0001 (****)	p = 0.9380 (ns)	p < 0.0001 (****)

Table 3.4: Comparison of magnitude of Ca^{2+} responses shown in Figure 3.4 A-F across two different stimulation irradiance settings. Sidak's multiple comparisons test results shown for comparisons.

Axons typically respond faster than dendrites

We next characterized the temporal dynamics of cells directly irradiated with the laser. The response time (latency) was computed as the time where $\Delta F/F$ exceeded five standard deviations above the baseline fluorescence. The latencies of the "contact" responses were shorter in the axons than the dendrites (Figure 3.5A, B): in other words, the dendritic response rises with a larger delay than the axonal response. For both axons and dendrites, higher intensities gave shorter latencies. The latencies of axonal "contact" responses were similar to those of "non-contact" responses (Figure 3.5A-B, Figure 3.2 E). Interestingly, the rising phases of the dendritic responses were almost simultaneous in all the dendritic regions, being within the 100 ms frame time of the camera, even though the latency was significantly longer (≥ 500 ms). For example, directly stimulating a peripheral dendrite gave a response in the same dendrite and in a dendrite on the other side of the cell body (>200 µm distance away) with a time-course that rose within 100 ms of each other (1 frame) (Figure 3.5C). This shows that the dendritic signals propagate at speeds >2 mm/s (= 200 µm / 100 ms).

Intriguingly, altering the irradiance had a significant impact on the response times/latencies of dendrites but not those of axons (Table 3.5). A stimulus with higher irradiance causes dendritic ROIs to respond faster, bringing them on par with the speed of the axonal response (Figure 3.5A, B). The speed of axonal responses, however, are consistent across both irradiance settings (Table 3.5).

We interpret these data as reinforcing our previous ideas about the difference between axonal and dendritic calcium transients. The faster axonal response is a proxy

for neural activation that underscores the function of Class IV neurons in mediating escape behaviors. As such, axon activation occurs quickly and uniformly across multiple variations of noxious stimuli. On the other hand, dendritic calcium transients are slower and demonstrate more variability in their response time. This is likely because the function of dendritic calcium transients in this context is distinct from that of the axonal pathway. Dendritic calcium transients are not essential for mediating escape behaviors, and thus presumably perform alternate functions on different time scales. We investigate some hypotheses on this front in Chapter 4.

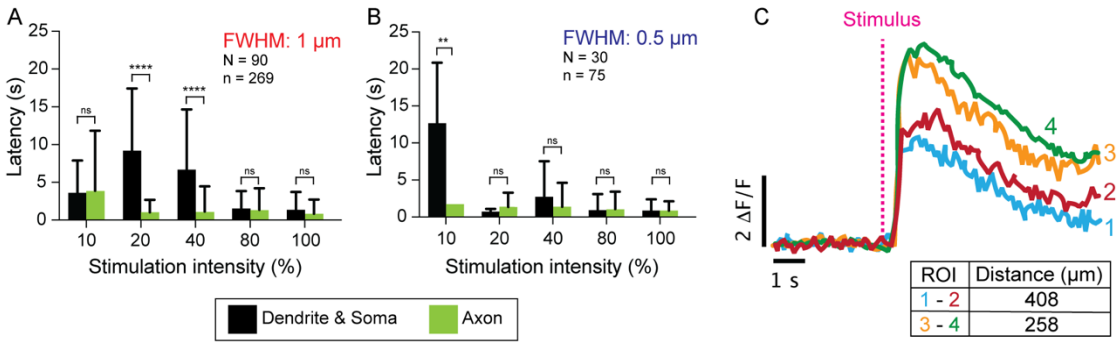

Figure 3.5: Response times/Latencies of axonal and non-axonal ROIs reacting to 405 nm stimulation via the "contact" dendrite pathway. Black histograms represent data from dendritic and soma ROIs. Green histograms represent data from axon ROIs. All data shown are means and standard deviations. (A-B) Response times for cells stimulated with a (A) broad stimulus profile (FWHM: 1 µm) and (B) tight stimulus profile (FWHM: 0.5 µm) at varying wattage levels (10-100%). Sidak's multiple comparisons test was used to evaluate statistical significance for pairwise comparisons of dendrite & soma versus axon response times. Ordinary one-way ANOVA shows no significant difference between Response Times for axons across all stimulation intensities at both irradiance settings (p=0.4163). (C) Dendrite ROIs >250 µm apart showing simultaneous rise after a lag (latency) post-stimulation (pink dashed line). Dendritic and somal regions show simultaneous responses within our time frame (100 ms).

	Figure 3.5A, B	Figure 3.5A, B
	Dendrite & Soma (black) **(FWHM: 1 µm)** vs. **Dendrite & Soma (black)** **(FWHM: 0.5 µm)**	**Axon (green)** **(FWHM: 1 µm)** vs. **Axon (green)** **(FWHM: 0.5 µm)**
10%	p = 0.0052 (**)	p = 0.9994 (ns)
20%	p < 0.0001 (****)	p > 0.9999 (ns)
40%	p < 0.0001 (****)	p > 0.9999 (ns)
80%	p = 0.9046 (ns)	p > 0.9999 (ns)
100%	p = 0.9537 (ns)	p > 0.9999 (ns)

Table 3.5: Comparison of Latencies for ROIs stimulated with two different irradiance settings in Figure 4. Sidak's multiple comparisons test results shown.

Magnitude of cellular calcium signals via the "contact" pathway is correlated with overlap of stimulus and dendrite geometry

Prior results demonstrated an interesting feature wherein distal stimulation of neurons consistently resulted in smaller Peak ΔF/F values. In addition, we found it curious that doubling the wattage or halving the FWHM of the stimulus resulted in similar Peak ΔF/F values across all stimulation locations (Figure 3.4 D, E, F, G, H, I). For example, if we consider soma-stimulated cells: stimulation at 80% wattage with high irradiance (40X) results in a mean Peak ΔF/F value of ~5. If we reduce the wattage by half to 40%, we get a mean Peak ΔF/F of ~2. Similarly, if instead of reducing the wattage by a factor of 2, we increase the FWHM of the stimulus by a factor of 2 (20X stimulus, broader profile than stimulus from 40X), we obtain a mean Peak ΔF/F of ~2. We sought to investigate the cause of these observations.

Careful measurement of individual dendritic processes revealed that dendrite diameters systematically taper radially away from the soma. Distal dendritic processes are considerably thinner (radius: 200 nm) than proximal dendrites near the cell body (radius: 500 nm) (Figure 3.6B, *Supplementary Materials*) (Liao and Howard, 2020). This led us to investigate if distal dendrites are, in fact, responding with equal magnitude when their smaller radii are accounted for. That is, we hypothesized that the stimulus-per-unit-dendrite could be the cause of these differences.

To test this, we generated a mathematical model by considering physical and geometric properties of the dendrites and the laser stimulus. The laser beam was modelled as a two-dimensional gaussian with measured parameters as input for the

standard deviation and amplitude (Figure 3.6A). Dendrites were modelled as cylinders with varying radii to represent proximal and distal processes (Figure 3.6B). For simplicity, the soma was modelled as a cylinder with radii significantly greater than proximal processes. We accounted for the non-linearity of the dose response by introducing an exponentiating factor, ***n***. Our model asked the question: are the observed Peak ΔF/F magnitudes a result of differing degrees of overlap between the stimulus and the dendrite? In other words, does stimulation of thinner dendrites result in smaller responses because a smaller fraction of stimulus is actually making contact with the process? To be thorough, we considered, both, overlap of the stimulus with the volume of the dendrite (volume model) and overlap with the surface area (surface model) of the dendrite (See *Materials and Methods)*. Using the various measured parameters as input (Tables 3.6- 3.7), we then computed values for free parameters, **n** and **γ**, that simultaneously minimized the sum of the least squares difference between experimental and theoretical values (Table 3.8, See *Materials and Methods*).

Indeed, our models show good agreement with experimental data for all permutations of wattage, irradiance, and stimulus location (Figure 3.6C, D, E, F, G, H, Table 3.8). Notably, we faithfully recapitulate the non-linearity observed with increasing stimulus intensity. Our models also predict that stimulation of distal processes results in smaller Peak ΔF/F values overall. This is a result of diminished contact between the stimulus and distal neurites: regions distal from the soma have less volume to receive the stimulus. Furthermore, our models predict the observed irradiance dependence seen in our data (red versus blue). A broader stimulus results in

lower Peak ΔF/F magnitudes as compared with a tighter stimulus. This arises from considerations of the overlap between the stimulus density and dendrite geometry. For example, the broader irradiance setting results in overfilling of distal dendritic regions – that is, a considerable portion of the stimulus is not delivered to the arbor but to neighboring regions (Figure 3.6B).

To see if we could gain any insight into differences between axon and dendrite ROIs, we considered the fit of both models (surface model, dashed line and volume model, dotted line) with axon ROIs and dendrite/soma ROIs independently. Yet again, we discovered a difference between axonal and dendritic regions. In particular, our models predict that Peak ΔF/F magnitudes resulting from stimulus overlap with the volume of the stimulated neurite (volume model) better capture dendrite and soma ROIs (Figure 3.6C, E, G). On the other hand, a model that considers overlap of the stimulus with the surface area of the dendrite (surface model) more faithfully captures data from axonal ROIs (Figure 3.6D, F, H) (Table 3.8).

Cumulatively, our modeling results clarify the origin of the subtle differences between the observed calcium signaling magnitudes in Figure 3.4. That is, experimental calcium signaling magnitudes are a result of the integrated overlap of the stimulus and dendrite geometry. Excellent theoretical and experimental agreement between the various permutations of data sets (wattage, irradiance, stimulus location) provides quantitative support for our model (Table 3.8). Importantly, our models also highlight new evidence that suggests that dendritic and axonal calcium transients are mediated via different receptor pathways. This lends further support to the idea that these two

pathways serve distinct functions. Agreement with the surface model for axonal ROIs and volume model for dendrite/soma ROIs also opens the door for investigation of corresponding biological receptors that may localize on the surface of dendrites or cytosol of dendrites, respectively.

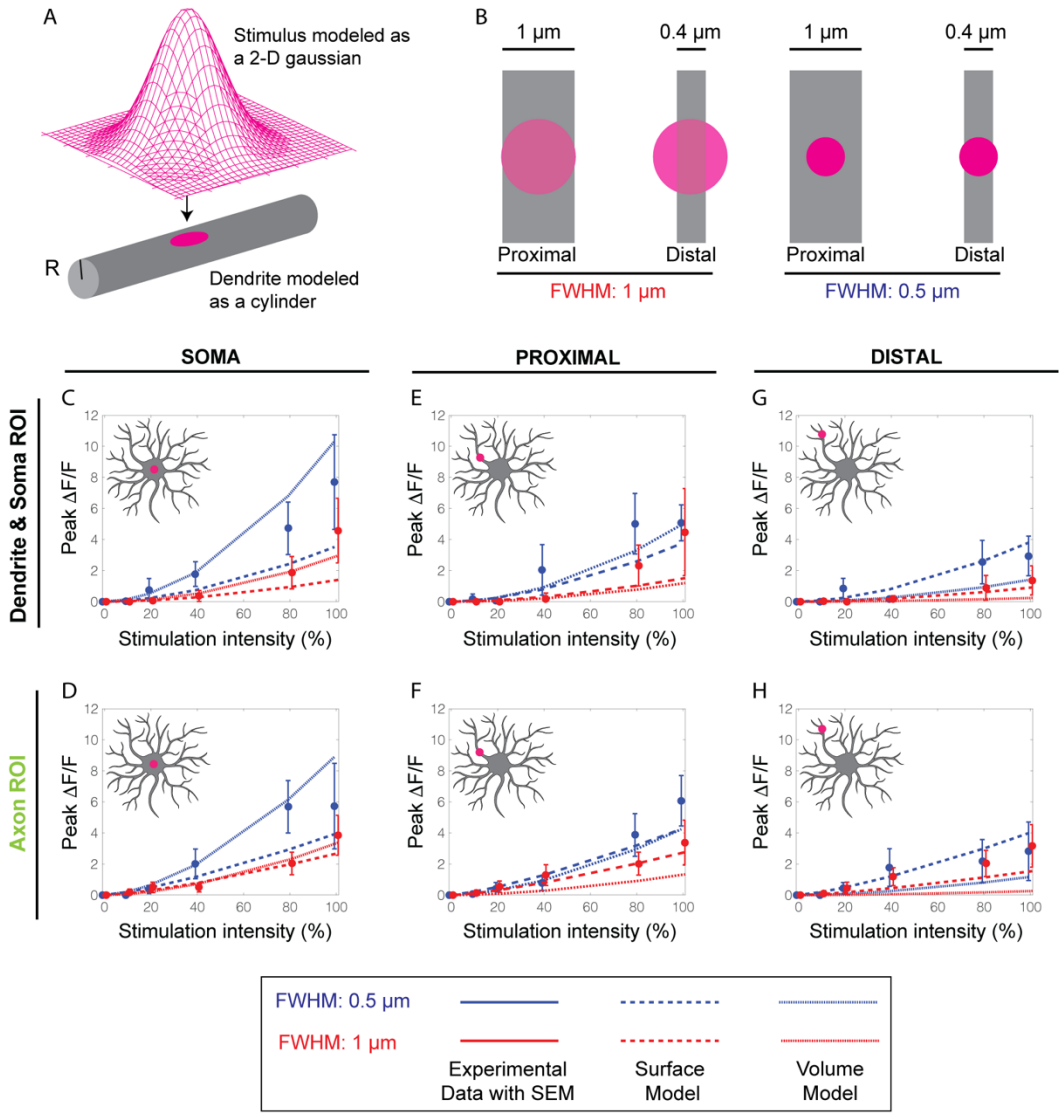

Figure 3.6: Overlap of stimulus and dendrite geometry underlie observed experimental calcium signaling magnitudes. (A) Schematic of the overlap model: the laser profile is approximated by a 2-D Gaussian and the dendrite modeled by a cylinder with radius R. (B) Top-down view of the two laser profiles projected onto proximal and distal dendrites. Proximal dendrites have radius 500 nm and distal dendrites have radius 200 nm. (C-H) Theoretical curves (lines) superimposed on the measured peak $\Delta F/F$ for somal (C, D), proximal dendrite (E, F) and distal dendrite (G, H) stimulation. Dashed lines represent the surface model and dotted line represents the volume model.

Power (P)	Laser Width (σ)	Radius (r)	Experimental ΔF/F (F)	Modeled SEM (WLS weight)
0	212.31	500	0	0.1445
10	212.31	500	0.068684925	0.168677094
20	212.31	500	0.392383484	0.282618986
40	212.31	500	0.782529208	0.419950281
80	212.31	500	3.872628207	1.507665129
100	212.31	500	6.07809914	2.283990897
0	212.31	200	0	0.1445
10	212.31	200	0.01168088	0.14861167
20	212.31	200	0.43328868	0.297017615
40	212.31	200	1.77380998	0.768881113
80	212.31	200	2.18446697	0.913432373
100	212.31	200	2.81976898	1.137058681
0	212.31	1000	0	0.1445
10	212.31	1000	0	0.1445
20	212.31	1000	0.360228787	0.271300533
40	212.31	1000	2.011095156	0.852405495
80	212.31	1000	5.684920583	2.145592045
100	212.31	1000	5.734179428	2.162931159
0	424.62	500	0	0.1445
10	424.62	500	0.140546121	0.193972235
20	424.62	500	0.54426786	0.336082287
40	424.62	500	1.292631317	0.599506224
80	424.62	500	2.027996352	0.858354716
100	424.62	500	3.37835648	1.333681481
0	424.62	200	0	0.1445
10	424.62	200	0.091146399	0.176583532
20	424.62	200	0.429240122	0.295592523
40	424.62	200	1.189055302	0.563047466
80	424.62	200	2.035088751	0.86085124
100	424.62	200	3.170241314	1.260424942
0	424.62	1000	0	0.1445
10	424.62	1000	0.182453729	0.208723713
20	424.62	1000	0.498731771	0.320053583
40	424.62	1000	0.500696023	0.320745
80	424.62	1000	2.037007512	0.861526644
100	424.62	1000	3.852882468	1.500714629

Table 3.6: Modeling input parameter values for axon ROIs.

Power (P)	Laser Width (σ)	Radius (r)	Experimental ΔF/F (F)	Modeled SEM (WLS weight)
0	212.31	500	0	0.1558
10	212.31	500	0.182350664	0.22717205
20	212.31	500	0.076460389	0.185726596
40	212.31	500	2.050158743	0.958232132
80	212.31	500	5.025163541	2.12264901
100	212.31	500	5.074426106	2.141930378
0	212.31	200	0	0.1558
10	212.31	200	0.005188064	0.157830608
20	212.31	200	0.860460567	0.492584266
40	212.31	200	0.164808405	0.22030601
80	212.31	200	2.548603702	1.153323489
100	212.31	200	2.948527166	1.309853533
0	212.31	1000	0	0.1558
10	212.31	1000	0.03473628	0.16939578
20	212.31	1000	0.763529255	0.45464535
40	212.31	1000	1.779650087	0.852355044
80	212.31	1000	4.722394194	2.004145087
100	212.31	1000	7.703064753	3.170779545
0	424.62	500	0	0.1558
10	424.62	500	0.008014336	0.158936811
20	424.62	500	0	0.1558
40	424.62	500	0.182200981	0.227113464
80	424.62	500	2.328810344	1.067296369
100	424.62	500	4.482075196	1.910084232
0	424.62	200	0	0.1558
10	424.62	200	0.022429348	0.164578847
20	424.62	200	0.008520127	0.159134778
40	424.62	200	0.163382325	0.219747842
80	424.62	200	0.892799903	0.505241882
100	424.62	200	1.369965549	0.692004516
0	424.62	1000	0	0.1558
10	424.62	1000	0.003978684	0.157357257
20	424.62	1000	0.076913166	0.185903813
40	424.62	1000	0.366020076	0.299060258
80	424.62	1000	1.869151273	0.887385808
100	424.62	1000	4.580236882	1.948504716

Table 3.7: Modeling input parameter values for dendrite and soma ROIs.

	Surface Model *(Equation 1)*			Volume Model *(Equation 2)*		
	n	**γ**	**Error**	**n**	**γ**	**Error**
Dendrites and Soma ROI	1.71	8.125	56.99	1.87	0.097	39.07
Axon ROI	1.33	0.346	24.29	1.66	0.015	42.19

Table 3.8: Summary of modeling fit parameters. Fit values for dendrite and soma ROI and axon ROIs using the surface model (equation 1, See *Materials and Methods*) and volume model (equation 2, See *Materials and Methods*). Visual plots of modeling results are shown in Figure 3.6 C-H.

Stimulus-induced calcium influx is mediated via voltage-gated calcium channels

Increases in cytoplasmic calcium concentrations can be the result of release of internal calcium stores or extra-cellular calcium. Inside the cell, the endoplasmic reticulum is the primary location where calcium is stored and buffered in large concentrations at concentrations on the order of 500μM (Stutzmann and Mattson, 2011). Alternatively, extracellular regions have calcium concentrations on the order of 1mM – approximately 10,000X greater than the concentration of calcium in the cytoplasm of the cell (Felix, 2001). As such, we wanted to investigate if internal or external calcium stores were the primary contributors to our observed calcium signaling events.

To test this, we generated mutant cell lines using TRiP flies (Perkins et al., 2015) expressing dsRNA for RNAi of the Ca-alpha1D under UAS control in either the VALIUM-10 or VALIUM-20 vectors. If extracellular calcium influx via L-type VGCC is the primary contributor to stimulus-evoked calcium signaling events, RNAi of Ca-alpha1D should result in attenuated calcium influx, and thus, lower overall calcium signaling magnitudes via GCaMP6f fluorescence. If, however, internal calcium stores are the primary contributor, RNAi should show no significant effect. As a control for the RNAi, we also used a fly which expressed dsRNA for RNAi of *white* eye gene. Using the same protocol for our earlier characterization experiments, we quantified the magnitude of the calcium signaling events post stimulation. To be thorough, we stimulated cells at two different stimulus wattages – 40% and 80%.

We found that, indeed, RNAi of the VGCC Ca-alpha1D (L-type VGCC) resulted in lower overall calcium signaling magnitudes at both wattage intensities.

Animals expressing the RNAi of *white* were not affected (Figure 3.7). The VALIUM 20-based vector showed a stronger phenotype than the VALIUM-10-based vector. This was likely due to stronger expression via VALIUM-20 and slightly leaky expression via VALIUM-10, as has been previous reported (Perkins et al., 2015). This is also in close agreement with findings in the literature where calcium signaling magnitudes in response to other types of stimuli (eg: thermal) were dampened via selective blockage of VGCCs (Kanamori et al., 2013; Terada et al., 2016). We did note, however, that although the calcium signaling magnitudes were attenuated, they were still present. This is likely because there are a number of non-selective cation channels on the cell membrane that also mediate extra-cellular calcium influx – for example, piezo and transient receptor potential (TRP) channels.

Cumulatively, our results, in close agreement with reported work, demonstrate that 405nm laser-evoked calcium responses in Class IV neurons are mediated via influx of extra-cellular calcium. L-type VGCCs are a key contributor to this process.

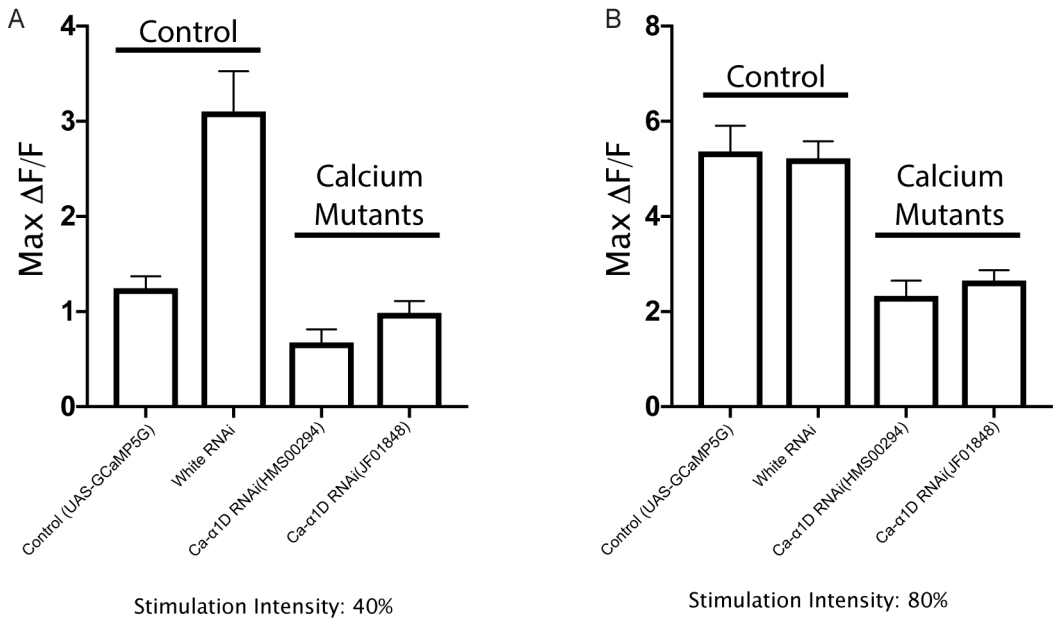

Figure 3.7: 405nm stimulus-induced calcium influx is mediated via voltage-gated calcium channels. Magnitudes of calcium transients from control (; UAS-GCaMP5G / ppk-GAL4; | N = 24, n = 72 and ; ppk-GAL4/+ ; white RNAi/+ / UAS-GCaMP5G | N = 24, n = 72) and mutant cells (; ppk-GAL4/ + ; *Ca-α1D RNAi* ^{JF01848} / UAS-GCaMP5G | N = 24, n = 72 and ; ppk-GAL4/+ ; *Ca-α1D RNAi* ^{HMS00294}/ UAS-GCaMP5G | N = 24, n = 72) irradiated at two different stimulation intensities, 40% (A) and 80% (B). Plots show mean and SEM.

3.4 Discussion

Using our assay, we have characterized somatosensory sensitivity of Class IV arbors and shown the presence of two distinct calcium signaling pathways: (i) a "non-contact" axonal pathway an (ii) a "contact" dendritic pathway (Figure 3.1). Three distinct pieces of evidence corroborated that these two pathways are distinct: (a) dendritic calcium transients require direct arbor contact; axonal calcium transients do not (Figures 3.1-3.4), (b) axonal calcium transients are more sensitive and faster than dendrites even when the stimulus is often >500μm away from the axon (Figure 3.5), and (c) a surface receptor model fits axon data better; a volume receptor model better fits dendrites and soma data (Figure 3.6). These differences suggest that the "non-contact" axonal pathway and the "contact" dendritic pathway serve distinct functions.

Why do axons of Class IV neurons respond even without direct contact with the stimulus? Axonal signals are canonically interpreted as a proxy for neuronal activation. Prior work has proposed that the dense tiling of Class IV neurons maximizes the probability of sensing noxious stimuli via direct contact (*See Introduction*). Yet, we observe that axons of Class IV neurons activate via the "non-contact" pathway even when arbors are not directly stimulated. We propose that extensive innervation of Class IV neurons allows neighboring damaged cells to release molecules that quickly diffuse and activate nearby Class IV processes to initiate axonal responses (Figure 3.8B). It has been shown that release of cytosolic ATP from damaged cells, for example, mediates pain perception via contact with P2X receptors on peripheral nociceptive cells in higher-order organisms (Hamilton and McMahon, 2000; Cook and McCleskey,

2002). While *Drosophila* lacks P2X receptors (Fountain and Burnstock, 2009), it is possible that other small molecules and acidification from surrounding epidermal cells might play an analogous role. The ASIC/ENaC, pickpocket, may be a good candidate for this role. Several pieces of evidence support this idea: (i) axon responses are highly sensitive and triggered under a wide range of stimulus permutations (Figure 3.2-3.4), (ii) the temporal dynamics of axons in Class IV cells are consistent with diffusion-mediated responses: given the Class IV neuron mesh size of 8 μm (Ganguly et al., 2016), a small molecule similar in size to ATP (diffusion coefficient on the order of 100 μm ^{2}/sec) will interact with a nearby dendrite in ~0.1 sec (Figure 3.5), and (iii) our model results predict that axonal calcium responses are better explained by considering receptors on the surface of dendritic processes, where diffusing molecules would make contact (Figure 3.6). Cumulatively, our data propose a slight modification to the biological reasoning unpinning extensive branching of Class IV dendritic arbors: the liberal tiling of Class IV neurons occurs not to maximize the ability of the cell directly sense stimuli, but to ensure that every part of the larval epidermis is within quick diffusing distance to a Class IV dendritic process.

The "contact" dendritic pathway, on the other hand, is more difficult to interpret. Thresholds for dendritic responses are reported to be higher than those for axonal responses (Häusser et al., 2000; Kole and Stuart, 2008). This may explain why direct arbor contact is necessary to trigger dendritic calcium signals (Fig 6C). But, if axonal activation occurs with or without direct contact, why do dendritic trees initiate coincident calcium transients in response to a direct stimulus >400 μm away from the site of stimulation at all? (Fig 4C) While very large calcium transients have been

observed to accompany cell death (Zhivotovsky and Orrenius, 2011; Bhosale et al., 2018), we confirmed that activation of the "contact" dendritic pathway did not result in cell or larval death 24 hours after stimulation (data not shown). Another possibility is that evoked dendritic calcium transients in Class IV neurons mediate morphological changes that occur on time scales longer than our imaging time. Dendritic calcium transients in dendrites of neurons have been previously implicated in morphoengineering dendritic arbors (Konur and Ghosh, 2005; Redmond and Ghosh, 2005; Kanamori et al., 2013). Thus, it is plausible that dendritic calcium spikes evoked in response to noxious stimuli may facilitate targeted reorganization of dendritic tips. This could be functionally beneficial as altered tip morphology may allow for increased coverage of the larval body wall, resulting in heightened ability to activate the "non-contact" axonal pathway. Alternatively, these dendritic spikes could be involved in long-term potentiation with neighboring cells to serve a similar function (Golding et al., 2002). Although these are exciting possibilities, it is worth noting, however, that we have not yet ruled out that our observed dendritic calcium transients are merely an epiphenomenon. These hypotheses are challenging to pinpoint because calcium dynamics are associated with a large number of cellular functions (Sabatini et al., 2001; Bootman et al., 2001; Clapham, 2007). Future work may consider studying the impact of evoked dendritic calcium transients on dendrite tip dynamics, connectivity, and overall arborization using robust tracking algorithms and long-term imaging.

One of the more surprising results of our model is the discovery of a cytoplasmic response factor. Our modelling results show that axonal responses are mediated via a cell surface – that is, membrane-localized – receptor. On the other hand, the dendritic

and somatic responses were better explained by a volume receptor: cytoplasmic localization. There is a considerable body of work that has implicated membrane receptors – TRP channels, Piezo channels, etc – in somatosensation of noxious heat and mechanical touch. However, the idea of a cytoplasmic sensors has not yet been proposed in this context. Yet, our model proposes that cytosolic proteins could be implicated in mediating cellular responses to when noxious stimuli exceeds a cellular threshold. Such a criterion could be based on physical parameters – for example, large number of sequential spikes or breakage of the cell membrane. On the other hand, if the stimulus is not of sufficient magnitude, such cytoplasmic proteins and their signaling pathways remain inactivated. This may explain why axonal responses – those mediated via membrane sensors – show higher sensitivity as compared with dendritic responses. Ongoing work in our laboratory is focused on identifying proteins that operate in such a capacity via targeted mutant screens.

Lastly, our results also demonstrate that spatiotemporal dynamics are paramount when analyzing calcium signaling assays. Although calcium imaging has become a ubiquitous technique in neuroscience, imaging experiments often consider many cells in aggregate or study individual cellular components in isolation. However, differential analysis of cellular compartments offers additional information by allowing nuanced interpretation of signals based on their spatial and temporal dynamics within the cell (Ali and Kwan, 2019). In our own system, this approach led us to discover the presence of distinct calcium signaling dynamics in dendrites versus axons. In fact, we also observed that sub-regions within cellular compartments showed varying behaviors (Figure 3.2-3.4). For example, distal axonal regions were much more

sensitive than proximal axonal regions (Figure 3.2). This could be a byproduct of denser localization of cationic channels in distal dendritic regions where synapses form. While we did not make any measurable distinction between the two in our analysis, future investigators may find it fruitful to consider even smaller cellular sub-compartments.

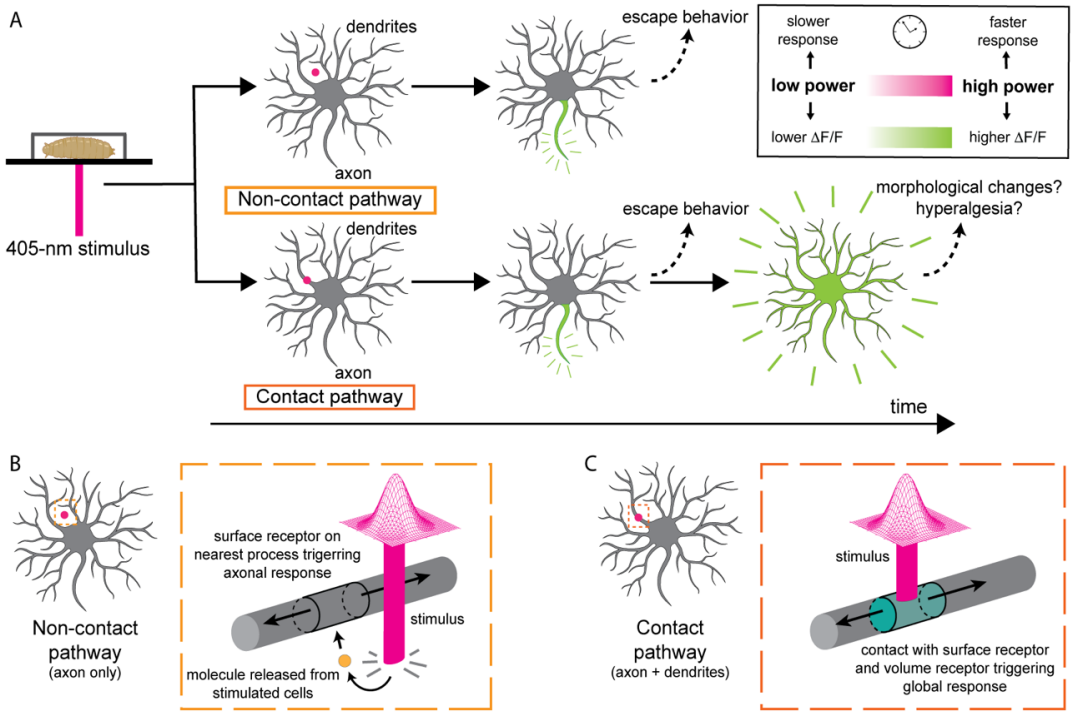

Figure 3.8: Stimulation of Class IV neurons evokes 2 distinct calcium signaling pathways. Schematic diagrams summarize features of both calcium signaling pathways. (A) Upper panels: "non-contact" stimulation (magenta dot) initiates axonal calcium responses. Lower panels: contact stimulation (magenta dot) initiates axonal and dendritic calcium responses. (B) Hypothetical mechanism underlying the "non-contact" response: damage to adjacent cells releases molecules (orange circle) that bind receptors on dendritic surface leading to cell depolarization. The depolarization is enough to trigger action potentials in the axon, which open calcium channels in the axon; the depolarization is insufficient to open calcium channels in the dendrites and soma. (C) Hypothetical mechanism underlying the "contact" response: direct damage to the dendrite strongly depolarizes the cell and opens calcium channels in dendrites, soma and axon. The contact stimulus is also expected to also trigger the "non-contact" pathway.

3.5 Materials and Methods

***Drosophila* Strains and Husbandry.** Fly lines were obtained from the Bloomington *Drosophila* Stock Center and through generous gifts from Damon Clark and Fernando Von Hoff. Fly stocks were maintained at 25°C in a humidity-controlled incubator (60% humidity) on standard apple-agar based food (Archon Scientific) with 12-hour light/dark cycles. Fly crosses were maintained in fly chambers on apple juice agar-based food (mixture of apple agar concentrate, propionic acid, phosphoric acid and water) with a generous dollop of yeast paste at 25°C, 60% humidity. Larvae 68-72 hours after egg laying were used for all imaging experiments. The following fly lines were used to image Class IV da neurons:

+ ; 20XUAS-GCaMP6f ; +	(Bloomington #42747)
+ ; ppk-Gal4 ; +	(Bloomington #32078)
+; ; ppk-CD4-tdTomato	(Bloomington #35845)
+ ; ppk-CD4-tdTomato ; +	(Bloomington #35844)
+ ; ; ppk-CD4-tdGFP	(Bloomington #35843)
+; +; shibire/(Tm6B)	
+; shibire/(Cyo); +	

Image Processing. Movies were analyzed using Image J (NIH). When necessary, movies were stabilized using the Template-Matching or Image Stabilizer plug-ins. For each cell, several regions of interest (ROI) were manually selected for each cell from 7 different locations along the entire dendritic tree to study any differential responses

within the same cell: soma (1 ROI), axon (2 ROIs), dendritic arbors (4 ROIs). Care was taken minimize background by contouring the ROI region to encompass only the cellular region being considered. Corresponding fluorescence values for each ROI were extracted in Image J and imported into MATLAB (Mathworks). Baseline fluorescence F_0 was calculated as the mean fluorescence for all frames before laser stimulation. The change in the fluorescence values from baseline (ΔF/F) was calculated as $\frac{F-F_0}{F_0-100}$ where 100 is the measured manufacturer camera offset in our system. The time series data was then cleaned by applying a median filter (width 7) to remove outliers resulting from noise or movement. Data points were linearly interpolated between known values to generate a smooth curve.

Calcium Imaging Response Criteria. The mean fluorescence value for all timepoints prior to the stimulus was designed as F_0. ROIs were scored as being responsive to the stimulus if the ΔF/F at any frame after stimulation was greater than 5 standard deviations above the baseline F_0. The largest ΔF/F value for all frames post stimulation was determined to be Peak ΔF/F (also called Max ΔF/F). The timepoint when ΔF/F was equal to or greater than 5 standard deviations above F_0 was scored as the rise time.

Modeling. Our models aim to develop a framework for the observed dendritic calcium signal magnitudes as a function of changing wattage and irradiance. As such, we inquired if physical considerations of the stimulus and dendrite geometry can account for the observed differences. The laser was modeled as a two-dimensional Gaussian

with experimentally measured wattage values as the amplitude. The spatial profile of the laser was experimentally measured using IRM by analyzing the reflection of the laser on a coverslip and using a line scan in ImageJ. A Gaussian was fit over the line scan in MATLAB to compute the standard deviation $\boldsymbol{\sigma}$. To test whether the observed laser-activated calcium transients are a surface or volume process, we considered two different models. First, we considered overlap of the laser profile with the surface of a dendrite modeled as a cylinder (Eq 1). In the second model, we considered overlap of the laser profile with the volume of a dendrite modeled as a cylinder (Eq 2), shown below:

$$F_{\mathrm{s}} = \gamma \int_{-R}^{R} \int_{-\infty}^{+\infty} \left(\frac{P}{2\pi\sigma^2}\right)^n \left(e^{\frac{-x^2-y^2}{2\sigma^2}}\right)^n \cdot 2\sqrt{1 + \frac{x^2}{R^2 - x^2}}\, dx\, dy \quad (Eq\ 1)$$

$$F_{\mathrm{v}} = \gamma \int_{-R}^{R} \int_{-\infty}^{+\infty} \left(\frac{P}{2\pi\sigma^2}\right)^n \left(e^{\frac{-x^2-y^2}{2\sigma^2}}\right)^n \cdot 2\sqrt{R^2 - x^2}\, dx\, dy \qquad (Eq\ 2)$$

Here, $\boldsymbol{F_s}$ and $\boldsymbol{F_v}$ are the theoretical Peak ΔF/F corresponding to each model, $\boldsymbol{P}$ is the laser power, $\left(\frac{1}{2\pi\boldsymbol{\sigma}^2}\right)$ is a Gaussian normalization constant, $\boldsymbol{\sigma}$ is the standard deviation of the Gaussian, and $\boldsymbol{R}$ is the radius of the dendrite being considered. Rather than considering the soma as a sphere, a simplification was made by modeling the soma with a cylindrical radius $\boldsymbol{R}$ significantly larger than that of proximal and distal dendrites. This simplification is justified as the laser profile dies off exponentially and $\boldsymbol{\sigma} << \boldsymbol{R_{soma}}$. The variable $\boldsymbol{n}$ is a free parameter introduced to account for the observed nonlinearity in

experimental values, and $\boldsymbol{\gamma}$ is a free parameter corresponding to a unit conversion factor.

$\boldsymbol{P}$ ranged between 0 to 100 based on the power output of the laser. $\boldsymbol{\sigma}$ was set at 212.31 nm or 424.62 nm, corresponding to the two different stimulation irradiance settings. Existing measurements made in the lab were used as input parameters for the radii of dendritic processes: $\boldsymbol{R}$ was 500 nm for proximal dendrites, 200 nm for distal dendrites, and 1000 nm for soma. Because Peak ΔF/F (also referred to as Max ΔF/F) exhibited unequal variances (heteroskedasticity) across the range of stimulation wattages, we had to perform a weighted least square fitting procedure. We computed a set of weights for use in our weighted least squares fitting by performing a linear regression between the ΔF/F and the experimental SEM. A strong linear correlation between ΔF/F and the experimental SEM was found (see Supplementary Materials).

MATLAB's *fminsearch* was then used to compute the values for **n** and $\boldsymbol{\gamma}$ that simultaneously minimized the sum of the squared errors between all theoretical and experimental values. The search was initialized by arbitrarily choosing initial parameters for **n** and $\boldsymbol{\gamma}$ (**n** = 2 and $\boldsymbol{\gamma}$ = 100). Minimization was performed by considering data from axon ROIs and non-axon ROIs separately. Values predicted by the surface model were plotted with a dashed line and values predicted by the volume model were plotted with a dotted line, as denoted in the figure legend.

Statistical Analysis. Sample sizes are listed for each data set on the corresponding plots. Capitalized 'N' indicates number of larvae; lowercase n is number of neurons.

Statistical analysis was performed in Prism 8 (GraphPad). Sidak's test was used when making pairwise comparisons of multiple comparisons. One-way analysis of variance (ANOVA) was used to determine if statistically significant differences existed between the means of three or more independent groups. For plots showing Peak ΔF/F, all data points (open circles) and experimental means (lines) are shown on graphs to demonstrate experimental variability. For plots showing Rise Time, experimental means and SD are shown. Significance was evaluated at $p<0.05$.

3.6 Supplementary Materials

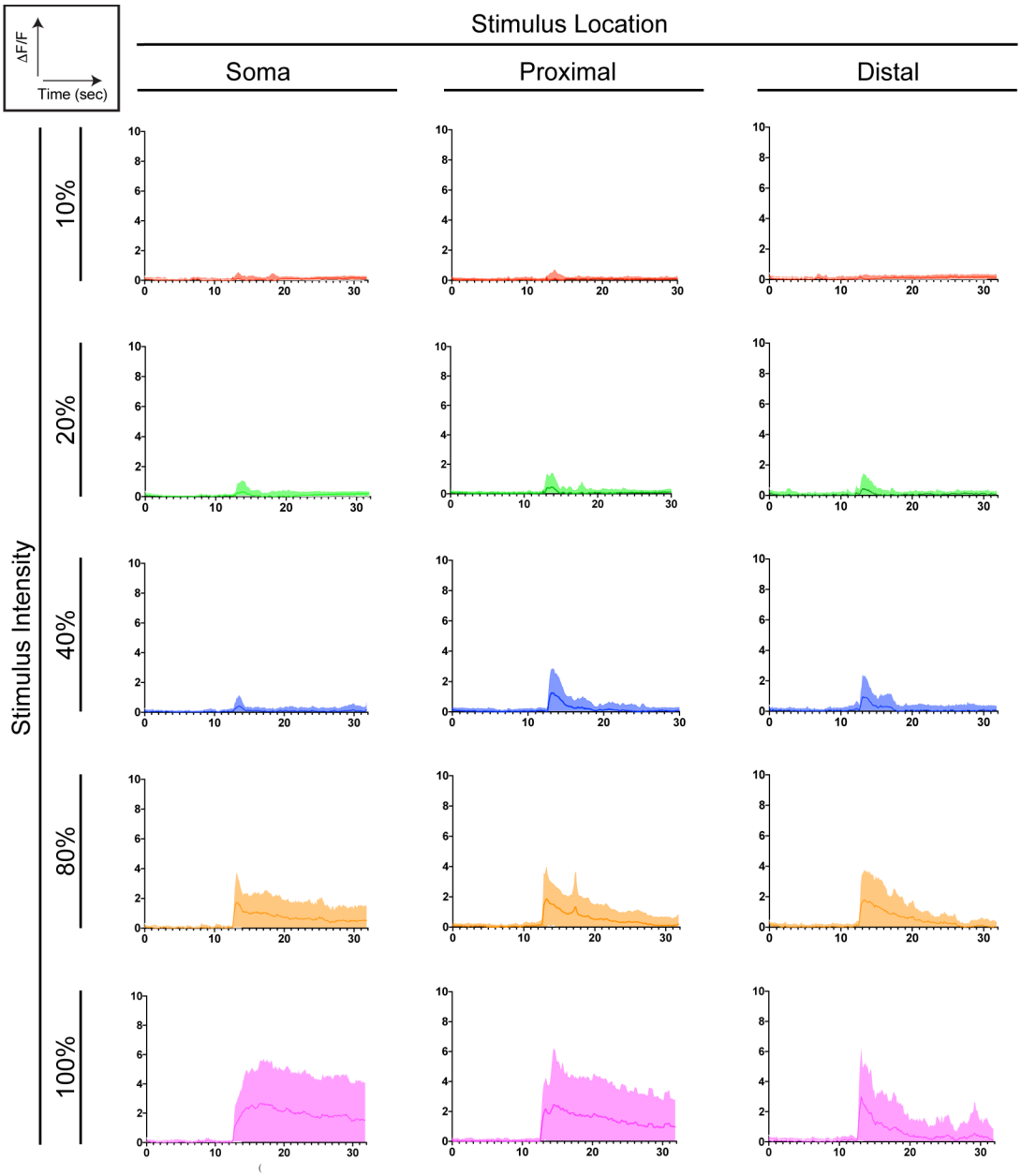

Supplementary Figure 3.1: Representative ΔF/F traces of only axon ROIs for varying stimulation locations and wattages. Stimulus was activated at the 12.43 second mark (100 frames). Data across all experiments were combined. Mean and SD shown.

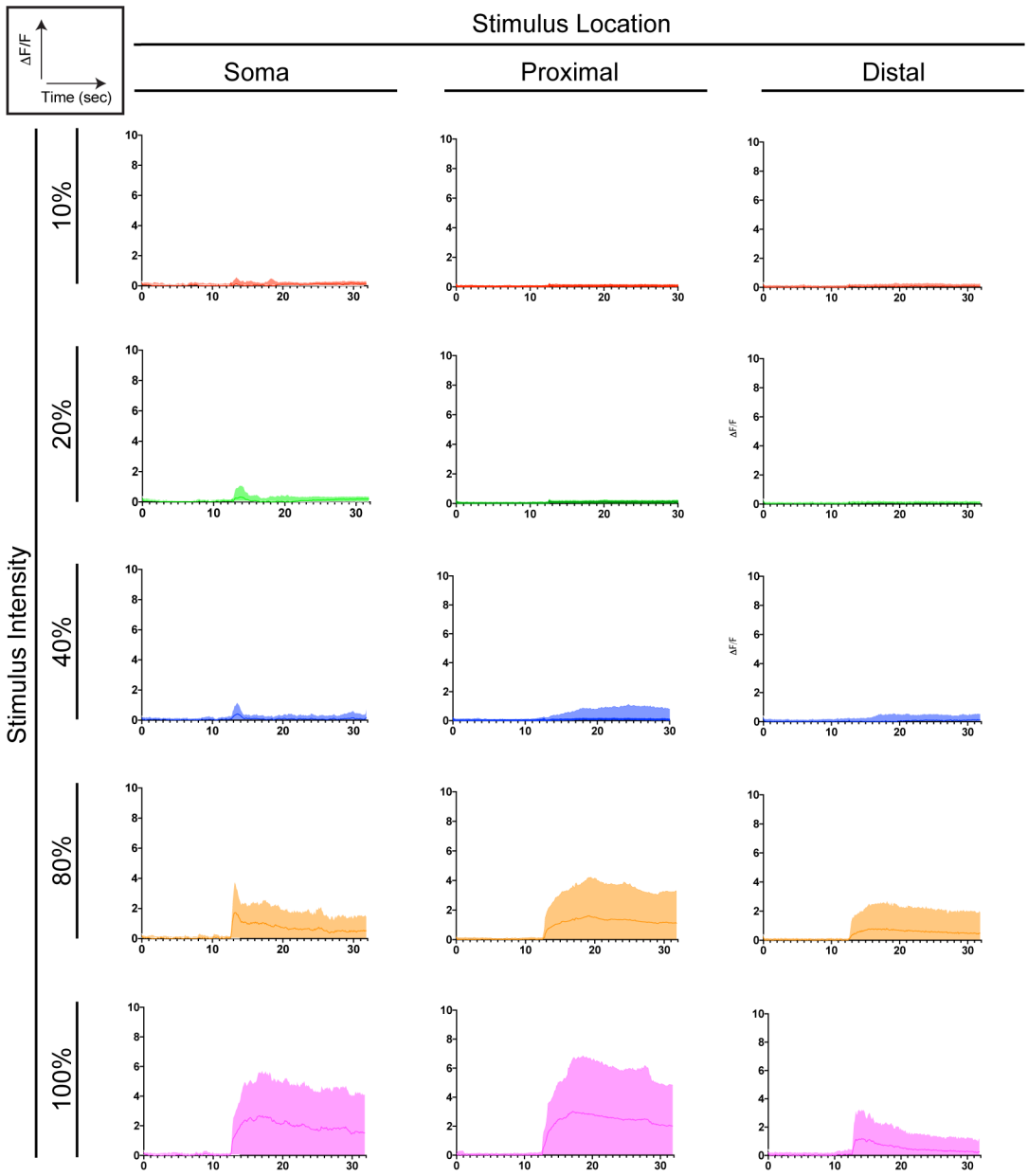

Supplementary Figure 3.2: Representative ΔF/F traces of only dendrite & soma ROIs (combined) for varying stimulation locations and wattages. Stimulus was activated at the 12.43 second mark (frame 101). Data across all experiments were combined. Mean and SD shown.

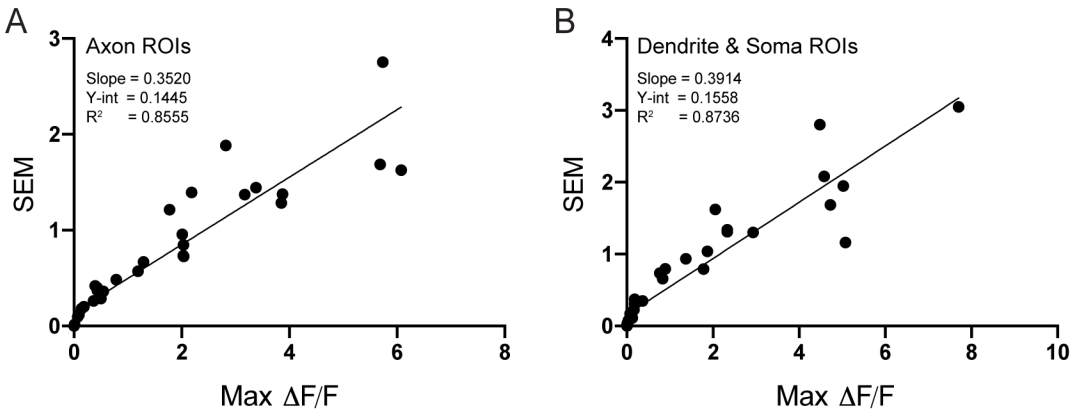

Supplementary Figure 3.3: Linear correlation between Peak ΔF/F (Max ΔF/F) and Standard Error of the Mean (SEM) was used to generate a noise model for Weighted Least Square (WLS) regression weights. Goodness of fit parameters are shown within corresponding plots in Figure 3.6 and Table 8. (A) Relationship between SEM and Peak ΔF/F for data from all axon ROIs. (B) Relationship between SEM and Peak ΔF/F for data from all dendrite and soma ROIs, combined.

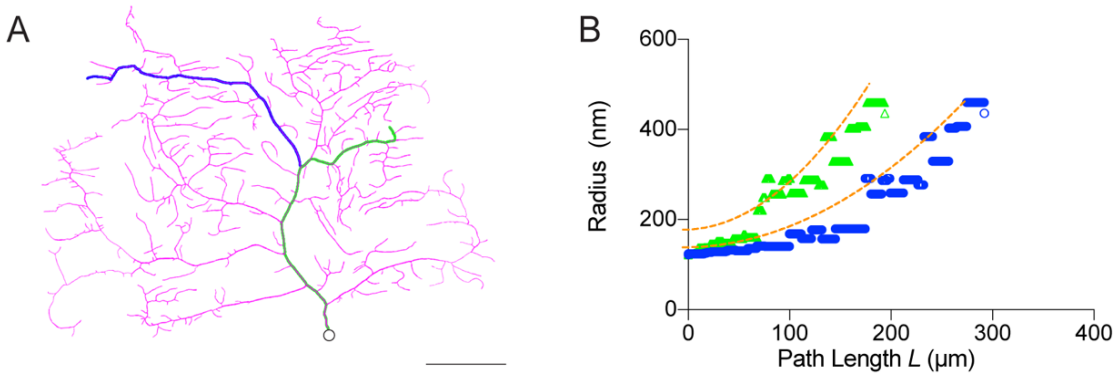

Supplementary Figure 3.4: The diameter of dendritic arbors in CLIV neurons taper away from the cell body. Larvae expressing *shibire* and ppk-CD4-Td-Tomato were imaged 130 hours AEL. (A) Skeletonized image of Class IV neuron highlighting arbors that were measured. Scale bar is 50 μm. (B) Radius of corresponding dendritic arbors. Measurements taken by Dr. Maijia Liao.

3.7 Research Contributions

All experiments and modelling were conceptualized in conjunction with Dr. Jonathon Howard. Automation of the image analysis protocol in MATLAB was done in collaboration with Dr. Sabyasachi Sutradhar. Gratitude to Dr. Ania Luchniak and Dr. Sonal Shree, who helped optimize experimental conditions used for sample immobilization and calcium imaging. Part of the data shown was collected in collaboration with Christian Freniere during his laboratory rotation.

Nothing ever exists entirely alone;
everything is in relation to everything else.

–Gautama Buddha (563 - 483 B.C., *approx.*)

Chapter 4:
Investigating Downstream Effects on Functional Dynamics and Arbor Morphometrics

4.1 Abstract

Having studied somatosensory properties in Class IV neurons (Chapter 3), we next turned our attention to the functional purpose of the dendritic "contact" pathway. Based on preliminary evidence, we focused our efforts on probing two main questions: (i) do global dendritic calcium transients in response to stimulation result in nociceptive cellular hypersensitization? (ii) do evoked dendritic calcium signals actively alter morphological features of Class IV arbors? To test the former, we stimulated Class IV neurons at periodic intervals and analyzed the resulting calcium signaling magnitudes. For the latter, we studied morphometric properties of Class IV arbors before and after stimulation using an in-house software capable of tracking dendritic arbors to sub-pixel accuracy. While we do not find evidence of hypersensitization in Class IV cells, we do observe changes to the morphology of stimulated arbors. However, the precise the role calcium in mediating these structural changes requires further investigation.

4.2 Introduction

In Chapter 3, we characterized the receptive properties of Class IV dendritic arbors and found the presence of two distinct calcium signaling pathways based on the location of the stimulus. While we could reasonably reconcile the "non-contact" axonal pathway as being part of the canonical neuronal circuit associated with neuronal activation, the purpose of the "contact" dendritic pathway remained unclear. This chapter details some of our efforts in trying to uncover the functional motivation for activation of the "contact" dendritic pathway. Broadly, our thinking revolved around two distinct ideas: (i) cellular nociceptive sensitization and (ii) morphological dynamicity.

Do sensory evoked calcium transients result in nociceptive sensitization in individual Class IV neurons?

First, we wanted to see if global dendritic calcium transients were altering functional features of Class IV neurons. More specifically, we were interested in seeing if activation of the dendritic pathway was changing the cellular sensory properties that we investigated in Chapter 3. Evidence from other systems drove our motivation into this line of inquiry (Simonetti et al., 2013; Marger et al., 2011). For example, nociceptive hypersensitivity in response to tissue damage, a well-studied phenomenon in vertebrate and invertebrate model organisms, serves as a crucial defense mechanism that results in enhanced behavioral responses while the afflicted tissue undergoes healing. It has been reported that exposure to noxious stimuli results in nociceptive

sensitization in organisms including *Aplysia* (Illich and Walters, 1997), *Manduca sexta* (Walters et al., 2001; McMackin et al., 2016), and *Hirudo medicinalis* (Burrell and Sahley, 1998). In *Drosophila*, nociceptive sensitization has been reported via involvement of BMP/SMAD (Follansbee et al., 2017), cytokine signaling/tumor necrosis factor (Babcock et al., 2009), Hedgehog (Hh) (Babcock et al., 2011b), and tachykinin (TK) (Im et al., 2015) pathways in response to ultraviolet- and thermal-induced sensitization of larval tissue. Given this background, we hypothesized that focal puncture wounds to the larval body wall may similarly result in heightened sensitization to stimuli at the single cell level, which we could measure via altered calcium signaling magnitudes as compared with baseline (Chapter 3). If true, this could be rationalized as a larval defense mechanism and would open up additional lines of inquiry regarding the precise role of the induced dendritic calcium transients.

Do sensory evoked calcium transients result in measurable morphological changes to arbors of Class IV neurons?

In looking for a potential downstream effect of the "contact" dendritic pathway (Chapter 3), we also studied the impact of evoked dendritic calcium signals on the morphology of Class IV dendritic arbors. This line of inquiry was motivated by several pieces of evidence. First, prior studies have suggested that Class IV arbors tile the larval body wall to near uniform coverage without overlapping regions to maximize their ability to sense and mediate escape behaviors to noxious stimuli (Grueber et al., 2002; Hwang et al., 2007a; Ganguly et al., 2016). Larvae with aberrant or underdeveloped or silenced Class IV neurons demonstrate markedly reduced ability to

initiate rolling and writhing behaviors needed for effective evasion of noxious stimuli (Robertson et al., 2013; Hwang et al., 2007a). Thus, there is an in-built, well-studied link between the morphology and function of Class IV neurons. Secondly, there is evidence showing that compartmentalized calcium transients in neurons spatiotemporally regulate dendritic growth and pruning events in a number of biological systems (Rosenberg and Spitzer, 2011). For example, timed dendritic calcium signaling events mediate localized pruning in Class IV neurons and blockage of voltage-gated calcium channels results in impaired ability to eliminate branches (Kanamori et al., 2013). Relatedly, studies in zebrafish (Ashworth and Bolsover, 2002; Vargas et al., 2015) and *Aplysia* (Spira et al., 2001) have shown that spontaneous and evoked intra-cellular elevations in calcium concentrations contribute to axonal regeneration and degradation, and calcium transients actively regulate the formation, stability, and dynamics of cytoskeletal structures like microtubules and F-actin in mouse neurons (Merriam et al., 2013; Oertner and Matus, 2005) and other systems (Gasperini et al., 2017). Third, we observed subtle visual cues during our prior experiments of altered dendritic tip dynamics (for details, see Chapter 1) in Class IV arbors in response to stimulation. Notably, we observed on a number of occasions that regions >500um away from the site of stimulation demonstrated elevated levels of dynamic growth and shrinkage events as compared with control unstimulated cells (data not shown). Taken together, these pieces of evidence led us to consider the possibility that the "contact" dendrite pathway may be involved in morphoregulation of dendritic arbors by either increasing or decreasing tip dynamics, and, as a result, overall branch growth and shrinkage rates. This could plausibly be useful from a

behavioral standpoint. For example, increase tip dynamics in response to noxious stimuli could increase coverage density of Class IV arbors or act as associative signals for synaptic plasticity, thereby enhancing ability to sense any subsequent stimuli.

As a way to test this hypothesis, we segmented our experiments into two lines of inquiry. First, we wanted to study the "bulk" properties – i.e., total branch length, total branch number, total coverage area – of Class IV cells before and after stimulation. Secondly, we evaluated the remodeling of individual growing and shrinking dendritic tips as a metric for morphological dynamicity. Using an in-house tip segmentation and tracking software, we set out to evaluate the dynamicity of dendritic tips in pre- and post- stimulation conditions. We find that although our results show evidence of morphological changes in response to stimulation, the role of the evoked dendritic calcium signals in this context is inconclusive and warrants further careful investigation.

4.3 Results

Single class IV neurons do not show evidence of nociceptive hypersensitization

To test if activation of the dendritic contact pathway was resulting in hypersensitization of Class IV neurons we probed cells in a number of ways: in the first set of experiments, we stimulated the same set of cells seven times – first three stimuli were at a low power setting (10%), fourth was at a high power setting (80%) and the last three were again at a low power setting (10%). We reasoned that if the response threshold of individual class IV neurons could be altered by large dendritic calcium signaling events, we would notice a difference in signaling magnitudes between the first three and last three low power stimuli. In the second set of experiments, we probed the same set of cells at high power (80%) four times consecutively and analyzed the resulting calcium signaling magnitudes. In this case, as an alternate approach to the first experiment, we hypothesized that any induced hypersensitivity would manifest in larger signaling magnitudes for stimulations subsequent to the first.

In the first set of experiments, we observed response frequencies and calcium signaling magnitudes that were consistent with our prior experiments. Probes at 10% power resulted in a low frequency of responses and small calcium signaling magnitudes ~0 Peak ΔF/F across all three stimulations (Figure 4.1A). The fourth stimulation at 80%, as expected, resulted in a much high response frequency (100%) and large calcium signaling magnitudes: Mean Peak ΔF/F of ~6 for all ROIs combined (Figure 4.1A). The last set of stimuli at 10%, again, resulted in responses in line our previous observations at 10% power at ~ 0 Peak ΔF/F. Contrary to our expectation, we did not find any

difference between the first three and last three stimulations at 10% power (one-way ANOVA, not significant); there was no evidence of heightened cellular responsiveness as measured by calcium signaling magnitudes.

We then performed the second test of probing the same set of cells repeatedly at 80% power on proximal dendritic arbors (<50um from the cell body). To ensure that we were not stimulating an arbor severed by a preceding stimulus, we focused our laser in a new location for each subsequent stimulus. Our first probe at 80% resulted in cellular response magnitudes comparable to those we had observed before (average Peak ΔF/F of ~6 for all ROIs combined) (Figure 4.1B). Interestingly, subsequent stimulations resulted in responses that were smaller in magnitude. To be certain that this was not an artifact of persistent elevated calcium levels after each stimulus, we waited 2-3 minutes between each stimulus till the baseline fluorescence was on par with pre-stimulus levels. We find that, although Class IV neurons are capable of responding multiple times to stimuli, large stimuli result in cellular "fatigue" wherein responses subsequent to the first are less frequent and smaller in magnitude (Figure 4.1B). Thus, rather than hypersensitization, we see some evidence that could be interpreted as lowered sensitivity, as measured by calcium signaling magnitudes (though there are considerations of elevated baseline calcium levels as a result of initial stimulation). Although we did not pursue this further, future work interested in characterizing these properties may benefit from longer rest intervals between consecutive stimuli. This may highlight any changes to cellular response properties that require some latency before they materialize.

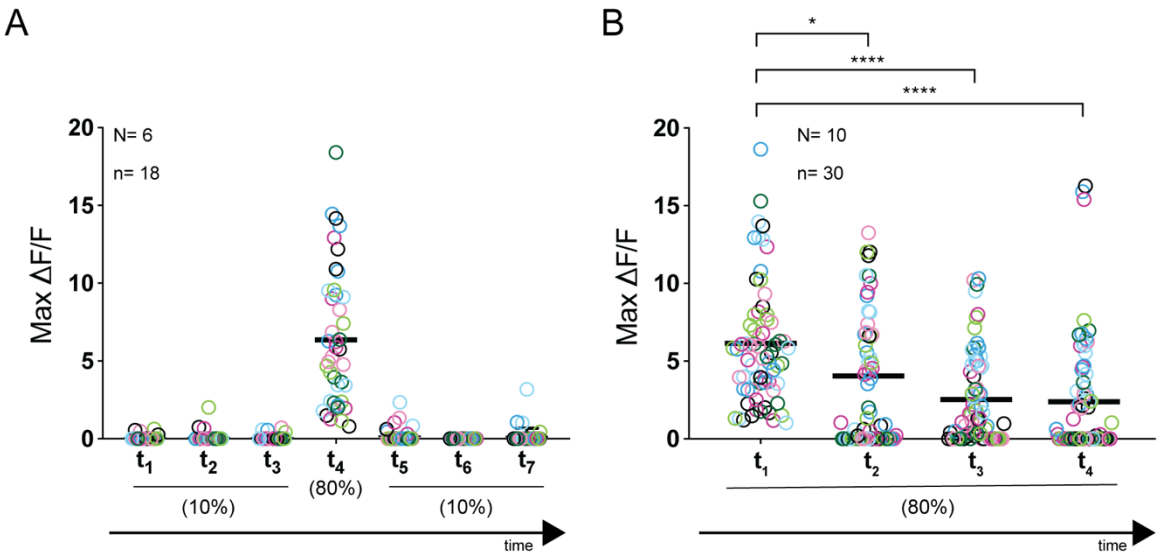

Figure 4.1: Individual Class IV neurons do not show evidence of nociceptive hypersensitization post stimulation. Black lines denote mean of all ROIs. FWHM of stimulus was 0.5 µm (40X objective). Plots are color coded as described previously (Chapter 2, *Materials and Methods*). (A) Calcium signaling magnitudes for cells stimulated seven consecutive times at varying locations along the dendritic tree. First three stimuli were at 10% power, fourth stimulation was at 80% power, and last three stimuli were at 10% power. Stimulus was rendered for 100ms in each instance. Interval between each consecutive stimulation was 60-90 seconds. No difference between average magnitudes of cells stimulated at 10% power (Ordinary one-way ANOVA, p = 0.2228, not significant) (B) Calcium signaling magnitudes for cells stimulated at 80% power four consecutive times at varying locations along the dendritic tree. 100ms exposure. Interval between each consecutive stimulation was 2-3 minutes to allow intracellular calcium levels to return to baseline.

405nm stimulation does not result in detectable short-term changes to bulk morphometric properties of Class IV arbors

We next investigated if calcium transients evoked via the "contact" dendritic pathway could be affecting "bulk" morphological properties of Class IV neurons. The use of the work "bulk" is meant to draw contrast with dynamics at the level of individual tips, which we explore later. Building on prior work that has implicated spontaneous calcium transients in morpho-regulation, we hypothesized that stimulus-evoked calcium signaling events may trigger accelerated growth or global pruning of dendritic arbors. To study this, we used a custom, in-house, semi-automated software that is capable of skeletonizing images of dendritic arbors and computing locations of dendritic tips to sub-pixel accuracy (For details, see Supplementary Materials Figure 4.1 - 4.3 and *Materials & Methods*). Using this method, we were able to measure morphometric properties (for example, overall branch length, branch number) of entire dendritic arbors in control and stimulated cells over time.

We first established a set of baseline values by studying 10 cells (6 larvae) over a 30-minute period. To do this, we measured values for total branch length and branch number via maximum-projected z-stacks acquired every 5-minutes. Although we observed normal dendritic tip dynamics (Figure 4.2 A-F), control cells did not show large changes to overall bulk morphometric properties over 30 minutes (Figure 4.2 G, H). We next performed the same analysis for 6 cells (6 larvae) that were stimulated at the 5-minute mark (80% power, 100 msec exposure). Our results did not show any measurable departure from the dynamics observed for control cells (Figure 4.2 I-J). It is possible, however, that any changes to the bulk morphometrics may occur over

longer time scales. Since our current experimental set-up limited us to ~30 minutes of continuous imaging (Chapter 2), we were not able to directly probe that possibility in this experiment.

We were curious to see similar response features were consistent across all stages of larval development. Since dynamicity of dendritic tips is highest in the embryo and early instar stages (*unpublished data*, Howard lab), we hypothesized that reorganization of dendritic tips may be more readily apparent in younger larval samples. To test this, we repeated the same experiment on samples 18 hours AEL using a slight modification of the imaging protocol (Supplementary Figure 4.4). While control cells (no stimulus) were completely unaffected (Supplementary Figure 4.4A, B, E), interestingly, stimulation of larvae 18 hours AEL showed prominent morphological changes in response to stimulation. Rather than localized pruning of the stimulated arbor, the entire dendritic arbor demonstrated severe signs of degradation (Supplementary Figure 4.4C, D, F). Closer inspection revealed that our stimulation assay was lethal to these younger samples – 8 out of 10 embryos did not develop into larvae (we had previously confirmed that our protocol was non-lethal to larvae >65 hours AEL, See Chapter 2). This is likely due to the much thinner and structurally less robust cuticle and epidermis of younger larvae. In light of this, we limited our investigations to larval samples 68-72 hours AEL henceforth.

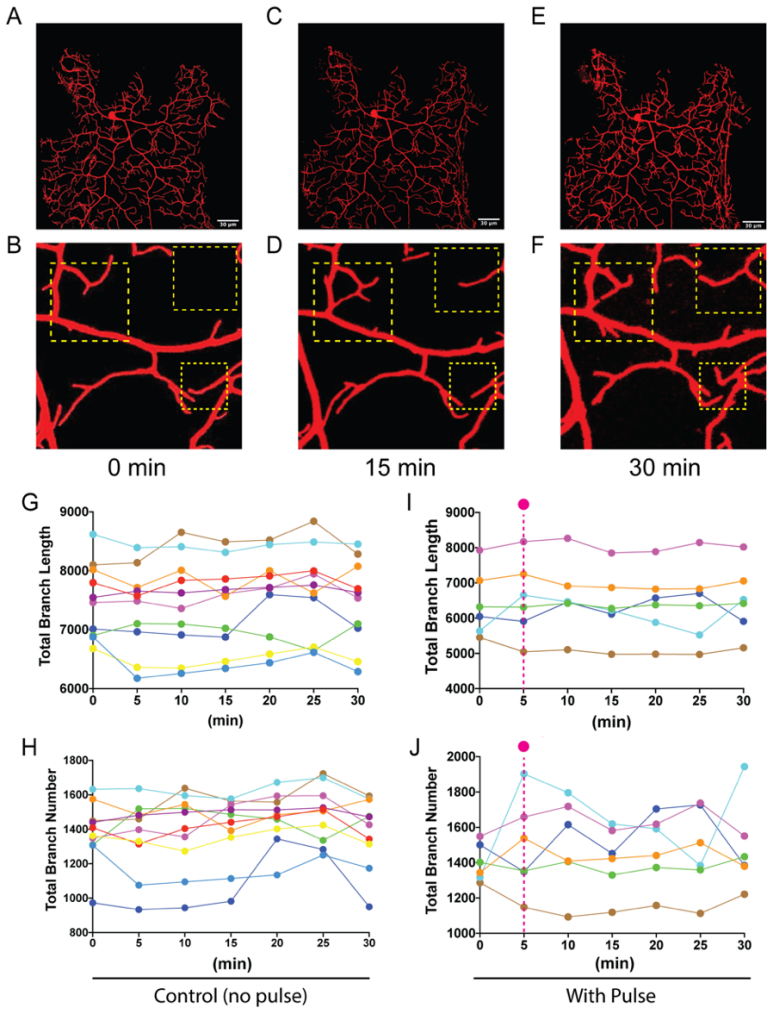

Figure 4.2: There are no detectable net changes to "bulk" morphometric properties of Class IV dendritic arbors within 25 minutes following stimulation. Images are of cells are expressing CD4-td-Tomato. (A-F) Maximum projection images from z-stacks unstimulated Class IV neurons in late second instar larvae (~68-72 hours AEL) demonstrating dendritic tip dynamics. Cell boundaries in max-projections were cropped using user-defined ROIs. Panels in second row (B, D, F) are zoom-ins of corresponding images above. Dashed yellow boxes highlight example regions where tip reorganization is prominent. (G-H) Morphometric properties of control cells (no stimulus) showing (G) total branch length as a function of time and (H) total branch number as a function of time. (I-J) Morphometric properties of stimulated cells (80% power) showing (I) total branch length as a function of time and (J) total branch number as a function of time. Stimulus was rendered at the 5-minute mark for 100 ms.

Localized puncture injuries to Class IV cells results in localized pruning of stimulated dendritic arbor over longer time scales

We were interested in testing for the possibility that morphological changes to dendritic arbors were occurring on time scales longer than we were previous imaging. To circumvent our ~30 minute continuous imaging constraint (Chapter 2), we adopted an alternate imaging protocol. Samples were pulsed and a z-stack of the stimulated cell and its neighboring cell were taken before they were recovered back to apple agar plates. The same cells were located and imaged again 24 hours later. Samples were probed directly on arbors ("contact" dendritic pathway, See Chapter 3) and also in regions not tiled by dendrites ("non-contact" axonal pathway, See Chapter 3). As an additional control, neighboring cells were imaged but not stimulated.

We found that, barring expected growth, there were no apparent changes to the morphology of control cells (no stimulus). The same was true for samples where the stimulus did not directly make contact with the dendritic arbors, over a 24-hour period (Figure 4.3A, B) (N=6). Morphological features of cells were largely unchanged and cells tiled the larval body with uniform coverage. However, cells directly contacted by the stimulus (80% Stimulus Intensity) did show significant morphological changes (N= 6) Notably, the pulsed arbor was entirely pruned over 24 hours, leaving behind a region completely untiled by Class IV processes (N= 6) (Figure 4.3C, D). This was true for 100% of samples where contact was made with a dendritic arbor (6 out of 6). Contrary to our expectations, neighboring arbors within the same cell were unaffected. To investigate if this effect was localized or systemic, we also imaged cells neighboring to stimulated neuron. Cell neighbors on either side showed no apparent changes to the

morphological features of neighboring cells in all instances (N = 6), suggesting that the effect of the stimulus was limited only to the afflicted arbor (Figure 4.3 E, F).

Interestingly, we noticed a few new processes in the untiled regions left behind by the pruned arbor (Figure 4.3D, F). Similar invasion of dendritic processes has been reported before in Class IV dendrites (Parish, 2010). However, in our case, it was not clear if these processes were previously present at the time of stimulation or if they were the result of (i) invagination from neighboring arbors or (ii) regrowth of the pruned arbor. The persistent reorganization of dendric tips and technical challenges with imaging and image analysis (tracking of individual arbors) make this a challenging question to answer. We are in the process of investigating alternate methods to perform time-lapse imaging over 24-48 hours at 4-6-hour intervals, which would provide additional insight into the onset and dynamics of the degradation and/or regrowth processes.

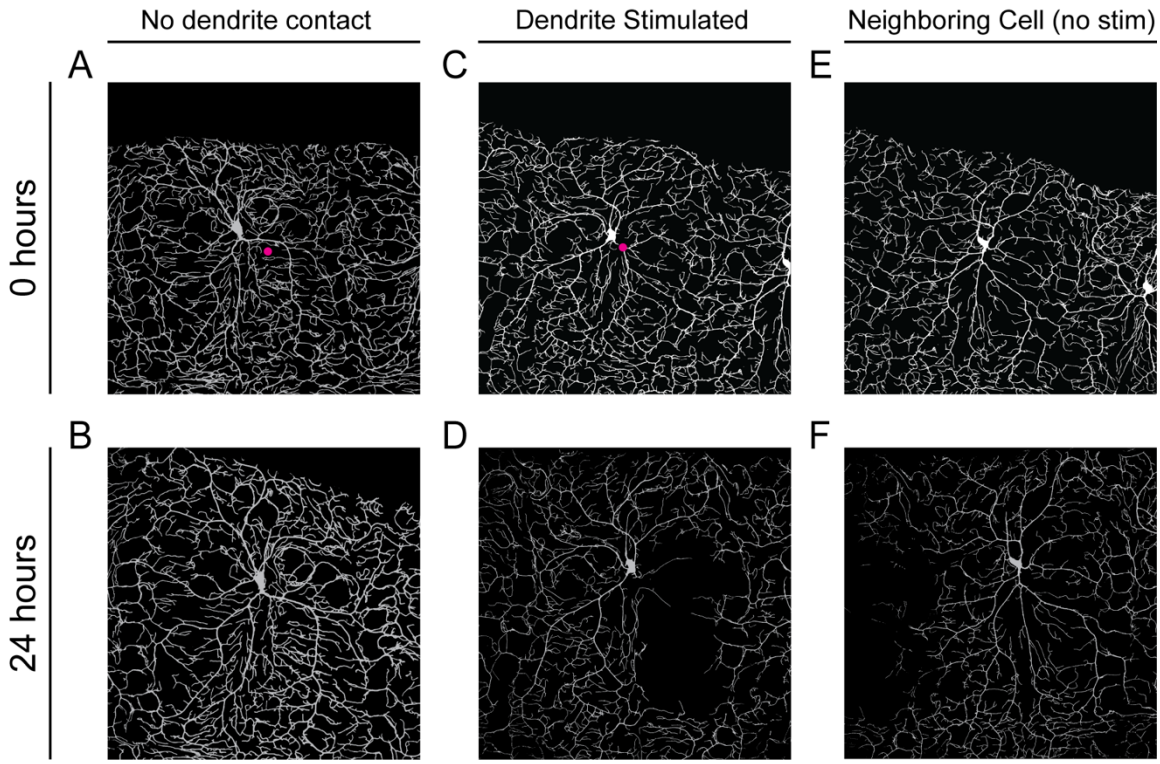

Figure 4.3: Direct contact with Class IV arbors results in localized pruning over 24 hours. Samples were 68-72 hours AEL. Magenta dot denotes location of stimulus. Cells were expressing CD4-td-GFP. All images are maximum-projected z-stacks. (A) Image Class IV neuron immediately before stimulation. Stimulus was directed at empty regions not tiled by dendritic arbors. (B) Image of Class IV neuron from panel A 24 hours following stimulation. (C) Image of Class IV neuron immediately before stimulation (80% stimulation intensity). Stimulus was directed to make contact with dendritic arbor. (D) Image of Class IV neuron from panel B 24 hours following stimulation. (E-F) Image of Class IV neuron immediately neighboring cell shown in panels C and D prior to stimulation and 24 hours after stimulation.

Focal puncture wounds to Class IV neurons results in altered tip velocities and transition rates within 15 minutes of stimulation

As a follow up to our results showing pruning in response to 405 nm stimulation, we decided to look closer at the dynamics of individual dendritic tips. While our previous experiment conclusively demonstrated that the stimulated arbors undergo degradation over 24 hours (Figure 4.3), it remained unclear if dendritic tips on unstimulated arbors within the same cell were affected. We reasoned that while our analysis of "bulk" morphometric properties did not yield measurable changes, it was still possible that stimulation of Class IV cells resulted in changes at the level of individual dendritic tips (tip growth velocities, trajectories, etc) (see Chapter 1). We thus asked the question: do focal puncture injuries result in altered tip dynamics in stimulated Class IV neurons? To test this, we analyzed the trajectories and transition frequencies of a representative sample of dendritic tips from cells under control conditions and then re-analyzed then post-stimulation conditions (for details, see *Materials and Methods*).

We spent a considerable amount of time rigorously establishing a baseline set of values for the growth dynamics of dendritic tips under control conditions. As expected, we found that dendritic tips in cells imaged under standard conditions with no stimulation showed net positive growth over 15 minutes (0.017 μm/min, N= 10 larvae, 217 dendrite tips) (Figure 4.4 A-C). The average growth rate and variance of the data was in good agreement with exiting data in our laboratory studying the growth dynamics of larvae ~72 hours AEL (Howard Lab, data not shown). Likewise, the velocities and distribution of tips in growing, paused, and shrinking states were in line

with our previous observation for larvae of our given age (Figure 4.4D). The distribution of tips was 33% (paused state), 33% (shrinkage state) and 34% (growing state); average velocity values were (2.00 ± 0.50 μm/min, growing tips), (-1.81 in ± 0.49 μm/min, shrinking tips) and (0 ± 0.35 μm/min, paused tips) (Figure 4.4). Our analysis of the transition rates between these states further established a baseline against which we could compare any deviations in stimulated cells (Figure 4.4F).

Having established a set of baseline values, we next turned our attention to cells in the post-stimulus condition. Cells were pulsed for 100ms in proximal dendrites at 80% wattage – conditions which we previously demonstrated can reliably damage the larval cuticle and induce nociceptive responses in Class IV neurons (see Chapter 2, Chapter 3, *Results*). Importantly, in order to make an apples-to-apple comparison, the same cells that we studied in our control experiments were pulsed and evaluated again under post-stimulation conditions.

Interestingly, analysis of dendritic tips post-stimulation (N = 10 larvae, 144 dendrite tips) demonstrated overall decline in average tip length 15 minutes post stimulation – net negative growth rate of -0.023 μm/min. This is in contrast to our control baseline value of 0.017 μm/min ($p = 0.0435$, t-test with Welch's correction). The distribution of dendritic tips in each state also deviated from controls with more tips in growing and shrinkage states and less tips in the paused state: 29% of tips were in the paused state, 35% of tips were in the shrinkage state, and 36% of tips were in the growing state (Figure 4.4E). In addition, both, the velocities of growing and shrinking tips were higher in post stimulation conditions; whereas control movies demonstrated mean velocities of -1.8 ± 0.49 μm/sec (shrinkage) and 2.0 ± 0.50 μm/sec

(growth), pulsed cells showed increased dynamics with values of -2.45 ± 0.54 μm/sec (shrinkage) and 2.54 ± 0.57 μm/sec (growth) (Figure 4.4E). This corresponds to a velocity change on the order of 35% (shrinkage) and 27% (growth) (Figure 4.4D-E).

Furthermore, transition rates between states echoed a similar trend: the rate of transitions between *growth* → *shrinkage* states and *shrinkage* → *growth* states were increased in post-stimulation conditions as compared with baseline. (Figure 4.4F, G). Whereas control cells showed *growth* → *shrinkage* transition rates of 0.67 ± 0.029 transitions • min^{-1}, post-stimulus cells demonstrated *growth* → *shrinkage* rates of 0.82 ± 0.041 transitions • min^{-1} (Figure 4.4F, G). Likewise, stimulated cells showed *shrinkage* → *growth* transition rates of 0.75 ± 0.031 transitions • min^{-1}, post-stimulus cells showed *shrinkage* → *growth* rates of 0.97 ± 0.045 transitions • min^{-1} (Figure 4.4F, G). The transition rate to and from the paused state, on the other hand, were lower in post-stimulus conditions (Figure 4.4F, G).

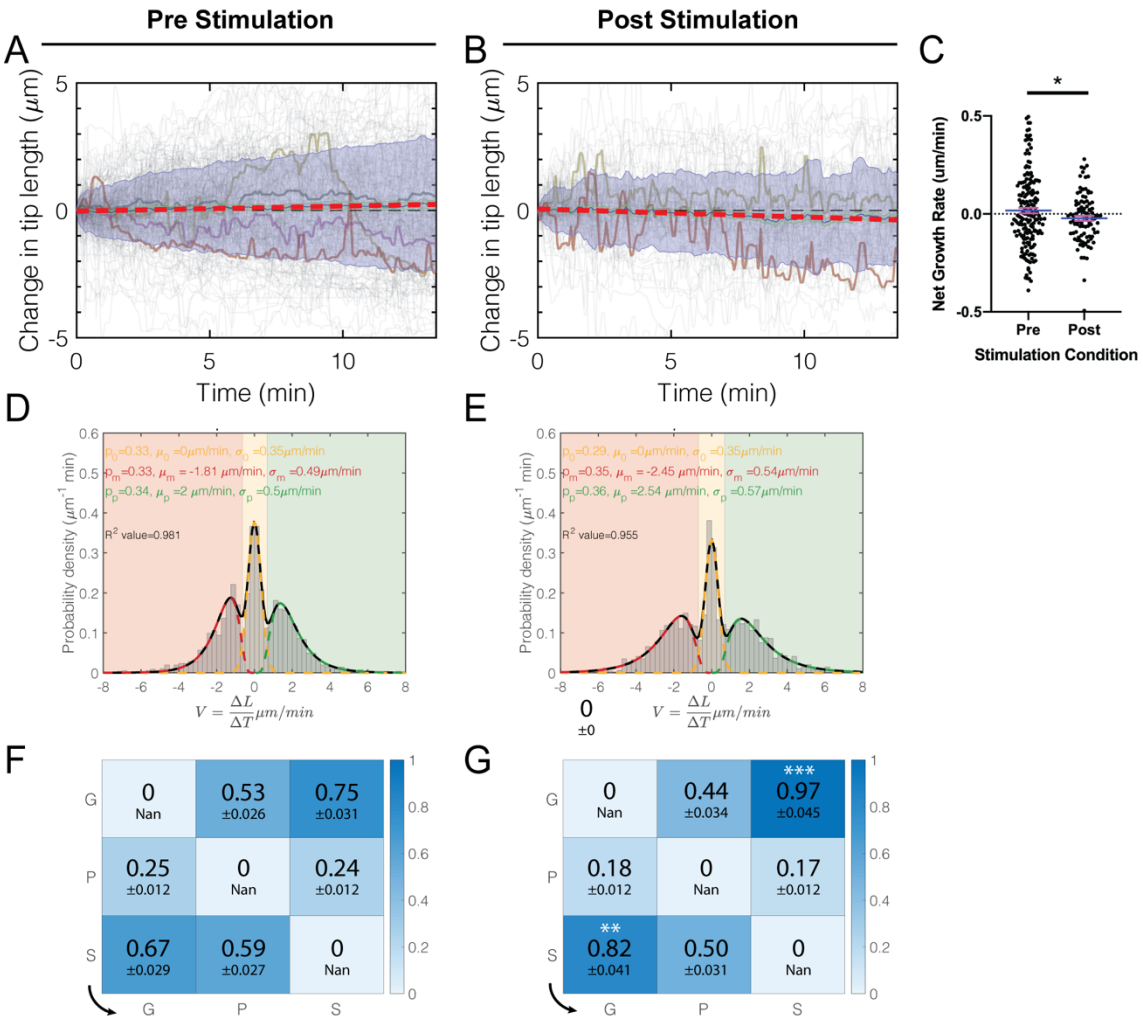

Figure 4.4: Quantification of dendritic tip dynamics pre- and post- 405 nm stimulus. (A-B) Length of dendritic tips over time for (A) pre-stimulation conditions (n_{tips} = 217, n_{cells} = 10, N = 10) and (B) post-stimulation conditions (n_{tips} = 144, n_{cells} = 10, N = 10). Red line indicates mean change in tip length. Dashed black lines indicates zero change. Highlighted region in blue represents standard deviation of all traces. Some representative traces are highlighted. (C) Net overall growth rate for dendritic tips in the pre-stimulation condition (0.017 μm/min) and post-stimulation condition (-0.023 μm/min). (D-E) Distribution of dendritic tip velocities in growing, shrinkage and paused states for (D) pre-stimulation conditions and (E) post-stimulation conditions. (F-G) Matrix showing transition rates between growing (G), paused (P) and shrinkage (S) states ± SEM. Units of min^{-1}.

4.4 Discussion

In this section, we investigated several hypotheses for downstream effects of the "contact" dendritic pathway. First, we investigated if puncture wounds to Class IV cells induced hypersensitization of individual neurons. Prior work has found that UV- and thermal - induced damaged to cell tissue in *Drosophila* causes hyperalgesia, resulting in accentuated behavioral responses to sub-traumatic stimuli (Follansbee et al., 2017; Babcock et al., 2009, 2011a). However, it is worth noting that the stimulus used in these studies is not entirely comparable our assay. Whereas these studies irradiate larval tissue with UV-light (λ = 254 nm) using semi-widefield illumination, our assay is delivering highly focal wounds to the larval body with light in the visible spectrum (λ = 405 nm) that are localized only to Class IV neurons and the immediate surrounding tissue. Furthermore, whereas the authors found that UV irradiation results in behavioral changes, whether this hypersensitization manifests similarly in individual Class IV cells is not known. Our assay offered a method for us to evaluate this question.

In our experiments, we did not find evidence to show that individual Class IV cells demonstrate altered somatosensory responses after stimulation (Figure 4.1). However, this is not necessarily at odds with prior evidence – our data does not preclude the possibility that laser-induced injury results in enhanced sensitivity in cells other than Class IV neurons. Furthermore, we found it interesting that, completely contrary to our expectations, repeated stimulation of Class IV cells resulted in cellular fatigue (Figure 4.1B). The interpretation of this observation, though, remains unclear: using our existing set-up we were unable to test if diminishing magnitude of responses

in Class IV cells resulted in commensurate reduction in initiation of behavioral responses. While we would expect that not be the case, it is possible that stimuli that cause sufficiently large calcium spikes result in the initiation of cellular degeneration / death pathways (Zhivotovsky and Orrenius, 2011; Bhosale et al., 2018).

But if the evolutionary purpose of Class IV neurons is to sense noxious stimuli, why would direct stimulation of their arbors in result in degradation? We hypothesized that such a process would mediate invasion by neighboring, unstimulated – ergo, healthier – cells into the untiled territory. This would ensure that the larval body wall remains tiled by these critical sensors, but also remove cells damaged by external stimuli. A number of pieces of evidence lead us to construct this hypothesis: (i) there is published evidence of cellular invagination into untiled territory (Parrish et al., 2009), (ii) Class IV dendrite tips undergo dynamic reorganization throughout their lifetime, even after they have reached peak coverage (see Chapter 1) (why would they expend the energy to constantly undergo this energetically expensive process?) and (iii) we had visually observed subtle changes to dendritic tip dynamics under post stimulation conditions. To see if our idea had any merit, we decided to carefully quantify morphological features of Class IV neurons in pre- and post- stimulation conditions. To do this, we studied "bulk" morphometric properties and also quantified the behavior of individual dendritic tips.

Looking first at bulk morphometric properties, we did not find evidence of changes to the total branch length and total branch number within 30 minutes of stimulation (Figure 4.2). This could be rationalized in three different ways: (i) there is no change post stimulation, (ii) any changes were below the resolving limit of our

analysis protocol, and (iii) though cellular dynamicity increases considerably, the *net* change is imperceptible because growth and shrinkage rates increase by commensurate levels. We decided to further investigate the latter in light of visual cues during imaging.

To test the second and third hypotheses, we first decided to study the long-term effect of stimulation of Class IV cells. We reasoned that imaging over a 24-hour period could reveal changes that we could not resolve with our imaging and analysis protocol. Indeed, stimulated cells demonstrated gross morphological changes with entire sections of the dendritic arbor being pruned over a 24-hour period (Figure 4.3) Additionally, we found some evidence of invagination from neighboring arbors (Figure 4.3D), in accordance with prior reports. Subsequent analysis of individual dendritic tips provided strong evidence supporting our third hypothesis: both growth and shrinkage velocities of tips and transition rates between states increase in response to stimulation (Figure 4.4). This provided an explanation for why our "bulk" morphometric measurements did not yield a measurable change: the increase in the growth rate was offset by a commensurate increase in the shrinkage rates (Figure 4.4F, G), resulting in changes that were imperceptible over our measurement timescale. Ongoing work is focused on studying these changes over longer time period to quantify how long these effects persist (Howard lab, *unpublished data*).

It important to note, however, that although we see a morphological phenotype as a result of stimulation, our experiments do not implicate dendritic calcium transients directly. Instead, a number of other factors could be contributing to our results. We are currently in the process of performing similar quantitation in VGCC RNAi knock-down

and mutant flies (See Chapter 3) as a way to investigate to what extent dendritic calcium signaling events are involved in mediating these processes.

Finally, considerable time and effort was invested in method development and optimization to enable these experiments. The resulting filament tracking package has proven to be a powerful tool for analysis of neuronal processes, enabling high resolution quantitation of dendritic tip dynamics and overall morphometric properties (Sutradhar, Howard et. al., *manuscript in preparation*). Independent of our use, this method will likely enable a wide range of future studies on neuronal morphometrics or related subjects where semi-automated quantitative tracking of filament structures is required (for example, tracking of *in vitro* microtubule growth and catastrophe events, mitotic spindle dynamics).

4.5 Materials and Methods

Live-cell Confocal Imaging. Larvae were timed and selected between 18-72 hours AEL for imaging, depending on the experiment. Preparation, immobilization, and imaging of larval samples for imaging was done as described in Chapter 1 and 2. For embryonic and early first instar samples, immobilization was done by using an agar pad and gently sandwiching samples between a glass side and a coverslip. For experiments studying morphometrics of dendritic arbors over 30 minutes, samples were manually focused and z-stacks were acquired at 30-50% illumination intensity at 10-second intervals. To isolate individual cells, boundaries for cells were manually defined and cropped using the segmented line feature in Image J. Maximum projected images were then analyzed using our in-house custom skeletonization software, detailed below.

Neuron skeletonization and morphometric analysis. To quantify the dynamical properties of the tips, we had to develop an algorithm that was able to robustly track dendritic tips. To do this, we first devised a method to determine the central longitudinal axis of each dendritic filament being considered. We then tracked along this central axis to determine the tip extension position.

The central axis was computed by fitting Gaussians to the cross-sectional intensity profiles at regular intervals along the backbone of the dendrite or filamentous structure (Supplementary Figure 4.1A, B, C):

$$\boldsymbol{I = I_0\, e^{\frac{-(x - x_c)^2}{2\sigma^2}} + d}$$

Here, $\boldsymbol{I_0}$ represents the peak intensity value, $\boldsymbol{x_c}$ represents the center of the gaussian, $\boldsymbol{\sigma}$ is the standard deviation, $\boldsymbol{d}$ is the measured camera offset in our system (100). After determining the central axis, we fit a 2-dimensional Gaussian function convolved with an error function to compute the location of the tip extension:

$$\boldsymbol{I = I_0\, e^{\frac{-[(y-y_{tip})cos\theta-(x-x_{tip})sin\theta]^2}{2{\sigma_v}^2}} * erfc\frac{(y\ -\ y_{tip})cos\theta-(x\ -\ x_{tip})sin\theta}{\sigma_p} + d}$$

A number of *in silico* experiments were performed to quantify the precision with which this algorithm is able to perform tip tracking: (i) we analyzed synthetic images of capped cylindrical tubes with fluorophores placed randomly on their surfaces (30% labeling) and convolved with an appropriate point spread function (250 nm width). To ensure that our algorithm could perform robustly under a variety of imaging conditions, we tested its ability to perform filling on images taken using a variety of techniques (Supplementary Figure 4.2A, B, C). The typical precision was <1 pixel even for low experimental signal-to-background ratios. (ii) We tracked the position of real tips in long-term paused states and found that the average standard deviation of position was 0.1 μm. This accuracy is comparable and, in some cases, better than available software, such as, FIESTA (Ruhnow et al., 2011)and JFilament (Smith et al., 2010)and Simple Neurite Tracer (Longair et al., 2011). Using this parallelized method, several hundred tips can be tracked simultaneously.

Having validated this method, we used a semi-automated MATLAB tracking package developed in our lab that measures the length and location of dendritic tips in

the arbor. After imaging, 40-60 dendritic tips were manually selected and cropped from maximum-projected images in ImageJ based on the signal-to-noise ratio and their separation from the neighboring tips. Supplemental Figure 4.3A shows an example of a maximum projected image of a Class IV neuron and a corresponding set dendritic tips that were isolated. These tips were then manually cleaned to remove aberrant noise and optical garbage by zeroing out pixel intensity values in local regions determined to be potentially problematic (Supplementary Figure 4.3B). After manually checking all tip ROIs for inconsistencies (movements, frame jumps, etc), we then imported into MATLAB to generate a curve representing tip extension position over time (Supplementary Figure 4.3C). These individual trajectories were again checked for discontinuities or large jumps to ensure that our tracking algorithm was performing as we expected.

In MATLAB tip trajectories such as that shown in Supplementary Figure 4.3C were segmented into periods of constant velocity. Since a perfect fit can always be achieved with a large enough number of segments equal to the number of data point minus one, the tracking algorithm constrained the maximum number of segments to be the number of points divided by the estimated temporal resolution (6 frames). A piecewise linear function with this number of segments (with the positions of the segment ends a free variable) were then fit to each trace. Adjacent segments were then merged using a velocity (slope) threshold determined by the intersections of the velocity distribution curves (see Figure 4.4D, E) This allowed classification of the trajectories into transitions between three discrete states: growing, shrinking and paused (for rationale, see Chapter 1). This enabled estimation of the distributions of the

growth and shrinkage velocities (Figure 4.4D, E), and the transition rates (Figure 4.4F, G) for the given dendritic tips over time.

A caveat of this method is that it is only able to track filaments that are reasonably free of optical garbage and excessive noise. This is because tracking of the filaments is accomplished via a set fluorescence threshold value, and autofluorescence of optical garbage or additional sources of fluorescence above our set threshold can result in misidentification. Additionally, accurate tracking requires filaments with no breaks, discontinuities or overlapping segments (for example, circular patterns in arbors). As a result, our algorithm was unable to skeletonize and track cells that were undergoing rapid degradation (Supplementary Figure 4.4C, D) and regions when dendrites self-overlapped or crossed paths with a neighboring process (not shown). As an alternative, in such scenarios, arbors were tracked manually using the Simple Neurite tracer (SNT) plug-in and the ImageJ segmented line feature.

4.6 Supplementary Materials

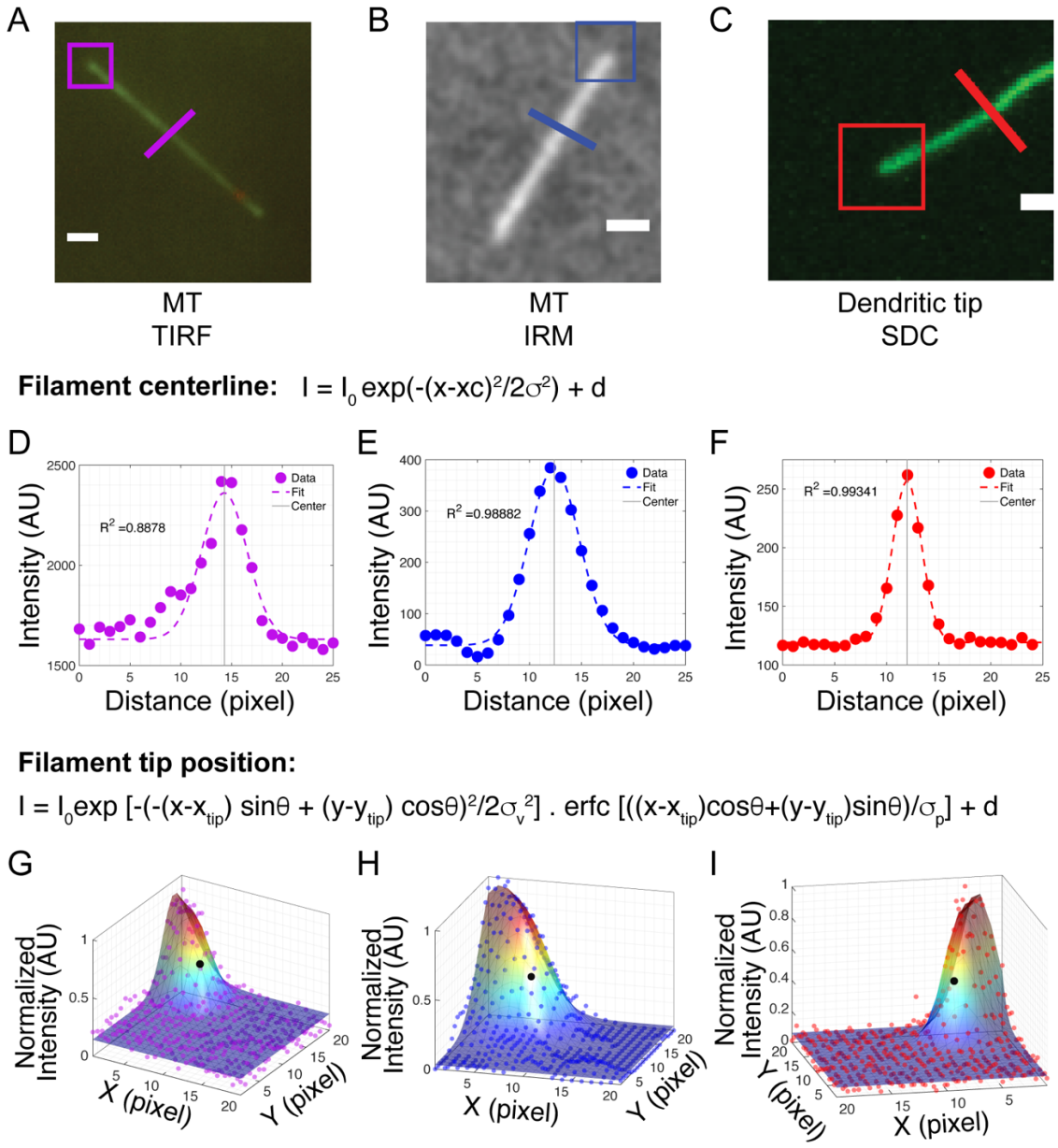

Supplementary Figure 4.1: Functional forms used to determine position of dendritic tips. Scale bar is 1 μm. (A-C) Experimental images of filamentous structures taken via (A) TIRF (microtubule) (B) IRM (microtubule) and (C) spinning disc confocal microscopy (Class IV dendrite tip). (D-F) Fitting to determine the central line of corresponding filaments in panels A-C. (G-I) Fitting to determine peripheral tip position of corresponding filaments in panels A-C.

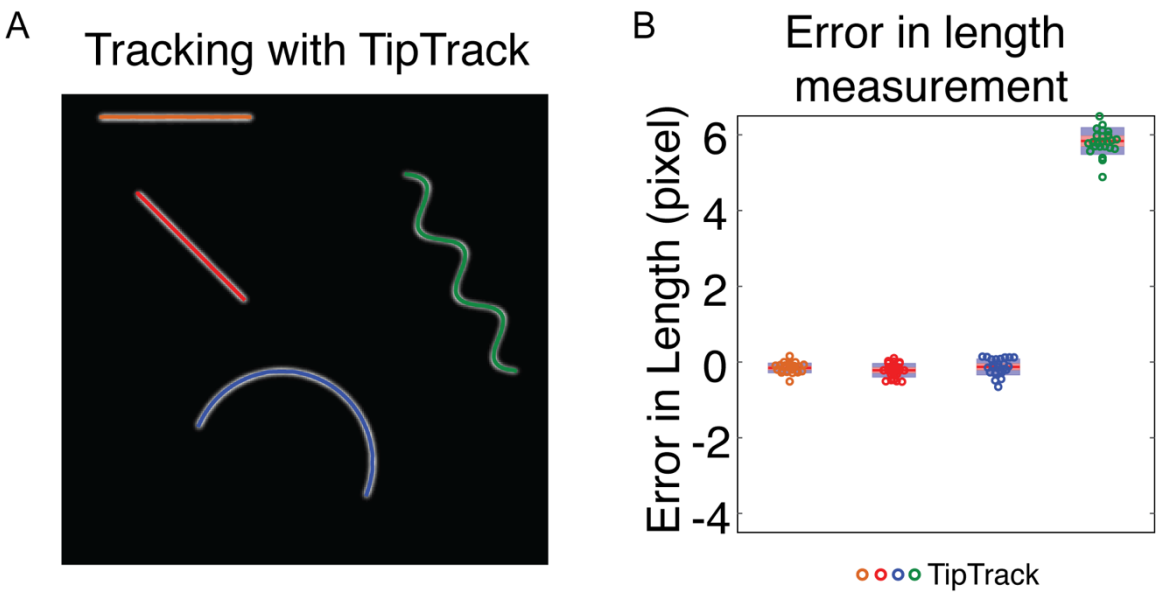

Supplementary Figure 4.2: Validation of tracking software — our tracking algorithm, TipTrack, skeletonizes and measures variety of filamentous shapes with high precision. (A) Examples of simulated shapes skeletonized with TipTrack. (B) Errors (unit: pixels) in measurement of simulated shapes, color coded as in panel A.

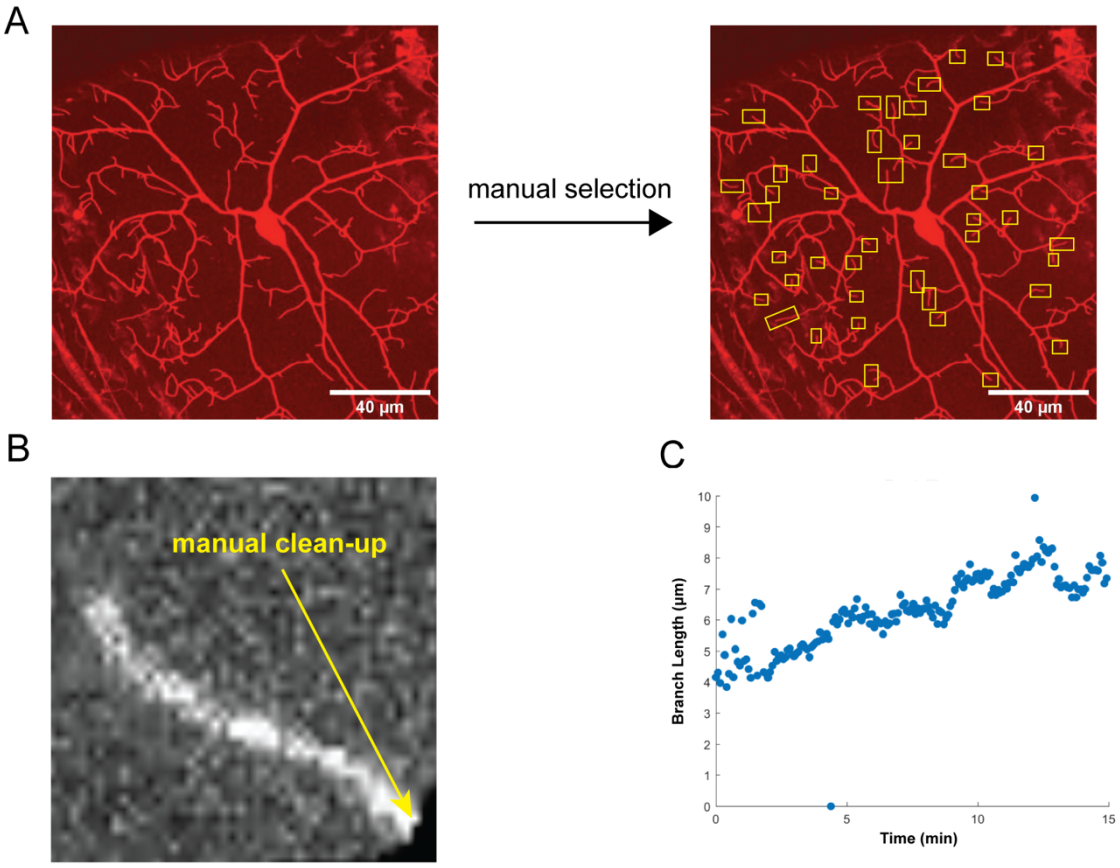

Supplementary Figure 4.3: Analysis protocol – tip tracking algorithm requires selection of individual dendritic tips. (A) Max-projected image of Class IV neuron and example of isolated dendritic tips (B) Example of isolated dendritic tip ROI post clean-up. (C) Representative trace of branch length over time for dendritic tip shown in panel B.

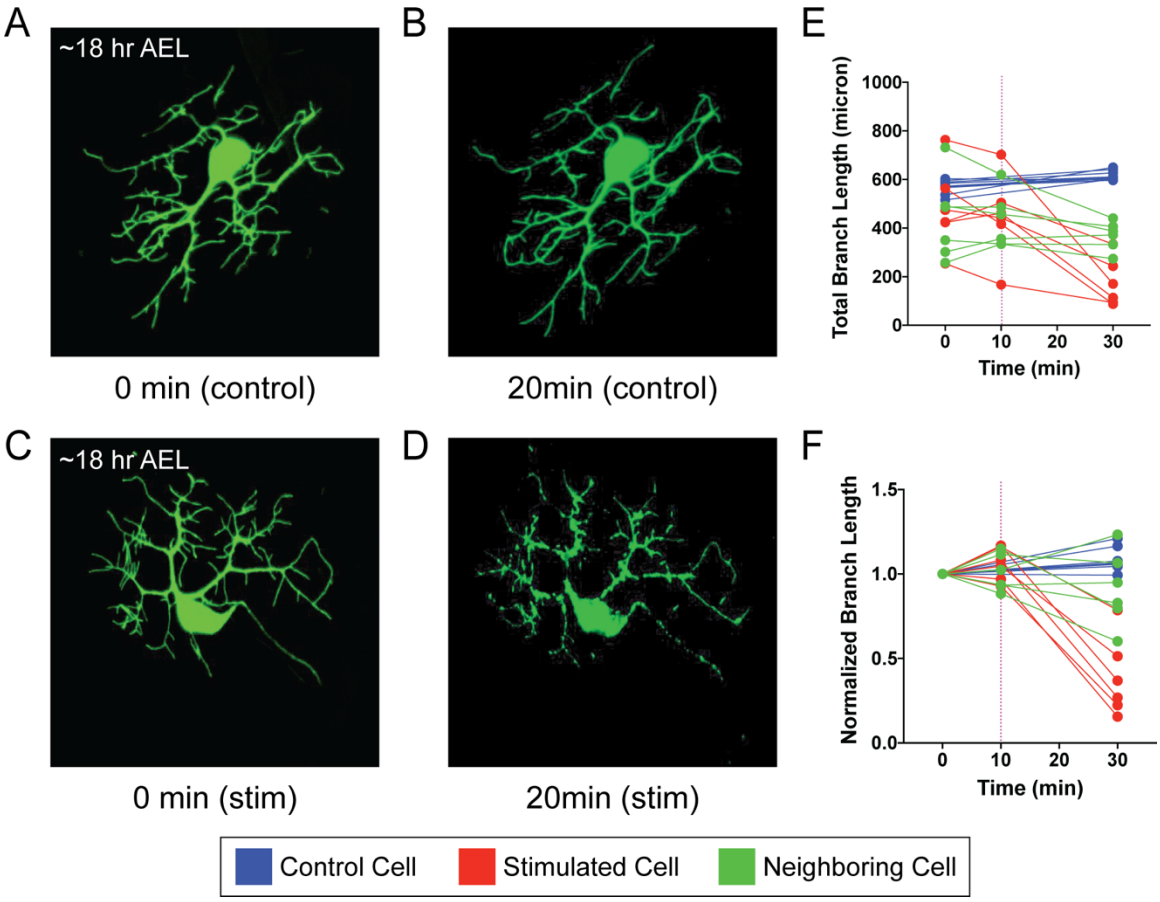

Supplementary Figure 4.4: Impact of 405nm stimulation on Class IV neurons in embryo/early first instar larvae. (A-B) Example of unstimulated Class IV neuron at (A) 0 min and (B) 20 mins, demonstrating robust tip reorganization. (C-D) Example of stimulated Class IV neuron (80% power) at (C) 0 min and (D) 20 mins. (E-F) Morphometric analysis of control (blue, no stimulation), stimulated (red) and neighboring cells (green, no stimulation) showing (E) total branch length and (F) normalized branch length.

4.6 Research Contributions

All experiments and modelling were conceptualized in conjunction with Dr. Jonathon Howard. The tip tracking automation package used in these studies was conceptualized and developed by Dr. Sabyasachi Sutradhar and Dr. Jonathon Howard. The long-term imaging protocol used to study *Drosophila* larvae morphometrics was optimized in conjunction with Dr. Sonal Shree.

Science is a way of thinking
much more than it is a body of knowledge.

–Carl Sagan (1934 – 1996)

Chapter 5:
Conclusions & Future Work

Conclusions

This work has focused on elucidating somatosensory properties of nociceptive neurons *in vivo*. *Drosophila melanogaster* dendritic arborization neurons were the choice of model system for these studies (Chapter 1). Using existing and newly developed techniques, we have provided the first known systemic characterization of somatosensory sensitivities of individual Class IV arbors. This provides novel insight into cell-specific receptive properties and their integration with the overall organism.

New method development was a critical part of this project. Namely, to understand how localized mechanical stimuli trigger cellular responses in Class IV neurons, we developed a novel, tunable, non-lethal assay for cellular nociception that offers advantages of optical techniques (spatio-temporal precision, profile, etc) while emulating ethologically realistic scenarios that larvae encounter in nature (mechanical oviposition) (Chapter 2). After validating this system, we studied Class IV neurons in whole-mount *Drosophila* larvae with a spatial resolution of 0.1615 μm (40X), 0.3225 μm (20X), and a 100ms temporal resolution using calcium imaging. While prior studies

have used optical techniques to probe Class IV cells, this is the first study, to our knowledge, to probe differential sensitivities within the dendritic arbors of single cells. This is important because it sheds light on developmental and functional reasons underlying extensive arborization of Class IV neurons. Additionally, our assay is easily amenable for microsurgical ablation, targeted photo-bleaching/activation, optogenetics, and related experiments. Thus, in addition to our use, our assay will likely be beneficial to researchers studying a variety of other systems.

Our primary research finding is that there are two distinct calcium signaling responses in Class IV cells: (i) a "non-contact" response observed primarily in axons, and (ii) a "contact" response seen in axons, dendrites and cell bodies (Figure 3.8). The existence of two response pathways is supported by three pieces of evidence: (a) axonal calcium signals do not require the laser spots to make direct contact with the dendritic processes whereas dendritic calcium signals require direct contact (Figure 3.1); (b) axonal calcium signals are more sensitive and faster than dendritic calcium transients even when the stimulus is as far as 400 μm away from the axon (Fig 3.2, 3.5); and (c) the surface model provides a better fit to the axon responses while the volume model provides a better fit to the dendrite and soma data (Fig 3.6, Table 3.6-3.8). Therefore, we conclude that localized mechanical damage induced by the laser triggers "non-contact" responses in the axons and "contact" responses in all cellular compartments. The conclusion that the axon-only response is indirect is strengthened by the observation that "non-contact" wide-profile illumination gives smaller axonal responses despite it having more power at larger distances (that could potentially directly stimulate the dendrite).

Given that stimulation with a focused laser shares several features with stimulation by an ovipositor – localized tissue damage, melanotic spots, behavioral responses, axonal signals – we postulate that the ovipositor can excites the Class IV neuron through both the "contact" and "non-contact" mechanisms. There are, however, some potential caveats to this conclusion. First, a wasp ovipositor punctures the cuticle via mechanical pressure, whereas our laser is likely damaging the cuticle via localized heating or production of reactive oxygen species by autofluorescence or GCaMP6f fluorescence. Second, while both the ovipositor and the focused laser produce localized damage, they are both expected to produce more delocalized effects on the tissue. The ovipositor is expected to generate a large strain field as the cuticle is indented before it ruptures. This strain field could evoke mechanoreceptive responses. The laser generates stray light over a wide area of the tissue through reflection and scattering, though the intensity is greatly attenuated. This stray light could excite photoreceptors (Xiang et al., 2010) or the reactive-oxygen-species response (Kim and Johnson, 2014). However, the stray light evidently does not excite dendritic calcium responses. Despite differences between laser and ovipositor stimulation, and the considerable uncertainty about the precise effects of ovipositor penetration and laser illumination on the tissue, we believe that the ovipositor likely stimulates both "contact" and "non-contact" responses.

We propose the following pathways to account for the "contact" and "non-contact" calcium responses. First, direct contact of high-power laser illumination damages the Class IV cell's plasma membrane, making it more permeable to sodium and inducing a local depolarization of the membrane potential (Tracey, 2017). The

depolarization then spreads electrotonically throughout the dendrite, to the cell body and the axon. Modeling electrotonic spread in the thin axons of primate rods and cones (which have diameters 0.45 and 1.6 μm respectively), shows that there is little signal decrement over 400 μm even at frequencies up to 50 Hz, which corresponds to a time constant <10 ms (Hsu et al., 1998). Therefore, electrotonic spread of depolarization is likely fast enough to reach all parts of the Class IV cell. If the depolarization exceeds the threshold needed to open L-type (and potentially other) calcium channels, then calcium will enter and a GCaMP6f fluorescent signal produced. If there are calcium channels in the dendrites, cell body and axon, then fluorescence changes will be observed throughout the cell.

Second, we propose that if high-power laser illumination makes no contact with the Class IV cell, it will, never-the-less damage adjacent cells, such as the overlying epithelial (epidermal) cells and underlying muscle cells (Grueber et al., 2002). These cells could then release small metabolites or acidify the extracellular space. These signals then spread by diffusion to the membrane of the Class IV cells where they open receptor-gated or the acid-sensing channels — for example, pickpocket or ripped pocket (Boiko et al., 2011; Adams et al., 1998). This mechanism would be analogous to release of cytosolic ATP from damaged cells, which mediates pain perception via contact with P2X receptors on peripheral nociceptive cells in vertebrates (Hamilton and McMahon, 2000; Cook and McCleskey, 2002). While *Drosophila* lacks P2X receptors (Fountain and Burnstock, 2009), it is possible that other small cytoplasmic molecules or protons released by surrounding cells might play an analogous role. Opening of receptor-linked channels like pickpocket or ripped

pocket is expected to locally depolarize the cell membrane, and this depolarization will spread electrotonically to the cell body and axon, where, if it exceeds a threshold, leads to axonal action potentials which in turn trigger the opening of calcium channels. If the receptor mechanism leads to less depolarization in Class IV dendrites than direct damage, as is reasonable, then "non-contact" stimulation may be above threshold for action potentials in the axons (which then open calcium channels), but below threshold for opening calcium channels in the dendrites and soma. Hence, only axons respond to "non-contact" stimulation. Because direct contact is also likely to damage adjacent cells and trigger the "non-contact" response as well, axon responses are likely to be triggered by both pathways. Thus, there are likely two pathways by which localized damage by ovipositor barbs leads to electrophysiological and calcium responses.

Interestingly, the existence of these two pathways provides evidence that the dendrites of Class IV cell are not electrically excitable. If they were excitable, then we would expect that axonal action potentials would back propagate and in turn stimulate calcium entry through voltage-gated channels in the dendrites; but the "non-contact" response does not stimulate calcium responses in dendrites. A related point is that when direct contact is made, the axonal calcium signals (Supplementary Figure 3.1) are usually more transient than the dendritic signals (Supplementary Figure 3.2). A possible explanation is that calcium entry opens calcium-activated potassium channels in the axons, which depolarizes the axonal membrane tending to inhibit spiking and additional calcium entry. This delayed negative feedback would attenuate the calcium signal in the axon at longer times. The existence of axonal calcium-activated potassium channels could account for the "unconventional spikes" (US) recorded from the cell body and

the axon bundle (Terada et al., 2016): these spikes are characterized by an ensuing refractory period during which there is no spiking; the US and refractory period correlates with calcium signals in the dendrites and may be a consequence of the opening of calcium-activated potassium channels.

The existence of the "non-contact" pathway sheds new light on the highly branched morphology of Class IV cells. Because the mesh size — the average distance between dendrites in the arbor — is about 5 μm, it has been suggested that the reason these cells are highly branched is to maximize direct contact with ovipositor barbs (Ganguly et al., 2016). However, the "non-contact" pathway implies that direct damage to the Class IV cell is not necessary to stimulate the axonal pathway. Still, the Class IV cells still need to be highly branched and make a fine mesh so that extracellular signals can still diffuse sufficiently quickly to activate membrane receptors: a small molecule similar in size to ATP (diffusion coefficient on the order of 100 μm^2/sec) will reach a dendrite 5 μm away in ~0.1 second. To diffuse a distance three times as far (15 μm), for example, would take ~1 second, too slow to account for the axonal responses. Thus, our data lead us to propose a new function underlying extensive branching and interdigitation of Class IV dendritic arbors: the fine meshwork minimizes diffusion times to ensure that "non-contact" response is rapidly transduced.

While the function of the axonal response is clear – to convey nociceptive signals to the central nervous system, the function of the dendritic responses is not. Dendritic signals are often centrifugal, moving away from the cell body; they are therefore not on the cell-to-central nervous system pathway. One implication is that dendritic calcium signals in Class IV cells are not necessarily good proxies for neuronal

excitation. Calcium signals are often assumed to be reporters of cell excitation, though a number of researchers have cautioned against this assumption (Ali and Kwan, 2019; Higley and Sabatini, 2008). Since the "contact" dendritic pathway signals not just to the axon and CNS but also throughout the dendritic array, even to regions that are peripheral to the stimulus, we investigated potential links to arbor morphometrics and cellular nociceptive hypersensitivity. We found evidence that activation of the "contact" dendritic pathway results in morphological changes to the arbor via altered tip dynamicity, but not hypersensitivity at the level of individual Class IV cells. (Chapter 4). Ongoing work in our lab is focused on further investigating morphometrics of Class IV arbors post dendritic calcium signals and the possible impact of these changes on larval behavior and cellular connectivity (Howard Lab).

Taken together, our *in vivo* data provide novel insight into somatosensory properties of Class IV dendritic arbors and proposes differing functional interpretations of dendritic and axonal calcium signals.

Future work & outlook

There are several follow-up studies that will provide additional color to the results presented. Regarding the downstream effects of the "contact" dendrite calcium signaling pathways, although we have shown some evidence that activation results in some morphological changes to tip dynamicity in arbors, the precise role of calcium in mediating these changes is unclear. Additional investigations via RNAi knockdown experiments provide a convenient method to probe this (*ongoing*; Howard Lab). A characterization of potential dose-response effects via stimulation at varying intensities

may also shed light on the extent to which cytosolic calcium signaling magnitudes are mediating these changes. Long-term imaging experiments studying the impact of evoked dendritic calcium transients on cytoskeletal structures (microtubules, F-actin) also hold promise to deliver insight into regulatory and mechanistic features underlying morphoregulation of Class IV arbors.

The presence of the surface versus volume response factors for the axonal and dendritic pathways (Figure 3.6), respectively, also opens up an interesting line of inquiry for the identification of corresponding receptors that localize on the membrane or cytosol of Class IV dendritic arbors. Although we have some existing evidence for candidates that may be mediating the surface receptor-based axonal response (pickpocket1, ripped pocket, dTRPA1 channels, dmPiezo, for example), researchers in search of cytoplasmic receptors mediating this process will be in novel territory.

Voltage imaging and *in vivo* electrophysiology in Class IV cells are also interesting avenues that will likely shed light on dendritic versus axonal spiking in Class IV cells. A key caveat of our approach using calcium imaging is that calcium concentrations are a second-order measurement of neuronal activity. Direct analysis of voltage events in Class IV neurons will provide additional information about propagation of signals within Class IV neurons and its neighboring cells. Are signals attenuated at branch nodes? Are signals initiated in the axons or throughout the arbor? Do signals propagate to neighboring Class IV neurons and other dendritic arborization cells? Answers to such questions, paired with our calcium imaging data, will further clarify the architecture of Class IV neurons and their related circuits.

Additionally, although we have characterized sensory properties in Class IV neurons specifically, it is not known if these properties are cell-type specific or if they extend to other multidendritic neurons in *Drosophila*. For example, are Class I or Class III neurons also differentially activated via localized stimuli at different thresholds? Does the dual signaling pathway paradigm extend to other dendritic arborization neurons, or is it specific to Class IV cells? Cell-specific drivers similar to the one we have used to visualize Class IV neurons makes it possible to readily address these questions. Ongoing work will provide more insight into functional reasons underlying our reported results in the Class IV system.

Although rare events, our stimulation experiments also highlighted that Class IV neurons can "propagate" calcium signals to neighboring cells via neurite contacts (data not shown). This raises the question: do dendrites have bidirectional polarity in Class IV cells? That is, in addition to receiving synaptic input, are dendrites capable of sending outward signals to neighboring cells? Do Class IV neurons have synapses with neighboring cells within and outside the da class? Studies our lab are exploring localization and activation of tagged pre-synaptic markers (eg: synaptotagmin-tagged GCaMP) and propagation in mutants with aberrant morphology (i.e., over-branching and under-tiled arbors) as a way to probe these questions.

***

Literature Cited

Abraira, V.E., and D.D. Ginty. 2013. The Sensory Neurons of Touch. *Neuron*. 79:618–639. doi:10.1016/j.neuron.2013.07.051.

Adams, C.M., M.G. Anderson, D.G. Motto, M.P. Price, W.A. Johnson, and M.J. Welsh. 1998. Ripped Pocket and Pickpocket, Novel Drosophila DEG/ENaC Subunits Expressed in Early Development and in Mechanosensory Neurons. *J Cell Biology*. 140:143–152. doi:10.1083/jcb.140.1.143.

Ainsley, J.A., M.J. Kim, L.J. Wegman, J.M. Pettus, and W.A. Johnson. 2008. Sensory mechanisms controlling the timing of larval developmental and behavioral transitions require the Drosophila DEG/ENaC subunit, Pickpocket1. *Dev Biol*. 322:46–55. doi:10.1016/j.ydbio.2008.07.003.

Akerboom, J., T.-W. Chen, T.J. Wardill, L. Tian, J.S. Marvin, S. Mutlu, N.C. Calderón, F. Esposti, B.G. Borghuis, X.R. Sun, A. Gordus, M.B. Orger, R. Portugues, F. Engert, J.J. Macklin, A. Filosa, A. Aggarwal, R.A. Kerr, R. Takagi, S. Kracun, E. Shigetomi, B.S. Khakh, H. Baier, L. Lagnado, S.S.-H. Wang, C.I. Bargmann, B.E. Kimmel, V. Jayaraman, K. Svoboda, D.S. Kim, E.R. Schreiter, and L.L. Looger. 2012. Optimization of a GCaMP calcium indicator for neural activity imaging. *J Neurosci Official J Soc Neurosci*. 32:13819–40. doi:10.1523/jneurosci.2601-12.2012.

Akerboom, J., J.D.V. Rivera, M.M.R. Guilbe, E.C.A. Malavé, H.H. Hernandez, L. Tian, S.A. Hires, J.S. Marvin, L.L. Looger, and E.R. Schreiter. 2009. Crystal Structures of the GCaMP Calcium Sensor Reveal the Mechanism of Fluorescence Signal Change and Aid Rational Design*S. *J Biological Chem*. 284:6455–6464. doi:10.1074/jbc.m807657200.

Ali, F., and A.C. Kwan. 2019. Interpreting in vivo calcium signals from neuronal cell bodies, axons, and dendrites: a review. *Proc Spie*. 7:1. doi:10.1117/1.nph.7.1.011402.

Anda, F.C. de, A.L. Rosario, O. Durak, T. Tran, J. Gräff, K. Meletis, D. Rei, T. Soda, R. Madabhushi, D.D. Ginty, A.L. Kolodkin, and L.-H. Tsai. 2012. Autism spectrum disorder susceptibility gene TAOK2 affects basal dendrite formation in the neocortex. *Nat Neurosci*. 15:1022–1031. doi:10.1038/nn.3141.

Ashworth, R., and S.R. Bolsover. 2002. Spontaneous activity-independent intracellular calcium signals in the developing spinal cord of the zebrafish embryo. *Dev Brain Res*. 139:131–137. doi:10.1016/s0165-3806(02)00538-2.

Babcock, D.T., C. Landry, and M.J. Galko. 2009. Cytokine signaling mediates UV-induced nociceptive sensitization in Drosophila larvae. *Curr Biology Cb*. 19:799–806. doi:10.1016/j.cub.2009.03.062.

Babcock, D.T., S. Shi, J. Jo, M. Shaw, H.B. Gutstein, and M.J. Galko. 2011a. Hedgehog Signaling Regulates Nociceptive Sensitization. *Curr Biol*. 21:1525–1533. doi:10.1016/j.cub.2011.08.020.

Babcock, D.T., S. Shi, J. Jo, M. Shaw, H.B. Gutstein, and M.J. Galko. 2011b. Hedgehog Signaling Regulates Nociceptive Sensitization. *Curr Biol*. 21:1525–1533. doi:10.1016/j.cub.2011.08.020.

Badura, A., X.R. Sun, A. Giovannucci, L.A. Lynch, and S.S.-H. Wang. 2014. Fast calcium sensor proteins for monitoring neural activity. *Proc Spie*. 1:025008–025008. doi:10.1117/1.nph.1.2.025008.

Baloyannis, S.J. 2009. Dendritic pathology in Alzheimer's disease. *J Neurol Sci*. 283:153–157. doi:10.1016/j.jns.2009.02.370.

Barnett, L.M., T.E. Hughes, and M. Drobizhev. 2017. Deciphering the molecular mechanism responsible for GCaMP6m's Ca2+-dependent change in fluorescence. *Plos One*. 12:e0170934. doi:10.1371/journal.pone.0170934.

Bartheld, C.S., J. Bahney, and S. Herculano-Houzel. 2016. The search for true numbers of neurons and glial cells in the human brain: A review of 150 years of cell counting. *J Comp Neurol*. 524:3865–3895. doi:10.1002/cne.24040.

Basak, R., S. Sutradhar, and J. Howard. 2021. Focal Laser Stimulation of Fly Nociceptors Activates Distinct Axonal and Dendritic Ca 2+ Signals. *undefined*. doi:10.1101/2021.03.04.433797.

Bassett, D.S., and M.S. Gazzaniga. 2011. Understanding complexity in the human brain. *Trends Cogn Sci*. 15:200–209. doi:10.1016/j.tics.2011.03.006.

Beaulieu, C., and M. Colonnier. 1989. Number and size of neurons and synapses in the motor cortex of cats raised in different environmental complexities. *J Comp Neurol*. 289:178–187. doi:10.1002/cne.902890115.

Bellen, H.J., C. Tong, and H. Tsuda. 2010. 100 years of Drosophila research and its impact on vertebrate neuroscience: a history lesson for the future. *Nat Rev Neurosci*. 11:514–522. doi:10.1038/nrn2839.

Benzer, S. 1967. BEHAVIORAL MUTANTS OF Drosophila ISOLATED BY COUNTERCURRENT DISTRIBUTION. *Proc National Acad Sci*. 58:1112–1119. doi:10.1073/pnas.58.3.1112.

Berni, J., S.R. Pulver, L.C. Griffith, and M. Bate. 2012. Autonomous Circuitry for Substrate Exploration in Freely Moving Drosophila Larvae. *Curr Biol*. 22:1861–1870. doi:10.1016/j.cub.2012.07.048.

Berridge, M.J. 2016. The Inositol Trisphosphate/Calcium Signaling Pathway in Health and Disease. *Physiol Rev*. 96:1261–1296. doi:10.1152/physrev.00006.2016.

Bhosale, G., J.A. Sharpe, S.Y. Sundier, and M.R. Duchen. 2018. Calcium signaling as a mediator of cell energy demand and a trigger to cell death. *Ann Ny Acad Sci*. 1350:107–116. doi:10.1111/nyas.12885.

Bier, E. 2005. Drosophila, the golden bug, emerges as a tool for human genetics. *Nat Rev Genet*. 6:9–23. doi:10.1038/nrg1503.

Boiko, N., B.A. Eaton, and J.D. Stockand. 2011. Identification of pH-sensitive currents in Drosophila sensory neurons. *Faseb J*. 25:860.5-860.5. doi:10.1096/fasebj.25.1_supplement.860.5.

Bootman, M.D., T.J. Collins, C.M. Peppiatt, L.S. Prothero, L. MacKenzie, P.D. Smet, M. Travers, S.C. Tovey, J.T. Seo, M.J. Berridge, F. Ciccolini, and P. Lipp. 2001. Calcium signalling—an overview. *Semin Cell Dev Biol*. 12:3–10. doi:10.1006/scdb.2000.0211.

Borst, A., and M. Egelhaaf. 1994. Dendritic processing of synaptic information by sensory interneurons. *Trends Neurosci*. 17:257–263. doi:10.1016/0166-2236(94)90009-4.

Botas, J. 2007. Drosophila researchers focus on human disease. *Nat Genet*. 39:589–589. doi:10.1038/ng0507-589.

Branco, T., and M. Häusser. 2010. The single dendritic branch as a fundamental functional unit in the nervous system. *Curr Opin Neurobiol*. 20:494–502. doi:10.1016/j.conb.2010.07.009.

Brand, A.H., and E.-L. Dormand. 1995. The GAL4 system as a tool for unravelling the mysteries of the Drosophila nervous system. *Curr Opin Neurobiol*. 5:572–578. doi:10.1016/0959-4388(95)80061-1.

Burgos, A., K. Honjo, T. Ohyama, C.S. Qian, G.J. Shin, D.M. Gohl, M. Silies, W.D. Tracey, M. Zlatic, A. Cardona, and W.B. Grueber. 2018. Nociceptive interneurons control modular motor pathways to promote escape behavior in Drosophila. *Elife*. 7:e26016. doi:10.7554/elife.26016.

Burrell, B.D., and C.L. Sahley. 1998. Generalization of habituation and intrinsic sensitization in the leech. *Learn Mem Cold Spring Harb N Y*. 5:405–19.

Cameron, S., and Y. Rao. 2010. Molecular mechanisms of tiling and self-avoidance in neural development. *Mol Brain*. 3:28. doi:10.1186/1756-6606-3-28.

Campana, G., and R. Rimondini. 2014. Opioid Receptors, Methods and Protocols. *Methods Mol Biology*. 1230:229–231. doi:10.1007/978-1-4939-1708-2_18.

Carafoli, E., and J. Krebs. 2016. Why Calcium? How Calcium Became the Best Communicator*. *J Biol Chem*. 291:20849–20857. doi:10.1074/jbc.r116.735894.

Cerella, C., M. Diederich, and L. Ghibelli. 2010. The Dual Role of Calcium as Messenger and Stressor in Cell Damage, Death, and Survival. *Int J Cell Biology*. 2010:546163. doi:10.1155/2010/546163.

Chattopadhyay, A., A.V. Gilstrap, and M.J. Galko. 2012. Local and global methods of assessing thermal nociception in Drosophila larvae. *J Vis Exp Jove*. e3837. doi:10.3791/3837.

Chen, T.-W., T.J. Wardill, Y. Sun, S.R. Pulver, S.L. Renninger, A. Baohan, E.R. Schreiter, R.A. Kerr, M.B. Orger, V. Jayaraman, L.L. Looger, K. Svoboda, and D.S. Kim. 2013. Ultrasensitive fluorescent proteins for imaging neuronal activity. *Nature*. 499:295–300. doi:10.1038/nature12354.

Chiang, A.-S., C.-Y. Lin, C.-C. Chuang, H.-M. Chang, C.-H. Hsieh, C.-W. Yeh, C.-T. Shih, J.-J. Wu, G.-T. Wang, Y.-C. Chen, C.-C. Wu, G.-Y. Chen, Y.-T. Ching, P.-C. Lee, C.-Y. Lin, H.-H. Lin, C.-C. Wu, H.-W. Hsu, Y.-A. Huang, J.-Y. Chen, H.-J. Chiang, C.-F. Lu, R.-F. Ni, C.-Y. Yeh, and J.-K. Hwang. 2011. Three-Dimensional Reconstruction of Brain-wide Wiring Networks in Drosophila at Single-Cell Resolution. *Curr Biol*. 21:1–11. doi:10.1016/j.cub.2010.11.056.

Chin, M.R., and W.D. Tracey. 2017. Nociceptive Circuits: Can't Escape Detection. *Curr Biol*. 27:R796–R798. doi:10.1016/j.cub.2017.07.031.

Chklovskii, D.B. 2004. Synaptic Connectivity and Neuronal Morphology Two Sides of the Same Coin. *Neuron*. 43:609–617. doi:10.1016/j.neuron.2004.08.012.

Clapham, D.E. 2007. Calcium Signaling. *Cell*. 131:1047–1058. doi:10.1016/j.cell.2007.11.028.

Cline, H.T. 2001. Dendritic arbor development and synaptogenesis. *Curr Opin Neurobiol*. 11:118–126. doi:10.1016/s0959-4388(00)00182-3.

Consoulas, C., L.L. Restifo, and R.B. Levine. 2002. Dendritic Remodeling and Growth of Motoneurons during Metamorphosis of Drosophila melanogaster. *J Neurosci*. 22:4906–4917. doi:10.1523/jneurosci.22-12-04906.2002.

Cook, K.R., A.L. Parks, L.M. Jacobus, T.C. Kaufman, and K. Matthews. 2010. New research resources at the Bloomington Drosophila Stock Center. *Fly*. 4:88–91. doi:10.4161/fly.4.1.11230.

Cook, S.P., and E.W. McCleskey. 2002. Cell damage excites nociceptors through release of cytosolic ATP. *Pain*. 95:41–47. doi:10.1016/s0304-3959(01)00372-4.

Corty, M.M., B.J. Matthews, and W.B. Grueber. 2009. Molecules and mechanisms of dendrite development in Drosophila. *Development*. 136:1049–1061. doi:10.1242/dev.014423.

Cuntz, H., F. Forstner, A. Borst, and M. Häusser. 2010. One Rule to Grow Them All: A General Theory of Neuronal Branching and Its Practical Application. *Plos Comput Biol*. 6:e1000877. doi:10.1371/journal.pcbi.1000877.

Darmanis, S., S.A. Sloan, Y. Zhang, M. Enge, C. Caneda, L.M. Shuer, M.G.H. Gephart, B.A. Barres, and S.R. Quake. 2015. A survey of human brain transcriptome diversity at the single cell level. *Proc National Acad Sci*. 112:7285–7290. doi:10.1073/pnas.1507125112.

Delmas, P., J. Hao, and L. Rodat-Despoix. 2011. Molecular mechanisms of mechanotransduction in mammalian sensory neurons. *Nat Rev Neurosci*. 12:139–153. doi:10.1038/nrn2993.

Deneux, T., A. Kaszas, G. Szalay, G. Katona, T. Lakner, A. Grinvald, B. Rózsa, and I. Vanzetta. 2016. Accurate spike estimation from noisy calcium signals for ultrafast three-dimensional imaging of large neuronal populations in vivo. *Nat Commun*. 7:12190. doi:10.1038/ncomms12190.

Denis, J., R.F. Dard, E. Quiroli, R. Cossart, and M.A. Picardo. 2020. DeepCINAC: a deep-learning-based Python toolbox for inferring calcium imaging neuronal activity based on movie visualization. *Biorxiv*. 803726. doi:10.1101/803726.

Deo, C., and L.D. Lavis. 2018. Synthetic and genetically encoded fluorescent neural activity indicators. *Curr Opin Neurobiol*. 50:101–108. doi:10.1016/j.conb.2018.01.003.

Deuis, J.R., L.S. Dvorakova, and I. Vetter. 2017. Methods Used to Evaluate Pain Behaviors in Rodents. *Front Mol Neurosci*. 10:284. doi:10.3389/fnmol.2017.00284.

Deuis, J.R., and I. Vetter. 2016. The thermal probe test: A novel behavioral assay to quantify thermal paw withdrawal thresholds in mice. *Temp*. 3:199–207. doi:10.1080/23328940.2016.1157668.

DeVault, L., T. Li, S. Izabel, K.L. Thompson-Peer, L.Y. Jan, and Y.N. Jan. 2018. Dendrite regeneration of adult Drosophila sensory neurons diminishes with aging and is inhibited by epidermal-derived matrix metalloproteinase 2. *Gene Dev.* 32:402–414. doi:10.1101/gad.308270.117.

DeWeese, M.R. 2007. Whole-Cell Recording In Vivo. *Curr Protoc Neurosci.* 38:6.22.1-6.22.15. doi:10.1002/0471142301.ns0622s38.

Dierssen, M., and G.J.A. Ramakers. 2006. Dendritic pathology in mental retardation: from molecular genetics to neurobiology. *Genes Brain Behav.* 5:48–60. doi:10.1111/j.1601-183x.2006.00224.x.

Ding, J., A.F. Luo, L. Hu, D. Wang, and F. Shao. 2014. Structural basis of the ultrasensitive calcium indicator GCaMP6. *Sci China Life Sci.* 57:269–274. doi:10.1007/s11427-013-4599-5.

Dubin, A.E., and A. Patapoutian. 2010. Nociceptors: the sensors of the pain pathway. *J Clin Invest.* 120:3760–3772. doi:10.1172/jci42843.

Duffy, J.B. 2002. GAL4 system in drosophila: A fly geneticist's swiss army knife. *Genesis.* 34:1–15. doi:10.1002/gene.10150.

Ellström, I.D., S. Spulber, S. Hultin, N. Norlin, S. Ceccatelli, C. Hultling, and P. Uhlén. 2019. Spinal cord injury in zebrafish induced by near-infrared femtosecond laser pulses. *J Neurosci Meth.* 311:259–266. doi:10.1016/j.jneumeth.2018.10.035.

Emoto, K. 2011. Dendrite remodeling in development and disease. *Dev Growth Differ.* 53:277–286. doi:10.1111/j.1440-169x.2010.01242.x.

Emoto, K., Y. He, B. Ye, W.B. Grueber, P.N. Adler, L.Y. Jan, and Y.-N. Jan. 2004. Control of Dendritic Branching and Tiling by the Tricornered-Kinase/Furry Signaling Pathway in Drosophila Sensory Neurons. *Cell.* 119:245–256. doi:10.1016/j.cell.2004.09.036.

Felix, B. 2001. Extracellular and Intracellular Regulation of Calcium Homeostasis. *Sci World J.* 1:919–925. doi:10.1100/tsw.2001.489.

Fenno, L., O. Yizhar, and K. Deisseroth. 2011. The Development and Application of Optogenetics. *Neuroscience.* 34:389–412. doi:10.1146/annurev-neuro-061010-113817.

Fleury, V., A. Al-Kilani, O.P. Boryskina, A.J.M. Cornelissen, T.-H. Nguyen, M. Unbekandt, L. Leroy, G. Baffet, F. le Noble, O. Sire, E. Lahaye, and V. Burgaud. 2010. Introducing the scanning air puff tonometer for biological studies. *Phys Rev E.* 81:021920. doi:10.1103/physreve.81.021920.

Follansbee, T.L., K.J. Gjelsvik, C.L. Brann, A.L. McParland, C.A. Longhurst, M.J. Galko, and G.K. Ganter. 2017. Drosophila Nociceptive Sensitization Requires BMP Signaling via the Canonical SMAD Pathway. *J Neurosci*. 37:8524–8533. doi:10.1523/jneurosci.3458-16.2017.

Fortini, M.E., M.P. Skupski, M.S. Boguski, and I.K. Hariharan. 2000. A Survey of Human Disease Gene Counterparts in the Drosophila Genome. *J Cell Biology*. 150:F23–F30. doi:10.1083/jcb.150.2.f23.

Fountain, S.J., and G. Burnstock. 2009. An evolutionary history of P2X receptors. *Purinerg Signal*. 5:269–272. doi:10.1007/s11302-008-9127-x.

Fruhstorfer, H., W. Gross, and O. Selbmann. 2001. von Frey hairs: new materials for a new design. *Eur J Pain*. 5:341–342. doi:10.1053/eujp.2001.0250.

Galko, M.J., and M.A. Krasnow. 2004. Cellular and Genetic Analysis of Wound Healing in Drosophila Larvae. *Plos Biol*. 2:e239. doi:10.1371/journal.pbio.0020239.

Ganguly, S., O. Trottier, X. Liang, H. Bowne-Anderson, and J. Howard. 2016. Morphology of Fly Larval Class IV Dendrites Accords with a Random Branching and Contact Based Branch Deletion Model. *Arxiv*.

Gao, F.-B., J.E. Brenman, L.Y. Jan, and Y.N. Jan. 1999. Genes regulating dendritic outgrowth, branching, and routing in Drosophila. *Gene Dev*. 13:2549–2561. doi:10.1101/gad.13.19.2549.

Gasperini, R.J., M. Pavez, A.C. Thompson, C.B. Mitchell, H. Hardy, K.M. Young, J.K. Chilton, and L. Foa. 2017. How does calcium interact with the cytoskeleton to regulate growth cone motility during axon pathfinding? *Mol Cell Neurosci*. 84:29–35. doi:10.1016/j.mcn.2017.07.006.

Gaub, B.M., K.C. Kasuba, E. Mace, T. Strittmatter, P.R. Laskowski, S.A. Geissler, A. Hierlemann, M. Fussenegger, B. Roska, and D.J. Müller. 2019. Neurons differentiate magnitude and location of mechanical stimuli. *P Natl Acad Sci Usa*. 117:848–856. doi:10.1073/pnas.1909933117.

Ghannad-Rezaie, M., X. Wang, B. Mishra, C. Collins, and N. Chronis. 2012. Microfluidic chips for in vivo imaging of cellular responses to neural injury in Drosophila larvae. *Plos One*. 7:e29869. doi:10.1371/journal.pone.0029869.

Glausier, J.R., and D.A. Lewis. 2013. Dendritic spine pathology in schizophrenia. *Neuroscience*. 251:90–107. doi:10.1016/j.neuroscience.2012.04.044.

Gochin, P.M., M. Colombo, G.A. Dorfman, G.L. Gerstein, and C.G. Gross. 1994. Neural ensemble coding in inferior temporal cortex. *J Neurophysiol*. 71:2325–2337. doi:10.1152/jn.1994.71.6.2325.

Golding, N.L., N.P. Staff, and N. Spruston. 2002. Dendritic spikes as a mechanism for cooperative long-term potentiation. *Nature*. 418:326–331. doi:10.1038/nature00854.

Grueber, W.B., L.Y. Jan, and Y.N. Jan. 2002. Tiling of the Drosophila epidermis by multidendritic sensory neurons. *Dev Camb Engl*. 129:2867–78.

Grueber, W.B., B. Ye, A.W. Moore, L.Y. Jan, and Y.N. Jan. 2003. Dendrites of Distinct Classes of Drosophila Sensory Neurons Show Different Capacities for Homotypic Repulsion. *Curr Biol*. 13:618–626. doi:10.1016/s0960-9822(03)00207-0.

Gu, P., J. Gong, Y. Shang, F. Wang, K.T. Ruppell, Z. Ma, A.E. Sheehan, M.R. Freeman, and Y. Xiang. 2019. Polymodal Nociception in Drosophila Requires Alternative Splicing of TrpA1. *Curr Biol*. 29:3961-3973.e6. doi:10.1016/j.cub.2019.09.070.

Guillery, R.W. 2005. Observations of synaptic structures: origins of the neuron doctrine and its current status. *Philosophical Transactions Royal Soc B Biological Sci*. 360:1281–1307. doi:10.1098/rstb.2003.1459.

Guo, Y., Y. Wang, Q. Wang, and Z. Wang. 2014. The Role of PPK26 in Drosophila Larval Mechanical Nociception. *Cell Reports*. 9:1183–1190. doi:10.1016/j.celrep.2014.10.020.

Hales, K.G., C.A. Korey, A.M. Larracuente, and D.M. Roberts. 2015. Genetics on the Fly: A Primer on the Drosophila Model System. *Genetics*. 201:815–842. doi:10.1534/genetics.115.183392.

Halligan, D.L., and P.D. Keightley. 2006. Ubiquitous selective constraints in the Drosophila genome revealed by a genome-wide interspecies comparison. *Genome Res*. 16:875–884. doi:10.1101/gr.5022906.

Hamilton, S.G., and S.B. McMahon. 2000. ATP as a peripheral mediator of pain. *J Autonom Nerv Syst*. 81:187–194. doi:10.1016/s0165-1838(00)00137-5.

Hardie, R.C., and B. Minke. 1992. The trp gene is essential for a light-activated Ca2+ channel in Drosophila photoreceptors. *Neuron*. 8:643–651. doi:10.1016/0896-6273(92)90086-s.

Häusser, M. 2000. The Hodgkin-Huxley theory of the action potential. *Nat Neurosci*. 3:1165–1165. doi:10.1038/81426.

Häusser, M., N. Spruston, and G.J. Stuart. 2000. Diversity and Dynamics of Dendritic Signaling. *Science*. 290:739–744. doi:10.1126/science.290.5492.739.

He, L., S. Gulyanon, M.M. Skanata, D. Karagyozov, E.S. Heckscher, M. Krieg, G. Tsechpenakis, M. Gershow, and W.D. Tracey. 2019. Direction Selectivity in Drosophila Proprioceptors Requires the Mechanosensory Channel Tmc. *Curr Biology Cb*. 29:945-956.e3. doi:10.1016/j.cub.2019.02.025.

Hegemann, P., and A. Möglich. 2011. Channelrhodopsin engineering and exploration of new optogenetic tools. *Nat Methods*. 8:39–42. doi:10.1038/nmeth.f.327.

Henricson, A., E.L. Sonnhammer, D.L. Baillie, and A.V. Gomes. 2004. Functional characterization in Caenorhabditis elegans of transmembrane worm-human orthologs. *Bmc Genomics*. 5:85. doi:10.1186/1471-2164-5-85.

Herculano-Houzel, S. 2009. The Human Brain in Numbers: A Linearly Scaled-up Primate Brain. *Front Hum Neurosci*. 3:31. doi:10.3389/neuro.09.031.2009.

Herzmann, S., I. Götzelmann, L.-F. Reekers, and S. Rumpf. 2018. Spatial regulation of microtubule disruption during dendrite pruning in Drosophila. *Development*. 145:dev.156950. doi:10.1242/dev.156950.

Herzmann, S., R. Krumkamp, S. Rode, C. Kintrup, and S. Rumpf. 2017. PAR-1 promotes microtubule breakdown during dendrite pruning in Drosophila. *Embo J*. 36:1981–1991. doi:10.15252/embj.201695890.

HF, M., L. J, S. F, C. A, and P. G. 2001. NSAID Antinociception Measured in a Chemical and a Thermal Assay in Mice. *Pain Res Management*. 6:190–196. doi:10.1155/2001/701427.

Hibi, M., K. Matsuda, M. Takeuchi, T. Shimizu, and Y. Murakami. 2017. Evolutionary mechanisms that generate morphology and neural-circuit diversity of the cerebellum. *Dev Growth Amp Differ*. 59:228–243. doi:10.1111/dgd.12349.

Higley, M.J., and B.L. Sabatini. 2008. Calcium Signaling in Dendrites and Spines: Practical and Functional Considerations. *Neuron*. 59:902–913. doi:10.1016/j.neuron.2008.08.020.

Hill, R.S., and C.A. Walsh. 2005. Molecular insights into human brain evolution. *Nature*. 437:64–67. doi:10.1038/nature04103.

Hirano, T. 2018. Purkinje Neurons: Development, Morphology, and Function. *Cerebellum*. 17:699–700. doi:10.1007/s12311-018-0985-7.

Hodge, R.D., T.E. Bakken, J.A. Miller, K.A. Smith, E.R. Barkan, L.T. Graybuck, J.L. Close, B. Long, N. Johansen, O. Penn, Z. Yao, J. Eggermont, T. Höllt, B.P. Levi, S.I. Shehata, B. Aevermann, A. Beller, D. Bertagnolli, K. Brouner, T. Casper, C. Cobbs, R. Dalley, N. Dee, S.-L. Ding, R.G. Ellenbogen, O. Fong, E. Garren, J. Goldy, R.P. Gwinn, D. Hirschstein, C.D. Keene, M. Keshk, A.L. Ko, K. Lathia, A. Mahfouz, Z. Maltzer, M. McGraw, T.N. Nguyen, J. Nyhus, J.G. Ojemann, A. Oldre, S. Parry, S. Reynolds, C. Rimorin, N.V. Shapovalova, S. Somasundaram, A. Szafer, E.R. Thomsen, M. Tieu, G. Quon, R.H. Scheuermann, R. Yuste, S.M. Sunkin, B. Lelieveldt, D. Feng, L. Ng, A. Bernard, M. Hawrylycz, J.W. Phillips, B. Tasic, H. Zeng, A.R. Jones, C. Koch, and E.S. Lein. 2019. Conserved cell types with divergent features in human versus mouse cortex. *Nature*. 573:61–68. doi:10.1038/s41586-019-1506-7.

Hodgkin, A.L., and A.F. Huxley. 1952. A quantitative description of membrane current and its application to conduction and excitation in nerve. *J Physiology*. 117:500–544. doi:10.1113/jphysiol.1952.sp004764.

Honjo, K., R.Y. Hwang, and W.D. Tracey. 2012. Optogenetic manipulation of neural circuits and behavior in Drosophila larvae. *Nat Protoc*. 7:1470–1478. doi:10.1038/nprot.2012.079.

Hori, M., K. Shibuya, M. Sato, and Y. Saito. 2014. Lethal effects of short-wavelength visible light on insects. *Sci Rep-uk*. 4:7383. doi:10.1038/srep07383.

Hsu, A., Y. Tsukamoto, R.G. Smith, and P. Sterling. 1998. Functional architecture of primate cone and rod axons. *Vision Res*. 38:2539–2549. doi:10.1016/s0042-6989(97)00370-2.

Huang, Z.J., and A. Paul. 2019. The diversity of GABAergic neurons and neural communication elements. *Nat Rev Neurosci*. 20:563–572. doi:10.1038/s41583-019-0195-4.

Hwang, R.Y., L. Zhong, Y. Xu, T. Johnson, F. Zhang, K. Deisseroth, and W.D. Tracey. 2007a. Nociceptive Neurons Protect Drosophila Larvae from Parasitoid Wasps. *Curr Biol*. 17:2105–2116. doi:10.1016/j.cub.2007.11.029.

Hwang, R.Y., L. Zhong, Y. Xu, T. Johnson, F. Zhang, K. Deisseroth, and W.D. Tracey. 2007b. Nociceptive Neurons Protect Drosophila Larvae from Parasitoid Wasps. *Curr Biol*. 17:2105–2116. doi:10.1016/j.cub.2007.11.029.

Illich, P.A., and E.T. Walters. 1997. Mechanosensory Neurons Innervating Aplysia Siphon Encode Noxious Stimuli and Display Nociceptive Sensitization. *J Neurosci*. 17:459–469. doi:10.1523/jneurosci.17-01-00459.1997.

Im, S.H., and M.J. Galko. 2012. Pokes, sunburn, and hot sauce: Drosophila as an emerging model for the biology of nociception. *Dev Dynam*. 241:16–26. doi:10.1002/dvdy.22737.

Im, S.H., K. Takle, J. Jo, D.T. Babcock, Z. Ma, Y. Xiang, and M.J. Galko. 2015. Tachykinin acts upstream of autocrine Hedgehog signaling during nociceptive sensitization in Drosophila. *Elife*. 4:e10735. doi:10.7554/elife.10735.

Inui, K., X. Wang, Y. Tamura, Y. Kaneoke, and R. Kakigi. 2004. Serial Processing in the Human Somatosensory System. *Cereb Cortex*. 14:851–857. doi:10.1093/cercor/bhh043.

Jan, Y.-N., and L.Y. Jan. 2001. Dendrites. *Gene Dev*. 15:2627–2641. doi:10.1101/gad.916501.

Jan, Y.-N., and L.Y. Jan. 2010. Branching out: mechanisms of dendritic arborization. *Nat Rev Neurosci*. 11:316–328. doi:10.1038/nrn2836.

Jenett, A., G.M. Rubin, T.-T.B. Ngo, D. Shepherd, C. Murphy, H. Dionne, B.D. Pfeiffer, A. Cavallaro, D. Hall, J. Jeter, N. Iyer, D. Fetter, J.H. Hausenfluck, H. Peng, E.T. Trautman, R.R. Svirskas, E.W. Myers, Z.R. Iwinski, Y. Aso, G.M. DePasquale, A. Enos, P. Hulamm, S.C.B. Lam, H.-H. Li, T.R. Laverty, F. Long, L. Qu, S.D. Murphy, K. Rokicki, T. Safford, K. Shaw, J.H. Simpson, A. Sowell, S. Tae, Y. Yu, and C.T. Zugates. 2012a. A GAL4-Driver Line Resource for Drosophila Neurobiology. *Cell Reports*. 2:991–1001. doi:10.1016/j.celrep.2012.09.011.

Jenett, A., G.M. Rubin, T.-T.B. Ngo, D. Shepherd, C. Murphy, H. Dionne, B.D. Pfeiffer, A. Cavallaro, D. Hall, J. Jeter, N. Iyer, D. Fetter, J.H. Hausenfluck, H. Peng, E.T. Trautman, R.R. Svirskas, E.W. Myers, Z.R. Iwinski, Y. Aso, G.M. DePasquale, A. Enos, P. Hulamm, S.C.B. Lam, H.-H. Li, T.R. Laverty, F. Long, L. Qu, S.D. Murphy, K. Rokicki, T. Safford, K. Shaw, J.H. Simpson, A. Sowell, S. Tae, Y. Yu, and C.T. Zugates. 2012b. A GAL4-Driver Line Resource for Drosophila Neurobiology. *Cell Reports*. 2:991–1001. doi:10.1016/j.celrep.2012.09.011.

Johnson, W.A., and J.W. Carder. 2012. Drosophila nociceptors mediate larval aversion to dry surface environments utilizing both the painless TRP channel and the DEG/ENaC subunit, PPK1. *Plos One*. 7:e32878. doi:10.1371/journal.pone.0032878.

Jones, E.G. 1999. Golgi, Cajal and the Neuron Doctrine. *J Hist Neurosci*. 8:170–178. doi:10.1076/jhin.8.2.170.1838.

Kakanj, P., S.A. Eming, L. Partridge, and M. Leptin. 2020. Long-term in vivo imaging of Drosophila larvae. *Nat Protoc*. 15:1158–1187. doi:10.1038/s41596-019-0282-z.

Kanamori, T., M.I. Kanai, Y. Dairyo, K. -i Yasunaga, R.K. Morikawa, and K. Emoto. 2013. Compartmentalized Calcium Transients Trigger Dendrite Pruning in Drosophila Sensory Neurons. *Science*. 340:1475–1478. doi:10.1126/science.1234879.

Kavaliers, M. 1988. Evolutionary and comparative aspects of nociception. *Brain Res Bull*. 21:923–931. doi:10.1016/0361-9230(88)90030-5.

Kellerth, J., C. Berthold, and S. Conradi. 1979. Electron microscopic studies of serially sectioned cat spinal α-motoneurons. III. Motoneurons innervating fast-twitch (type fr) units of the gastrocnemius muscle. *J Comp Neurol*. 184:755–767. doi:10.1002/cne.901840408.

Kim, M.-J., and W.A. Johnson. 2014. ROS-mediated activation of Drosophila larval nociceptor neurons by UVC irradiation. *Bmc Neurosci*. 15:14. doi:10.1186/1471-2202-15-14.

Kim, S.E., B. Coste, A. Chadha, B. Cook, and A. Patapoutian. 2012. The role of Drosophila Piezo in mechanical nociception. *Nature*. 483:209–12. doi:10.1038/nature10801.

Kitamura, K., and M. Häusser. 2011. Dendritic Calcium Signaling Triggered by Spontaneous and Sensory-Evoked Climbing Fiber Input to Cerebellar Purkinje Cells In Vivo. *J Neurosci*. 31:10847–10858. doi:10.1523/jneurosci.2525-10.2011.

Kling, S., N. Bekesi, C. Dorronsoro, D. Pascual, and S. Marcos. 2014. Corneal Viscoelastic Properties from Finite-Element Analysis of In Vivo Air-Puff Deformation. *Plos One*. 9:e104904. doi:10.1371/journal.pone.0104904.

Kling, S., and S. Marcos. 2013. Contributing Factors to Corneal Deformation in Air Puff MeasurementsCorneal Deformation in Air Puff Measurements. *Invest Ophth Vis Sci*. 54:5078–5085. doi:10.1167/iovs.13-12509.

Kole, M.H.P., and G.J. Stuart. 2008. Is action potential threshold lowest in the axon? *Nat Neurosci*. 11:1253–1255. doi:10.1038/nn.2203.

Konur, S., and A. Ghosh. 2005. Calcium Signaling and the Control of Dendritic Development. *Neuron*. 46:401–405. doi:10.1016/j.neuron.2005.04.022.

Kornreich, B.G. 2007. The patch clamp technique: Principles and technical considerations. *J Vet Cardiol*. 9:25–37. doi:10.1016/j.jvc.2007.02.001.

Kruger, L., A.R. Light, and F.E. Schweizer. 2003. Axonal terminals of sensory neurons and their morphological diversity. *J Neurocytol*. 32:205–216. doi:10.1023/b:neur.0000010080.62031.f0.

Kuo, C.T., L.Y. Jan, and Y.N. Jan. 2005. Dendrite-specific remodeling of Drosophila sensory neurons requires matrix metalloproteases, ubiquitin-proteasome, and ecdysone signaling. *P Natl Acad Sci Usa*. 102:15230–15235. doi:10.1073/pnas.0507393102.

Kweon, J.H., S. Kim, and S.B. Lee. 2017. The cellular basis of dendrite pathology in neurodegenerative diseases. *Bmb Rep*. 50:5–11. doi:10.5483/bmbrep.2017.50.1.131.

Lah, G.J., J.S.S. Li, and S.S. Millard. 2014. Cell-Specific Alternative Splicing of Drosophila Dscam2 Is Crucial for Proper Neuronal Wiring. *Neuron*. 83:1376–1388. doi:10.1016/j.neuron.2014.08.002.

Lai, C.-H., C.-Y. Chou, L.-Y. Ch'ang, C.-S. Liu, and W. Lin. 2000. Identification of Novel Human Genes Evolutionarily Conserved in Caenorhabditis elegans by Comparative Proteomics. *Genome Res*. 10:703–713. doi:10.1101/gr.10.5.703.

Lai, S.-L., and T. Lee. 2006. Genetic mosaic with dual binary transcriptional systems in Drosophila. *Nat Neurosci*. 9:703–709. doi:10.1038/nn1681.

Lambert, G.A., G. Mallos, and A.S. Zagami. 2009. Von Frey's hairs – a review of their technology and use – a novel automated von Frey device for improved testing for hyperalgesia. *J Neurosci Meth*. 177:420–426. doi:10.1016/j.jneumeth.2008.10.033.

Lee, H.-H., L.Y. Jan, and Y.-N. Jan. 2009. Drosophila IKK-related kinase Ik2 and Katanin p60-like 1 regulate dendrite pruning of sensory neuron during metamorphosis. *P Natl Acad Sci Usa*. 106:6363–8. doi:10.1073/pnas.0902051106.

Lent, R., F.A.C. Azevedo, C.H. Andrade-Moraes, and A.V.O. Pinto. 2012. How many neurons do you have? Some dogmas of quantitative neuroscience under revision. *Eur J Neurosci*. 35:1–9. doi:10.1111/j.1460-9568.2011.07923.x.

Li, Q.S., G.Y.H. Lee, C.N. Ong, and C.T. Lim. 2008. AFM indentation study of breast cancer cells. *Biochem Bioph Res Co*. 374:609–613. doi:10.1016/j.bbrc.2008.07.078.

Li, W.-C., T. Cooke, B. Sautois, S.R. Soffe, R. Borisyuk, and A. Roberts. 2007. Axon and dendrite geography predict the specificity of synaptic connections in a functioning spinal cord network. *Neural Dev*. 2:17. doi:10.1186/1749-8104-2-17.

Liao, M., and J. Howard. 2020. The Narrowing of Dendrite Branches across Nodes follows a well-defined Scaling Law. *Biorxiv*. 2020.04.13.039388. doi:10.1101/2020.04.13.039388.

Lichtneckert, R., and H. Reichert. 2005. Insights into the urbilaterian brain: conserved genetic patterning mechanisms in insect and vertebrate brain development. *Heredity*. 94:465–477. doi:10.1038/sj.hdy.6800664.

Liem, L.K., J.M. Simard, Y. Song, and K. Tewari. 1995. The Patch Clamp Technique. *Neurosurgery*. 36:382–392. doi:10.1227/00006123-199502000-00020.

Llin s, R.R. 2003. The contribution of Santiago Ramon y Cajal to functional neuroscience. *Nat Rev Neurosci*. 4:77–80. doi:10.1038/nrn1011.

Lockwood, D.B., J.C. Wataha, J.B. Lewis, W.Y. Tseng, R.L.W. Messer, and S.D. Hsu. 2005. Blue light generates reactive oxygen species (ROS) differentially in tumor vs. normal epithelial cells. *Dent Mater*. 21:683–688. doi:10.1016/j.dental.2004.07.022.

London, M., and M. Häusser. 2005. DENDRITIC COMPUTATION. *Annu Rev Neurosci*. 28:503–532. doi:10.1146/annurev.neuro.28.061604.135703.

Long, H., Y. Ou, Y. Rao, and D.J. van Meyel. 2009. Dendrite branching and self-avoidance are controlled by Turtle, a conserved IgSF protein in Drosophila. *Development*. 136:3475–3484. doi:10.1242/dev.040220.

Longair, M.H., D.A. Baker, and J.D. Armstrong. 2011. Simple Neurite Tracer: open source software for reconstruction, visualization and analysis of neuronal processes. *Bioinformatics*. 27:2453–2454. doi:10.1093/bioinformatics/btr390.

Lopez-Bellido, R., N.J. Himmel, H.B. Gutstein, D.N. Cox, and M.J. Galko. 2019. An assay for chemical nociception in Drosophila larvae. *Philosophical Transactions Royal Soc B*. 374:20190282. doi:10.1098/rstb.2019.0282.

López-Muñoz, F., J. Boya, and C. Alamo. 2006. Neuron theory, the cornerstone of neuroscience, on the centenary of the Nobel Prize award to Santiago Ramón y Cajal. *Brain Res Bull*. 70:391–405. doi:10.1016/j.brainresbull.2006.07.010.

Lumpkin, E.A., and D.M. Bautista. 2005. Feeling the pressure in mammalian somatosensation. *Curr Opin Neurobiol*. 15:382–388. doi:10.1016/j.conb.2005.06.005.

Lumpkin, E.A., and M.J. Caterina. 2007. Mechanisms of sensory transduction in the skin. *Nature*. 445:858–865. doi:10.1038/nature05662.

Marger, F., A. Gelot, A. Alloui, J. Matricon, J.F.S. Ferrer, C. Barrère, A. Pizzoccaro, E. Muller, J. Nargeot, T.P. Snutch, A. Eschalier, E. Bourinet, and D. Ardid. 2011. T-type calcium channels contribute to colonic hypersensitivity in a rat model of

irritable bowel syndrome. *Proc National Acad Sci*. 108:11268–11273. doi:10.1073/pnas.1100869108.

Martínez-Cerdeño, V. 2017. Dendrite and spine modifications in autism and related neurodevelopmental disorders in patients and animal models. *Dev Neurobiol*. 77:393–404. doi:10.1002/dneu.22417.

Matsubara, D., S. Horiuchi, K. Shimono, T. Usui, and T. Uemura. 2011. The seven-pass transmembrane cadherin Flamingo controls dendritic self-avoidance via its binding to a LIM domain protein, Espinas, in Drosophila sensory neurons. *Gene Dev*. 25:1982–1996. doi:10.1101/gad.16531611.

Matthews, B.J., M.E. Kim, J.J. Flanagan, D. Hattori, J.C. Clemens, S.L. Zipursky, and W.B. Grueber. 2007. Dendrite Self-Avoidance Is Controlled by Dscam. *Cell*. 129:593–604. doi:10.1016/j.cell.2007.04.013.

Matthews, K.A., T.C. Kaufman, and W.M. Gelbart. 2005. Research resources for Drosophila: the expanding universe. *Nat Rev Genet*. 6:179–193. doi:10.1038/nrg1554.

McCleskey, E.W., and M.S. Gold. 1999. ION CHANNELS OF NOCICEPTION. *Annu Rev Physiol*. 61:835–856. doi:10.1146/annurev.physiol.61.1.835.

McGuire, S.E., G. Roman, and R.L. Davis. 2004. Gene expression systems in Drosophila: a synthesis of time and space. *Trends Genet*. 20:384–391. doi:10.1016/j.tig.2004.06.012.

McMackin, M.Z., M.R. Lewin, D.R. Tabuena, F.E. Arreola, C. Moffatt, and M. Fuse. 2016. Use of von Frey filaments to assess nociceptive sensitization in the hornworm, Manduca sexta. *J Neurosci Meth*. 257:139–146. doi:10.1016/j.jneumeth.2015.09.015.

Merriam, E.B., M. Millette, D.C. Lumbard, W. Saengsawang, T. Fothergill, X. Hu, L. Ferhat, and E.W. Dent. 2013. Synaptic Regulation of Microtubule Dynamics in Dendritic Spines by Calcium, F-Actin, and Drebrin. *J Neurosci*. 33:16471–16482. doi:10.1523/jneurosci.0661-13.2013.

Millard, S.S., and S.L. Zipursky. 2008. Dscam-mediated repulsion controls tiling and self-avoidance. *Curr Opin Neurobiol*. 18:84–89. doi:10.1016/j.conb.2008.05.005.

Miller, F.D., and D.R. Kaplan. 2003. Signaling mechanisms underlying dendrite formation. *Curr Opin Neurobiol*. 13:391–398. doi:10.1016/s0959-4388(03)00072-2.

Mirzoyan, Z., M. Sollazzo, M. Allocca, A.M. Valenza, D. Grifoni, and P. Bellosta. 2019. Drosophila melanogaster: A Model Organism to Study Cancer. *Frontiers Genetics*. 10:51. doi:10.3389/fgene.2019.00051.

Mishra, B., M. Ghannad-Rezaie, J. Li, X. Wang, Y. Hao, B. Ye, N. Chronis, and C.A. Collins. 2014. Using Microfluidics Chips for Live Imaging and Study of Injury Responses in Drosophila Larvae. *J Vis Exp Jove*. 50998. doi:10.3791/50998.

Moolman, D.L., O.V. Vitolo, J.-P.G. Vonsattel, and M.L. Shelanski. 2004. Dendrite and dendritic spine alterations in alzheimer models. *J Neurocytol*. 33:377–387. doi:10.1023/b:neur.0000044197.83514.64.

Moreaux, L., and G. Laurent. 2008. A Simple Method to Reconstruct Firing Rates from Dendritic Calcium Signals. *Front Neurosci-switz*. 2:176–185. doi:10.3389/neuro.01.032.2008.

Morgan, T.H. 1910. Sex Limited Inheritance in Drosophila. *Science*.

Morrison, E.E., and R.M. Costanzo. 1990. Morphology of the human olfactory epithelium. *J Comp Neurol*. 297:1–13. doi:10.1002/cne.902970102.

Nagayama, S., R. Homma, and F. Imamura. 2014. Neuronal organization of olfactory bulb circuits. *Front Neural Circuit*. 8:98. doi:10.3389/fncir.2014.00098.

Nairn, J.G., K.S. Bedi, T.M. Mayhew, and L.F. Campbell. 1989. On the number of purkinje cells in the human cerebellum: Unbiased estimates obtained by using the "fractionator." *J Comp Neurol*. 290:527–532. doi:10.1002/cne.902900407.

Narayanan, N.S., E.Y. Kimchi, and M. Laubach. 2005. Redundancy and Synergy of Neuronal Ensembles in Motor Cortex. *J Neurosci*. 25:4207–4216. doi:10.1523/jneurosci.4697-04.2005.

Neely, G.G., A.C. Keene, P. Duchek, E.C. Chang, Q.-P. Wang, Y.A. Aksoy, M. Rosenzweig, M. Costigan, C.J. Woolf, P.A. Garrity, and J.M. Penninger. 2011. TrpA1 Regulates Thermal Nociception in Drosophila. *Plos One*. 6:e24343. doi:10.1371/journal.pone.0024343.

Newey, S.E., V. Velamoor, E. Govek, and L.V. Aelst. 2005. Rho GTPases, dendritic structure, and mental retardation. *J Neurobiol*. 64:58–74. doi:10.1002/neu.20153.

Nijs, J., L. Daenen, P. Cras, F. Struyf, N. Roussel, and R.A.B. Oostendorp. 2012. Nociception Affects Motor Output. *Clin J Pain*. 28:175–181. doi:10.1097/ajp.0b013e318225daf3.

Oertner, T.G., and A. Matus. 2005. Calcium regulation of actin dynamics in dendritic spines. *Cell Calcium*. 37:477–482. doi:10.1016/j.ceca.2005.01.016.

Ohyama, T., T. Jovanic, G. Denisov, T.C. Dang, D. Hoffmann, R.A. Kerr, and M. Zlatic. 2013. High-Throughput Analysis of Stimulus-Evoked Behaviors in Drosophila Larva Reveals Multiple Modality-Specific Escape Strategies. *Plos One*. 8:e71706. doi:10.1371/journal.pone.0071706.

Onodera, K., S. Baba, A. Murakami, T. Uemura, and T. Usui. 2017. Small conductance Ca2+-activated K+ channels induce the firing pause periods during the activation of Drosophila nociceptive neurons. *Elife*. 6:e29754. doi:10.7554/elife.29754.

Orgogozo, V., and W.B. Grueber. 2005. FlyPNS, a database of the Drosophila embryonic and larval peripheral nervous system. *Bmc Dev Biol*. 5:4. doi:10.1186/1471-213x-5-4.

Oswald, M., B. Rymarczyk, A. Chatters, and S. Sweeney. 2011. A novel thermosensitive escape behavior in Drosophila larvae. *Fly*. 5:304–306. doi:10.4161/fly.5.4.17810.

Owens, D.M., and E.A. Lumpkin. 2014. Diversification and Specialization of Touch Receptors in Skin. *Csh Perspect Med*. 4:a013656. doi:10.1101/cshperspect.a013656.

Pandey, U.B., and C.D. Nichols. 2011. Human Disease Models in Drosophila melanogaster and the Role of the Fly in Therapeutic Drug Discovery. *Pharmacol Rev*. 63:411–436. doi:10.1124/pr.110.003293.

Parrish, J.Z., P. Xu, C.C. Kim, L.Y. Jan, and Y.N. Jan. 2009. The microRNA bantam functions in epithelial cells to regulate scaling growth of dendrite arbors in drosophila sensory neurons. *Neuron*. 63:788–802. doi:10.1016/j.neuron.2009.08.006.

Perkins, L.A., L. Holderbaum, R. Tao, Y. Hu, R. Sopko, K. McCall, D. Yang-Zhou, I. Flockhart, R. Binari, H.-S. Shim, A. Miller, A. Housden, M. Foos, S. Randkelv, C. Kelley, P. Namgyal, C. Villalta, L.-P. Liu, X. Jiang, Q. Huan-Huan, X. Wang, A. Fujiyama, A. Toyoda, K. Ayers, A. Blum, B. Czech, R. Neumuller, D. Yan, A. Cavallaro, K. Hibbard, D. Hall, L. Cooley, G.J. Hannon, R. Lehmann, A. Parks, S.E. Mohr, R. Ueda, S. Kondo, J.-Q. Ni, and N. Perrimon. 2015. The Transgenic RNAi Project at Harvard Medical School: Resources and Validation. *Genetics*. 201:843–852. doi:10.1534/genetics.115.180208.

Perl, E.R. 2007. Ideas about pain, a historical view. *Nat Rev Neurosci*. 8:71–80. doi:10.1038/nrn2042.

Pnevmatikakis, E.A. 2019. Analysis pipelines for calcium imaging data. *Curr Opin Neurobiol*. 55:15–21. doi:10.1016/j.conb.2018.11.004.

Potter, C.J., and L. Luo. 2011. Using the Q system in Drosophila melanogaster. *Nat Protoc*. 6:1105–1120. doi:10.1038/nprot.2011.347.

Prigge, M., F. Schneider, S.P. Tsunoda, C. Shilyansky, J. Wietek, K. Deisseroth, and P. Hegemann. 2012. Color-tuned Channelrhodopsins for Multiwavelength Optogenetics. *J Biol Chem*. 287:31804–31812. doi:10.1074/jbc.m112.391185.

Redmond, L., and A. Ghosh. 2005. Regulation of dendritic development by calcium signaling. *Cell Calcium*. 37:411–416. doi:10.1016/j.ceca.2005.01.009.

Reich, D.S., F. Mechler, and J.D. Victor. 2001. Independent and Redundant Information in Nearby Cortical Neurons. *Science*. 294:2566–2568. doi:10.1126/science.1065839.

Reichert, H. 2009. Evolutionary conservation of mechanisms for neural regionalization, proliferation and interconnection in brain development. *Biol Letters*. 5:112–116. doi:10.1098/rsbl.2008.0337.

Reynolds, J.P., K. Zheng, and D.A. Rusakov. 2018. Multiplexed calcium imaging of single-synapse activity and astroglial responses in the intact brain. *Neurosci Lett*. 689:26–32. doi:10.1016/j.neulet.2018.06.024.

Riabinina, O., and C.J. Potter. 2016. Drosophila, Methods and Protocols. *Methods Mol Biology*. 53–78. doi:10.1007/978-1-4939-6371-3_3.

Robertson, J.L., A. Tsubouchi, and W.D. Tracey. 2013. Larval Defense against Attack from Parasitoid Wasps Requires Nociceptive Neurons. *Plos One*. 8:e78704. doi:10.1371/journal.pone.0078704.

Rodgers, J.B., and W.S. Ryu. 2020. Targeted thermal stimulation and high-content phenotyping reveal that the C. elegans escape response integrates current behavioral state and past experience. *Plos One*. 15:e0229399. doi:10.1371/journal.pone.0229399.

Rodríguez, A. del V., D. Didiano, and C. Desplan. 2012. Power tools for gene expression and clonal analysis in Drosophila. *Nat Methods*. 9:47–55. doi:10.1038/nmeth.1800.

Romanova, E.V., and J.V. Sweedler. 2018. Animal Model Systems in Neuroscience. *Acs Chem Neurosci*. 9:1869–1870. doi:10.1021/acschemneuro.8b00380.

Rosenberg, S.S., and N.C. Spitzer. 2011. Calcium Signaling in Neuronal Development. *Csh Perspect Biol.* 3:a004259. doi:10.1101/cshperspect.a004259.

Ruhnow, F., D. Zwicker, and S. Diez. 2011. Tracking Single Particles and Elongated Filaments with Nanometer Precision. *Biophys J.* 100:2820–2828. doi:10.1016/j.bpj.2011.04.023.

Russell, J.T. 2011. Imaging calcium signals in vivo: a powerful tool in physiology and pharmacology. *Brit J Pharmacol.* 163:1605–1625. doi:10.1111/j.1476-5381.2010.00988.x.

Sabatini, B.L. 2019. The impact of reporter kinetics on the interpretation of data gathered with fluorescent reporters. *Biorxiv*. 834895. doi:10.1101/834895.

Sabatini, B.L., M. Maravall, and K. Svoboda. 2001. Ca2+ signaling in dendritic spines. *Curr Opin Neurobiol.* 11:349–356. doi:10.1016/s0959-4388(00)00218-x.

Sattelle, D.B., and S.D. Buckingham. 2006. Invertebrate studies and their ongoing contributions to neuroscience. *Invertebr Neurosci.* 6:1–3. doi:10.1007/s10158-005-0014-7.

Scheffer, L.K., C.S. Xu, M. Januszewski, Z. Lu, S. Takemura, K.J. Hayworth, G.B. Huang, K. Shinomiya, J. Maitlin-Shepard, S. Berg, J. Clements, P.M. Hubbard, W.T. Katz, L. Umayam, T. Zhao, D. Ackerman, T. Blakely, J. Bogovic, T. Dolafi, D. Kainmueller, T. Kawase, K.A. Khairy, L. Leavitt, P.H. Li, L. Lindsey, N. Neubarth, D.J. Olbris, H. Otsuna, E.T. Trautman, M. Ito, A.S. Bates, J. Goldammer, T. Wolff, R. Svirskas, P. Schlegel, E. Neace, C.J. Knecht, C.X. Alvarado, D.A. Bailey, S. Ballinger, J.A. Borycz, B.S. Canino, N. Cheatham, M. Cook, M. Dreher, O. Duclos, B. Eubanks, K. Fairbanks, S. Finley, N. Forknall, A. Francis, G.P. Hopkins, E.M. Joyce, S. Kim, N.A. Kirk, J. Kovalyak, S. Lauchie, A. Lohff, C. Maldonado, E.A. Manley, S. McLin, C. Mooney, M. Ndama, O. Ogundeyi, N. Okeoma, C. Ordish, N. Padilla, C.M. Patrick, T. Paterson, E.E. Phillips, E.M. Phillips, N. Rampally, C. Ribeiro, M.K. Robertson, J.T. Rymer, S.M. Ryan, M. Sammons, A.K. Scott, A.L. Scott, A. Shinomiya, C. Smith, K. Smith, N.L. Smith, M.A. Sobeski, A. Suleiman, J. Swift, S. Takemura, I. Talebi, D. Tarnogorska, E. Tenshaw, T. Tokhi, J.J. Walsh, T. Yang, J.A. Horne, F. Li, R. Parekh, P.K. Rivlin, V. Jayaraman, et al. 2020. A connectome and analysis of the adult Drosophila central brain. *Elife.* 9:e57443. doi:10.7554/elife.57443.

Schmucker, D., J.C. Clemens, H. Shu, C.A. Worby, J. Xiao, M. Muda, J.E. Dixon, and S.L. Zipursky. 2000. Drosophila Dscam Is an Axon Guidance Receptor Exhibiting Extraordinary Molecular Diversity. *Cell.* 101:671–684. doi:10.1016/s0092-8674(00)80878-8.

Schüz, A., and G. Palm. 1989. Density of neurons and synapses in the cerebral cortex of the mouse. *J Comp Neurol*. 286:442–455. doi:10.1002/cne.902860404.

Scott, E.K., and L. Luo. 2001. How do dendrites take their shape? *Nat Neurosci*. 4:359–365. doi:10.1038/86006.

Shepherd, G.M. 1972. The neuron doctrine: a revision of functional concepts. *Yale J Biology Medicine*. 45:584–99.

Shepherd, G.M.G., A. Stepanyants, I. Bureau, D. Chklovskii, and K. Svoboda. 2005. Geometric and functional organization of cortical circuits. *Nat Neurosci*. 8:782–790. doi:10.1038/nn1447.

Sherrington, C.S. 1903. Qualitative difference of spinal reflex corresponding with qualitative difference of cutaneous stimulus. *J Physiology*. 30:39–46. doi:10.1113/jphysiol.1903.sp000980.

Sherrington, C.S. 1907. The Integrative Action of the Nervous System. *Nature*. 76:122–122. doi:10.1038/076122a0.

Sherwood, C.C., A.L. Bauernfeind, S. Bianchi, M.A. Raghanti, and P.R. Hof. 2012. Chapter 11 Human brain evolution writ large and small. *Prog Brain Res*. 195:237–254. doi:10.1016/b978-0-444-53860-4.00011-8.

Shibuya, K., S. Onodera, and M. Hori. 2018. Toxic wavelength of blue light changes as insects grow. *Plos One*. 13:e0199266. doi:10.1371/journal.pone.0199266.

Shimono, K., A. Fujimoto, T. Tsuyama, M. Yamamoto-Kochi, M. Sato, Y. Hattori, K. Sugimura, T. Usui, K. Kimura, and T. Uemura. 2009. Multidendritic sensory neurons in the adult Drosophila abdomen: origins, dendritic morphology, and segment- and age-dependent programmed cell death. *Neural Dev*. 4:37. doi:10.1186/1749-8104-4-37.

Simonetti, M., A.M. Hagenston, D. Vardeh, H.E. Freitag, D. Mauceri, J. Lu, V.P. Satagopam, R. Schneider, M. Costigan, H. Bading, and R. Kuner. 2013. Nuclear Calcium Signaling in Spinal Neurons Drives a Genomic Program Required for Persistent Inflammatory Pain. *Neuron*. 77:43–57. doi:10.1016/j.neuron.2012.10.037.

Šišková, Z., D. Justus, H. Kaneko, D. Friedrichs, N. Henneberg, T. Beutel, J. Pitsch, S. Schoch, A. Becker, H. von der Kammer, and S. Remy. 2014. Dendritic Structural Degeneration Is Functionally Linked to Cellular Hyperexcitability in a Mouse Model of Alzheimer's Disease. *Neuron*. 84:1023–1033. doi:10.1016/j.neuron.2014.10.024.

Sjöstedt, E., W. Zhong, L. Fagerberg, M. Karlsson, N. Mitsios, C. Adori, P. Oksvold, F. Edfors, A. Limiszewska, F. Hikmet, J. Huang, Y. Du, L. Lin, Z. Dong, L. Yang, X. Liu, H. Jiang, X. Xu, J. Wang, H. Yang, L. Bolund, A. Mardinoglu, C. Zhang, K. von Feilitzen, C. Lindskog, F. Pontén, Y. Luo, T. Hökfelt, M. Uhlén, and J. Mulder. 2020. An atlas of the protein-coding genes in the human, pig, and mouse brain. *Science*. 367:eaay5947. doi:10.1126/science.aay5947.

Smith, L.A., X. Wang, A.A. Peixoto, E.K. Neumann, L.M. Hall, and J.C. Hall. 1996. A Drosophila Calcium Channel α1 Subunit Gene Maps to a Genetic Locus Associated with Behavioral and Visual Defects. *J Neurosci*. 16:7868–7879. doi:10.1523/jneurosci.16-24-07868.1996.

Smith, M.B., H. Li, T. Shen, X. Huang, E. Yusuf, and D. Vavylonis. 2010. Segmentation and tracking of cytoskeletal filaments using open active contours. *Cytoskeleton*. 67:693–705. doi:10.1002/cm.20481.

Soba, P., S. Zhu, K. Emoto, S. Younger, S.-J. Yang, H.-H. Yu, T. Lee, L.Y. Jan, and Y.-N. Jan. 2007. Drosophila Sensory Neurons Require Dscam for Dendritic Self-Avoidance and Proper Dendritic Field Organization. *Neuron*. 54:403–416. doi:10.1016/j.neuron.2007.03.029.

Sokabe, T., S. Tsujiuchi, T. Kadowaki, and M. Tominaga. 2008. Drosophila painless is a Ca2+-requiring channel activated by noxious heat. *J Neurosci Official J Soc Neurosci*. 28:9929–38. doi:10.1523/jneurosci.2757-08.2008.

Solis, O., D.I. Limón, J. Flores-Hern ndez, and G. Flores. 2007. Alterations in dendritic morphology of the prefrontal cortical and striatum neurons in the unilateral 6-OHDA-rat model of Parkinson's disease. *Synapse*. 61:450–458. doi:10.1002/syn.20381.

Sotelo, C. 2003. Viewing the brain through the master hand of Ramon y Cajal. *Nat Rev Neurosci*. 4:71–77. doi:10.1038/nrn1010.

Spedden, E., and C. Staii. 2013. Neuron Biomechanics Probed by Atomic Force Microscopy. *Int J Mol Sci*. 14:16124–16140. doi:10.3390/ijms140816124.

Spira, M.E., R. Oren, A. Dormann, N. Ilouz, and S. Lev. 2001. Calcium, Protease Activation, and Cytoskeleton Remodeling Underlie Growth Cone Formation and Neuronal Regeneration. *Cell Mol Neurobiol*. 21:591–604. doi:10.1023/a:1015135617557.

Spruston, N. 2008. Pyramidal neurons: dendritic structure and synaptic integration. *Nat Rev Neurosci*. 9:206–221. doi:10.1038/nrn2286.

Stern, M., E. Shea-Brown, and D. Witten. 2020. Inferring the Spiking Rate of a Population of Neurons from Wide-Field Calcium Imaging. *Biorxiv*. 2020.02.01.930040. doi:10.1101/2020.02.01.930040.

Stewart, A., A. Tsubouchi, M.M. Rolls, W.D. Tracey, and N.T. Sherwood. 2012. Katanin p60-like1 promotes microtubule growth and terminal dendrite stability in the larval class IV sensory neurons of Drosophila. *J Neurosci Official J Soc Neurosci*. 32:11631–42. doi:10.1523/jneurosci.0729-12.2012.

Stringer, C., and M. Pachitariu. 2019. Computational processing of neural recordings from calcium imaging data. *Curr Opin Neurobiol*. 55:22–31. doi:10.1016/j.conb.2018.11.005.

Stutzmann, G.E., and M.P. Mattson. 2011. Endoplasmic Reticulum Ca2+ Handling in Excitable Cells in Health and Disease. *Pharmacol Rev*. 63:700–727. doi:10.1124/pr.110.003814.

Sugimura, K., M. Yamamoto, R. Niwa, D. Satoh, S. Goto, M. Taniguchi, S. Hayashi, and T. Uemura. 2003. Distinct Developmental Modes and Lesion-Induced Reactions of Dendrites of Two Classes of Drosophila Sensory Neurons. *J Neurosci*. 23:3752–3760. doi:10.1523/jneurosci.23-09-03752.2003.

Suk, H.-J., E.S. Boyden, and I. van Welie. 2019. Advances in the automation of whole-cell patch clamp technology. *J Neurosci Meth*. 326:108357. doi:10.1016/j.jneumeth.2019.108357.

Sun, X.R., A. Badura, D.A. Pacheco, L.A. Lynch, E.R. Schneider, M.P. Taylor, I.B. Hogue, L.W. Enquist, M. Murthy, and S.S.-H. Wang. 2013. Fast GCaMPs for improved tracking of neuronal activity. *Nat Commun*. 4:2170. doi:10.1038/ncomms3170.

Suster, M.L., L. Seugnet, M. Bate, and M.B. Sokolowski. 2004. Refining GAL4-driven transgene expression in Drosophila with a GAL80 enhancer-trap. *Genesis*. 39:240–245. doi:10.1002/gene.20051.

Tas, R.P., and L.C. Kapitein. 2018. Exploring cytoskeletal diversity in neurons. *Science*. 361:231–232. doi:10.1126/science.aat5992.

Terada, S.-I., D. Matsubara, K. Onodera, M. Matsuzaki, T. Uemura, and T. Usui. 2016. Neuronal processing of noxious thermal stimuli mediated by dendritic Ca(2+) influx in Drosophila somatosensory neurons. *Elife*. 5:e12959. doi:10.7554/elife.12959.

Theis, L., P. Berens, E. Froudarakis, J. Reimer, M. Rom n Rosón, T. Baden, T. Euler, A.S. Tolias, and M. Bethge. 2016. Benchmarking Spike Rate Inference in

Population Calcium Imaging. *Neuron*. 90:471–482. doi:10.1016/j.neuron.2016.04.014.

Tian, L., S.A. Hires, T. Mao, D. Huber, M.E. Chiappe, S.H. Chalasani, L. Petreanu, J. Akerboom, S.A. McKinney, E.R. Schreiter, C.I. Bargmann, V. Jayaraman, K. Svoboda, and L.L. Looger. 2009. Imaging neural activity in worms, flies and mice with improved GCaMP calcium indicators. *Nat Methods*. 6:875–881. doi:10.1038/nmeth.1398.

Tominaga, M., and M.J. Caterina. 2004. Thermosensation and pain. *J Neurobiol*. 61:3–12. doi:10.1002/neu.20079.

Tracey, W.D. 2017. Nociception. *Curr Biol*. 27:R129–R133. doi:10.1016/j.cub.2017.01.037.

Tracey, W.D., R.I. Wilson, G. Laurent, and S. Benzer. 2003. painless, a Drosophila Gene Essential for Nociception. *Cell*. 113:261–273. doi:10.1016/s0092-8674(03)00272-1.

Tsubouchi, A., J.C. Caldwell, and W.D. Tracey. 2012. Dendritic Filopodia, Ripped Pocket, NOMPC, and NMDARs Contribute to the Sense of Touch in Drosophila Larvae. *Curr Biol*. 22:2124–2134. doi:10.1016/j.cub.2012.09.019.

Ugur, B., K. Chen, and H.J. Bellen. 2016. Drosophila tools and assays for the study of human diseases. *Dis Model Mech*. 9:235–244. doi:10.1242/dmm.023762.

Ulfhake, B., and J. -O. Kellerth. 1981. A quantitative light microscopic study of the dendrites of cat spinal α-motoneurons after intracellular staining with horseradish peroxidase. *J Comp Neurol*. 202:571–583. doi:10.1002/cne.902020409.

Vaadia, R.D., W. Li, V. Voleti, A. Singhania, E.M.C. Hillman, and W.B. Grueber. 2019. Characterization of Proprioceptive System Dynamics in Behaving Drosophila Larvae Using High-Speed Volumetric Microscopy. *Curr Biol*. 29:935-944.e4. doi:10.1016/j.cub.2019.01.060.

Vannini, E., L. Restani, M. Pietrasanta, A. Panarese, A. Mazzoni, O. Rossetto, S. Middei, S. Micera, and M. Caleo. 2016. Altered sensory processing and dendritic remodeling in hyperexcitable visual cortical networks. *Brain Struct Funct*. 221:2919–2936. doi:10.1007/s00429-015-1080-1.

Vargas, M.E., Y. Yamagishi, M. Tessier-Lavigne, and A. Sagasti. 2015. Live Imaging of Calcium Dynamics during Axon Degeneration Reveals Two Functionally Distinct Phases of Calcium Influx. *J Neurosci*. 35:15026–15038. doi:10.1523/jneurosci.2484-15.2015.

Vetter, P., A. Roth, and M. Häusser. 2001. Propagation of Action Potentials in Dendrites Depends on Dendritic Morphology. *J Neurophysiol*. 85:926–937. doi:10.1152/jn.2001.85.2.926.

Veverytsa, L., and D.W. Allan. 2013. Subtype-specific neuronal remodeling during Drosophila metamorphosis. *Fly*. 7:78–86. doi:10.4161/fly.23969.

Vormberg, A., F. Effenberger, J. Muellerleile, and H. Cuntz. 2017. Universal features of dendrites through centripetal branch ordering. *Plos Comput Biol*. 13:e1005615. doi:10.1371/journal.pcbi.1005615.

Walters, E.T., P.A. Illich, J.C. Weeks, and M.R. Lewin. 2001. Defensive responses of larval Manduca sexta and their sensitization by noxious stimuli in the laboratory and field. *J Exp Biology*. 204:457–69.

Wang, Q., B. Shui, M.I. Kotlikoff, and H. Sondermann. 2008. Structural Basis for Calcium Sensing by GCaMP2. *Structure*. 16:1817–1827. doi:10.1016/j.str.2008.10.008.

Werner, Gerhard. 1977. CUTANEOUS STIMULUS REGISTRATION AND INFORMATION PROCESSING IN THE SOMESTHETIC CORTEX. *J Invest Dermatol*. 69:172–180. doi:10.1111/1523-1747.ep12497945.

Williams, D.W., and J.W. Truman. 2005. Cellular mechanisms of dendrite pruning in Drosophila: insights from in vivo time-lapse of remodeling dendritic arborizing sensory neurons. *Development*. 132:3631–3642. doi:10.1242/dev.01928.

Woolf, C.J., and Q. Ma. 2007. Nociceptors—Noxious Stimulus Detectors. *Neuron*. 55:353–364. doi:10.1016/j.neuron.2007.07.016.

Xiang, Y., Q. Yuan, N. Vogt, L.L. Looger, L.Y. Jan, and Y.N. Jan. 2010. Light-avoidance-mediating photoreceptors tile the Drosophila larval body wall. *Nature*. 468:921–926. doi:10.1038/nature09576.

Xu, C.S., M. Januszewski, Z. Lu, S. Takemura, K.J. Hayworth, G. Huang, K. Shinomiya, J. Maitin-Shepard, D. Ackerman, S. Berg, T. Blakely, J. Bogovic, J. Clements, T. Dolafi, P. Hubbard, D. Kainmueller, W. Katz, T. Kawase, K.A. Khairy, L. Leavitt, P.H. Li, L. Lindsey, N. Neubarth, D.J. Olbris, H. Otsuna, E.T. Troutman, L. Umayam, T. Zhao, M. Ito, J. Goldammer, T. Wolff, R. Svirskas, P. Schlegel, E.R. Neace, C.J. Knecht, C.X. Alvarado, D.A. Bailey, S. Ballinger, J.A. Borycz, B.S. Canino, N. Cheatham, M. Cook, M. Dreher, O. Duclos, B. Eubanks, K. Fairbanks, S. Finley, N. Forknall, A. Francis, G.P. Hopkins, E.M. Joyce, S. Kim, N.A. Kirk, J. Kovalyak, S.A. Lauchie, A. Lohff, C. Maldonado, E.A. Manley, S. McLin, C. Mooney, M. Ndama, O. Ogundeyi, N. Okeoma, C. Ordish, N. Padilla, C. Patrick, T. Paterson, E.E. Phillips, E.M. Phillips, N. Rampally, C. Ribeiro, M.K. Robertson, J.T.

Rymer, S.M. Ryan, M. Sammons, A.K. Scott, A.L. Scott, A. Shinomiya, C. Smith, K. Smith, N.L. Smith, M.A. Sobeski, A. Suleiman, J. Swift, S. Takemura, I. Talebi, D. Tarnogorska, E. Tenshaw, T. Tokhi, J.J. Walsh, T. Yang, J.A. Horne, F. Li, R. Parekh, P.K. Rivlin, V. Jayaraman, K. Ito, S. Saalfeld, et al. 2020. A Connectome of the Adult Drosophila Central Brain. *Biorxiv*. 2020.01.21.911859. doi:10.1101/2020.01.21.911859.

Xu, S.Y., C.L. Cang, X.F. Liu, Y.Q. Peng, Y.Z. Ye, Z.Q. Zhao, and A.K. Guo. 2006. Thermal nociception in adult Drosophila: behavioral characterization and the role of the painless gene. *Genes Brain Behav*. 5:602–613. doi:10.1111/j.1601-183x.2006.00213.x.

Yamanaka, N., N.M. Romero, F.A. Martin, K.F. Rewitz, M. Sun, M.B. O'Connor, and P. Léopold. 2013. Neuroendocrine control of Drosophila larval light preference. *Sci New York N Y*. 341:1113–6. doi:10.1126/science.1241210.

Yan, Z., W. Zhang, Y. He, D. Gorczyca, Y. Xiang, L.E. Cheng, S. Meltzer, L.Y. Jan, and Y.N. Jan. 2012. Drosophila NOMPC is a mechanotransduction channel subunit for gentle-touch sensation. *Nature*. 493:221–225. doi:10.1038/nature11685.

Yang, Y., N. Liu, Y. He, Y. Liu, L. Ge, L. Zou, S. Song, W. Xiong, and X. Liu. 2018. Improved calcium sensor GCaMP-X overcomes the calcium channel perturbations induced by the calmodulin in GCaMP. *Nat Commun*. 9:1504. doi:10.1038/s41467-018-03719-6.

Ye, L., M.A. Haroon, A. Salinas, and M. Paukert. 2017. Comparison of GCaMP3 and GCaMP6f for studying astrocyte Ca2+ dynamics in the awake mouse brain. *Plos One*. 12:e0181113. doi:10.1371/journal.pone.0181113.

Yoshino, J., R.K. Morikawa, E. Hasegawa, and K. Emoto. 2017. Neural Circuitry that Evokes Escape Behavior upon Activation of Nociceptive Sensory Neurons in Drosophila Larvae. *Curr Biol*. 27:2499-2504.e3. doi:10.1016/j.cub.2017.06.068.

Yuste, R. 2015. From the neuron doctrine to neural networks. *Nat Rev Neurosci*. 16:487–497. doi:10.1038/nrn3962.

Zhivotovsky, B., and S. Orrenius. 2011. Calcium and cell death mechanisms: A perspective from the cell death community. *Cell Calcium*. 50:211–221. doi:10.1016/j.ceca.2011.03.003.

Zhong, L., R.Y. Hwang, and W.D. Tracey. 2010. Pickpocket is a DEG/ENaC protein required for mechanical nociception in Drosophila larvae. *Curr Biology Cb*. 20:429–34. doi:10.1016/j.cub.2009.12.057.

Zimmerman, A., L. Bai, and D.D. Ginty. 2014. The gentle touch receptors of mammalian skin. *Science*. 346:950–954. doi:10.1126/science.1254229.